Fall 2018

Rock Strength: A Main Control of Yosemite's Topography?

Alex Jon Hutcherson
San Jose State University

ROCK STRENGTH: A MAIN CONTROL OF YOSEMITE'S TOPOGRAPHY?

A Thesis

Presented To

The Faculty of the Department of Geology

San José State University

In Partial Fulfillment

of the Requirements for the Degree

Master of Science

by

Alex Jon Hutcherson

December 2018

The Designated Thesis Committee Approves the Thesis Titled

ROCK STRENGTH: A MAIN CONTROL OF YOSEMITE'S TOPOGRAPHY?

by

Alex Jon Hutcherson

APPROVED FOR THE DEPARTMENT OF GEOLOGY

SAN JOSÉ STATE UNIVERSITY

December 2018

Emmanuel Gabet, Ph.D.	Department of Geology
Jonathan Miller, Ph.D.	Department of Geology
Robert Miller, Ph.D.	Department of Geology

ABSTRACT

ROCK STRENGTH: A MAIN CONTROL OF YOSEMITE'S TOPOGRAPHY?

by Alex Jon Hutcherson

Although contrasts in rock strength correlate to variations in topography, the role of rock strength in shaping the landscape of Yosemite National Park is uncertain. Magmatic processes may create variations in mineralogy within a single plutonic unit, while tectonic processes may result in contrasts in joint density and foliation, all of which may lead to variations in rock strength. For this study, the relationship between differences in mineralogy, joint density, and foliation in Yosemite National Park is analyzed to determine the role of rock strength in shaping Yosemite's topography. Modal mineral abundance and grain size are determined by analyzing cut rock samples, while joint density and foliation intensity are recorded at 83 sites. Also, a Schmidt hammer is used to compare rock strength readings to elevation at all 83 sites. This study finds that variations in joint density shape many topographic features, including Mount Hoffman, a topographic high point in Yosemite. High potassium feldspar and low plagioclase abundance may also be a factor in Mount Hoffman's erosion resistance. No significant relationship between foliation and other factors is observed. Schmidt hammer readings typically increase with elevation, which is likely a result of weathering differences. Decreasing joint density across Yosemite National Park is found to be associated with decreased forestation. Overall, while few correlations are observed across the entire landscape, rock strength shapes the landscape of Yosemite at varying scales.

ACKNOWLEDGMENTS

Thank you to my thesis advisor, Dr. Emmanuel Gabet, for the opportunity to research this subject, along with my thesis committee members, Dr. Robert Miller and Dr. Jonathan Miller, who provided valuable knowledge about plutonic rocks. Thank you to Torrance Magtoto and Andy Trigueros, who were valuable field assistants for the first third of my fieldwork. Also, thank you Stephanie Meursing and Shaelyn Silverman for your assistance during the final days of my fieldwork. Finally, thank you to my mom and sister for their support in me earning my M.S.

This acknowledgements section would not be complete without mentioning my father, Jon Hutcherson, who considered Yosemite National Park as one of his favorite places. This thesis was completed in his memory.

TABLE OF CONTENTS

LIST OF TABLES

LIST OF FIGURES

INTRODUCTION

Geomorphic processes are considered responsible for creating large variations in topography, but the role of the spatial variability in rock strength and rock strength's effect on topography may be underappreciated. Even within areas where one rock type dominates the landscape, subtle variations in mineralogy may lead to differences in landscape morphology (e.g., Flageollet, 1977 in Migón, 2006). These variations in rock strength (Zhang et al., 2013) and erodibility (Kühni and Pfiffner, 2001) may influence topography through differential erosion.

For granitic rocks, the relationship between mineral composition and topography has been explored in previous studies (Godard, 2001; Migón, 2006; Migón and Vieira, 2014). Godard (1965) sought to determine a relationship between elevation and erosion-resistant minerals, such as quartz, but found that there was a poor correlation between them (Godard 1965 in Godard et al., 2001). In contrast, Flageollet (1977) found that higher elevations were correlated with lower amounts of plagioclase and biotite (Flageollet, 1977 in Migón, 2006). Variations within a single granitic unit can also lead to contrasts in topography, such as in the Conway granite in the Appalachians, where differences in the amounts of biotite and plagioclase are associated with uplands and basins (Migón, 2006). In Portugal, Migón and Vieira (2014) determined that granites at higher elevations were generally fine to medium-grained while granites at lower elevations were medium to coarse-grained. In situ measurements of rock strength were also collected using a Schmidt hammer and rebound values were obtained. A general pattern was observed where fine-grained granites had higher rebound values than coarser grained granites,

indicating that they were stronger, although the authors urged caution when interpreting results as the readings were taken on surfaces with varying amounts of weathering.

Johnson (2015) described patterns in Yosemite National Park where fine-grained and quartz-rich rocks were found above bedrock channel knickpoints and coarse-grained and quartz-poor rocks were found below. These observations are supported by Tuğrul and Zarif (1999) who demonstrated in laboratory studies that high quartz content and fine grain sizes are associated with greater strength in granitic rocks, while larger grain sizes and high feldspar content are associated with weaker rocks. Rocks with more feldspars are likely weaker due to their cleavage and microfissures (Onodera and Asoka Kumara, 1980 in Tuğrul and Zarif, 1999), and rocks with more quartz have greater strength as quartz is interstitial other minerals (Tuğrul and Zarif, 1999). Similarly, rocks with finer grain sizes may be stronger as their tighter fabric makes them less susceptible to granular disintegration due to weathering processes (Migón, 2006), which may reduce in situ rock strength. Tuğrul and Zarif (1999) determined that mineralogical composition is one of the main properties controlling rock strength.

Eggler et al. (1969) described how the weathering of minerals also controls topography. In the Laramie Range of Wyoming, the Trail Creek granite supports topography covered by grus and comprised of gently rolling hills, in what is known as the Sherman surface (Eggler et al., 1969). The Trail Creek granite is one facies of the Sherman granite, which comprises the Sherman surface, and a second member, the Cap Rock quartz monzonite, supports parkland-tor topography, where open, grassy lands feature scattered clusters of tors. Eggler et al. (1969) determined that weathering rates,

especially of biotite, controlled the two different topographies. The Trail Creek granite rapidly weathers to grus, which is then transported away, leaving a relatively flat landscape with rolling topography. In contrast, the Cap Rock quartz monzonite weathers far slower and more selectively along fractures, which creates the different topography. Eggler et al. (1969) suggested that oxidation under high temperatures in the Precambrian when the Trail Creek granite crystallized likely led to alteration of biotites, which allowed for more accelerated subsequent weathering. Selective weathering of biotite and plagioclase has also been observed in other environments, such as in France's Massif Central (Flageollet, 1977 in Godard 2001). Differences in weathering rates between exposed and buried rocks may also be responsible for creating some of the topography of the Sierra Nevada Mountains. Buried granites turn into grus as biotite and feldspars weather, while exposed granites remain relatively unaltered (Wahrhaftig, 1965).

The varying grain sizes and mineral abundances in granitic rocks are the result of complex magmatic processes. Plutons are likely formed by many magmatic increments over millions of years rather than being formed in one large event (e.g., Pitcher and Berger, 1972; Glazner et al., 2004). These increments may vary in mineralogy and grain size, resulting in overall rock strength at different elevations within the same plutonic unit.

Other factors may also control topography. In glacial erosion, joint density controls whether plucking or abrasion is dominant, and as plucking is more efficient at erosion, joints can influence erosion rates. Also, streams often follow fractures (Scott and Wohl, 2018). Other possible influences of topography, as tested by Stutenbecker et al. (2016) in

the Rhône Basin in Central Europe, are uplift, glacial inheritance, and variations in precipitation. Although uplift and glaciation have an important role, variations in bedrock erodibility were determined to be the best explanation for the topography of that landscape.

The goal of this study is to expand our knowledge of rock strength and its effect on topography by collecting and analyzing rock samples from areas at different elevations in Yosemite National Park (Figure 1), along with obtaining Schmidt hammer, foliation, and joint data. The data were supplemented by data collected by former students affiliated with San Jose State University. For my study, I tested the hypothesis that stronger rocks support higher elevation terrain and weaker bedrock underlies topographic lows.

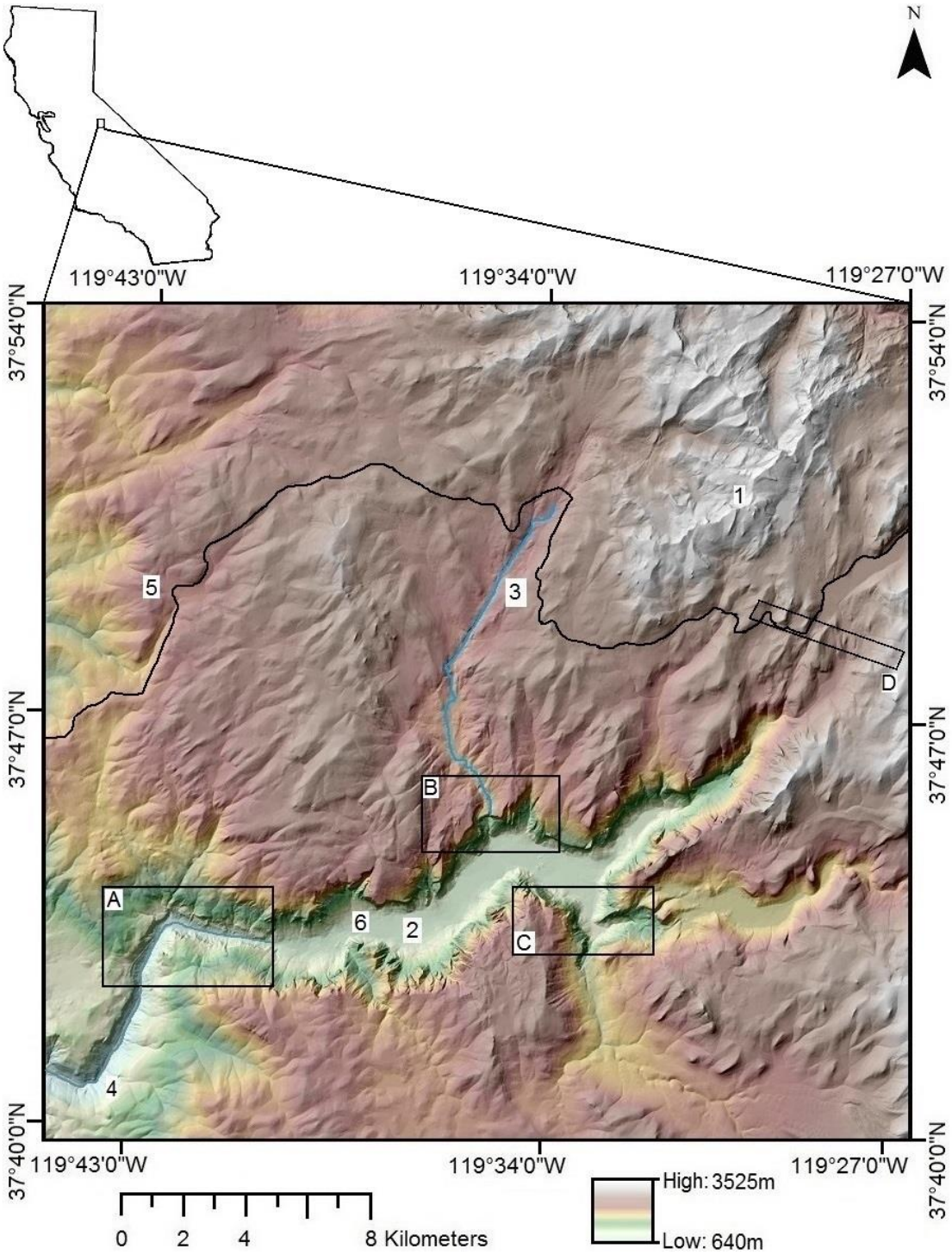

Figure 1. The study area, including areas sampled by supplemental theses. "1" shows the location of Mount Hoffman, "2" Yosemite Valley, "3" Yosemite Creek, "4" the Merced River, "5" Highway 120, and "6" El Capitan/ The Rockslides. "A" through "D" show the locations of topographic profiles presented later. The DEM data are available from the National Elevation Database (U.S. Geological Survey, 2014).

METHODS

Field Site

The Sierra Nevada mountain range (California, U.S.A.) extends from north to south for over 600 km, is 80 to 130 km wide and reaches elevations of more than 3,900 m near Yosemite. As the Sierra Nevada Range is dominated by plutonic igneous rocks (e.g. Bateman, 1992), Yosemite, which is characterized by mainly granitic (granite and granodiorite) lithology and high relief, is an ideal field site to test the correlation between rock strength and elevation among plutonic rocks.

The rocks at Yosemite are part of the Sierra Nevada Batholith, a group of plutonic rocks that extends throughout eastern California and western Nevada (Bateman and Wahrhaftig, 1966). Although it may have taken as much as 130 Ma to form the batholith (Huber et al., 1989), the majority of it formed in three distinct and separate events, with the third and final event occurring when most of the granitic units in the study area were intruded (Huber et al., 1989). Groundmass grain sizes in the central Sierras vary between 1-5 mm with potassium feldspar phenocrysts reaching several centimeters in length (Bateman and Wahrhaftig, 1966).

Yosemite features a variety of lithologic units (Figure 2). The granodiorite and granite units are the focus of this study, with the youngest dated unit, the Half Dome Granodiorite, having formed at approximately 86-88 Ma, and the oldest unit, the Granodiorite of Arch Rock and similar rocks, at 116 Ma (Huber et al., 1989). The majority of these units are grouped into intrusive suites by Huber et al. (1989), in which units within individual intrusive suites formed during the same magma-producing events.

In Figure 2, the units listed as aplite and pegmatite intrude the Granodiorite of Kuna Crest which is part of the Tuolumne Intrusive Suite. The Sentinel Granodiorite and Yosemite Creek Granodiorite also formed in the Late Cretaceous but are not listed as part of any intrusive suite (Huber et al., 1989).

Other units, such as granitic rocks, undivided (assumed to be from the Cretaceous), diorite and gabbro (Cretaceous and Jurassic), metasedimentary rock, undivided (assumed to be from the Jurassic), and the Granodiorite of Arch Rock are not mapped as part of any intrusive suite (Huber et al., 1989). The Granodiorite of Mount Hoffman, mapped by Kistler (1973) and Bateman et al. (1983), is part of the Yosemite Valley Intrusive Suite (e.g., Johnson, 2013).

Joints in the Sierra Nevada Batholith, including in Yosemite, are abundant and exist at scales from microscopic to regional (Migón, 2006), with a variety of spacing and lengths. For example, Segall and Pollard (1983) reported distances between joints ranging from approximately 20 cm to nearly 25 m, and lengths from 1 m up to 70 m in a study area south of Yosemite. Regional joints in the Sierras are often found in perpendicular sets and cut across plutons, indicating that they formed after the plutons had solidified (Bateman and Wahrhaftig, 1966). Major features such as streams, valley axes, gorges, ravines, trenches, and slope breaks are guided by these joints, often called master joints (Ericson et al., 2005). Vertical joints control the orientation of major features in Yosemite, such as Half Dome, while inclined joints control the topography of other minor features (Huber, 1987). Also, coarser-grained and more silica-rich plutonic rocks typically feature tighter joint spacing than finer-grained, less silica-rich rock

(Huber, 1987). Tabular fracture clusters, or groups of fractures clustered into tabular zones, likely control the topography of Tuolumne Meadows, just east of the study area (Becker et al., 2014).

The age of the landscape at Yosemite is subject to debate. After the Sierra Nevada Batholith was emplaced, the commonly accepted model for the creation of the Sierras involves unroofing of the batholith at approximately 65 Ma, creating a low relief landscape (Huber, 1987). According to Huber (1987), by approximately 25 Ma, tilting of the landscape had begun, which resulted in uplift and contemporaneous incision that cut canyons into the mountain block. However, the methods used to conclude late Cenozoic tilting and uplift of the Sierras may be unreliable (Gabet, 2014). In addition, ancient meteoric water data, gathered by analyzing hydrogen isotopes in volcanic glass, suggest that since the Miocene, the Sierras have been a major topographic feature with elevations similar to those seen today (Mulch et al., 2008).

Between 25 and 5 Ma, volcanoes erupted in the northern Sierras (Huber et al., 1989), burying the landscape north of Yosemite with lava flows (Huber, 1987; Huber et al., 1989). Approximately 2-3 Ma, glaciers and ice fields began to periodically cover the Sierras and Yosemite. These glaciers moved down valleys, carving and modifying the landscape. Lakes were created in the process, many of which have now been filled in by sediment (Huber, 1987). Glaciers likely disappeared from the Sierras by 5,000 years ago, although new, smaller glaciers formed by approximately 2,500 years ago, and as many as 500 glaciers, covering less than 1.3 km^2, still existed in the Sierras in 1980 (Huber, 1987).

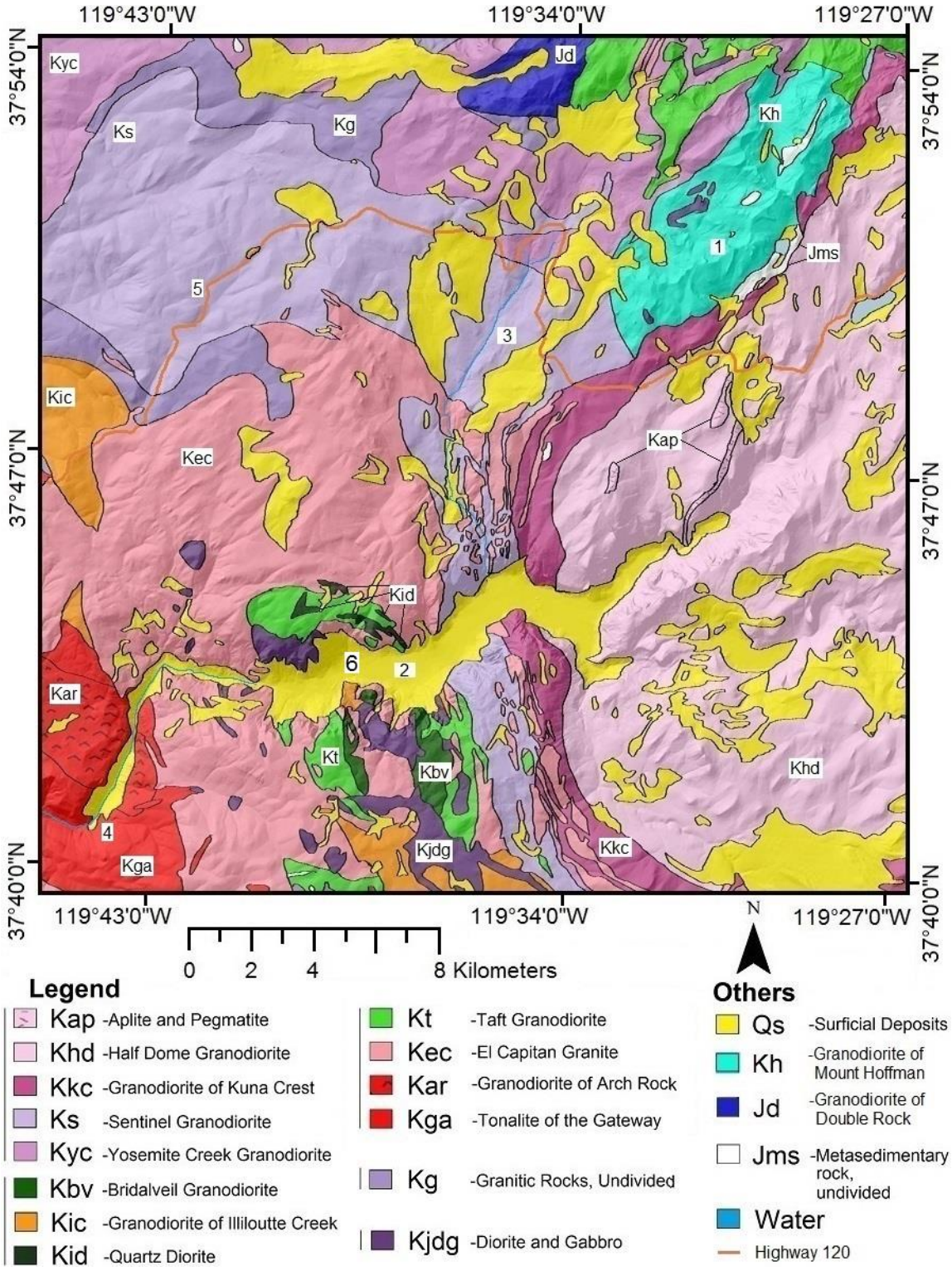

Figure 2. Geologic map of the study area from Figure 1, adapted from Huber et al. (1989), Bateman et al. (1983), and Kistler (1973). "1" through "6" represent the same locations as in Figure 1.

Rock mass failures have affected some parts of Yosemite. Differences in talus pile volume between diorite at the Rockslides and granite at El Capitan ("6," Figures 1, 2) demonstrate a connection between rock strength and topography in Yosemite. The diorite unit has the lowest silica content and the closest joint spacing of any plutonic rocks in Yosemite Valley, and rocks from it are usually finer grained than the granitic units (Huber, 1987). While these relatively weak rocks have produced massive talus piles, talus piles at the neighboring El Capitan are small due to El Capitan's resistance to erosion, a result of the lack of joints on the cliff. Also, several pinnacles on the north-facing side of the valley stand out due to their relatively high silica content (Huber, 1987). These are all evidence that joint spacing and silica content may be important.

Mineral Percentages and Grain Sizes

A total of 54 rock samples were collected from 83 sites in Yosemite National Park and analyzed; the resulting data were combined with mineral and grain size data from 53 samples collected by former and affiliated students of San Jose State University. Initially, approximately half of the 83 rock sampling sites were selected along transects to provide rock strength data at the base, sides, and tops of cliffs, while the remaining sites were chosen to provide data across the range of elevations in Yosemite.

After fieldwork was completed, samples were cut into slabs to analyze the modal mineralogy and grain size of each rock to determine how mineral properties varied across Yosemite. Forty-eight out of 54 samples were cut into slabs and stained so that the minerals could be easily identified using methods from Johnson (2015). Potassium feldspar grains were stained yellow and plagioclase were stained red. The remaining

samples either crumbled when cutting due to weathering or were too small and irregular to be cut into slabs.

Techniques based on Johnson (2015) were used for point counting and grain sizes. Stained slabs were scanned using a desktop printer-scanner. When scanning, a transparent ruler was placed next to all samples to provide a scale for determining grain sizes. The scans were imported into Adobe Illustrator and scaled to fit under a grid for point counting. A total of 300-400 combined potassium feldspar, plagioclase, mafic, and quartz points were counted per slab, as in Johnson (2015). The percentage of each mineral in a sample was determined by dividing the total number of points counted for each mineral type by the total number of points counted Mafic minerals such as hornblende and biotite were difficult to distinguish in the stained slabs, so any dark mineral was simply counted as being mafic and not further differentiated.

For grain sizes, the line tool was used to draw 6-13 transects on each sample, and the number of grains counted per transect was noted. Before counting, each line segment was compared with the scanned ruler to determine its length. The length and number of transects used varied depending on the dimensions of each slab, its variation in grain sizes, the irregularity of its shape, and the number of cracks (if present). Finally, the total length of line segments (transects) counted was divided by the total number of grains counted, resulting in an average grain size (mm/grain).

For the supplemental data sites 83-99, mineral percentages of quartz, plagioclase, and potassium feldspar, represented as a sum of the albite and anorthite end-members, were sourced from Bliekendaal (2012) and Van der Linde (2012), and sites 100-126 were

sourced from Fulmer and Kruijer (2009). The mineral data for sites 83-126 were generated by each theses' authors using Cross, Idings, Pirrson and Washington (CIPW) normative mineral calculations on geochemical data (e.g., Cross et al., 1902). Mineral data for sites 126-135 were obtained from Johnson (2015) who used point counts and grain size analysis to analyze cut and stained slabs. Grain size data from Johnson (2015), expressed as grains/cm, were converted to grain sizes of mm/grain by taking the inverse of and converting the grains/cm values.

Joint Density

To determine the potential effect of jointing on the strength of the entire rock mass, joint density was also estimated at all 83 sites. At each site, a maximum distance of 25 m was walked in a straight line from a central starting point and the number of joints crossing the walked path were counted. This was done a total of 4 times at each site until measurements had been taken north, south, east, and west of the starting point. A compass was used to ensure that the bearings from the starting point were consistent for each site. The total distance measured to the north and south was multiplied by the total distance measured to the east and west to calculate an area (m^2) for each site. Finally, the total number of joints counted were summed and then divided by the area to give a joint density in units of joints/m^2 for each site. Often, for logistical reasons, the number of paces walked in each direction was counted and later converted to meters rather than laying out a measuring tape. Since many sampling sites were on the edge of steep rock faces, the 25 m distance and measured lengths and widths were also approximate values

as joints extended to areas that were inaccessible without climbing gear and therefore could not be accessed for precise measuring.

Foliation

Rocks at all 83 sites were classified as either lightly to non-foliated, moderately foliated, or highly foliated to determine if there was any correlation between foliation and rock strength. Rocks classified as lightly foliated or non-foliated were given a value of "0" for foliation. Rocks in the moderately foliated category had minor yet visible foliation (layers or alignment of minerals), and were given a score of "1." Rocks in the highly foliated category were given a value of "2."

Schmidt Hammer Data

Schmidt hammer measurements were collected at all 83 sites. Due to wilderness regulations, the use of a power-sander was not permitted so rock surfaces were not polished or modified in any way before recording measurements. Ten Schmidt hammer measurements were taken and averaged to produce an average rebound value for the site. Rather than taking 10 measurements at the exact same point, impacts were separated by enough space so that no measurements overlapped. This method is similar to lab testing method T_1 described by Karaman and Kesimal (2014), except 10 measurements were taken at each site instead of 6. Measurements were taken at a variety of angles and the angle from horizontal was measured using a Brunton compass. Later, these measurements were normalized to account for differences in the measuring angle using the scale on the side of the Schmidt hammer. Finally, the 10 readings taken at each site were averaged to produce an average Schmidt value for the site. As a result, all Schmidt

hammer values represented as the Schmidt hammer rebound value for each site in all tables and figures are an average rebound value for the site rather than a single Schmidt rebound value.

Data Analysis

All data collected for this study were plotted against elevation to determine if there was any regional relationship between each category and elevation. Also, several factors were plotted against each other, such as plagioclase vs. potassium feldspar.

Microsoft Excel files containing each site's UTM coordinates (easting and northing) and each site's measurements, such as mineral percentage, were saved as .txt files. The .txt files were loaded into ArcGIS ArcMAP 10.6. Each file was then made into a map using the Kriging tool which interpolates values and produces a map based on the resulting values. Each factor, such as plagioclase percentage, was selected for the tool, where the setting of ordinary was selected for the Kriging method and the default semivariogram model was used. An interpolated map was produced as a result, and for each map, the location of data points used to create it was overlain on the map. All interpolated maps were also overlain on a hillshade of the study area. Six important geographic features, listed in Figure 2, were added to each interpolated map to aid map comparisons. As with the plots, these interpolated maps were created for all collected data. All plots and maps are visible in the results subsections.

Topographic Profiles

Plots of several transects were created to determine if there were any patterns

between elevation changes and changes in lithological characteristics. Areas with the greatest variations in topography and with numerous sample data were chosen to create the topographic profiles.

RESULTS

Mineral Percentages and Grain Sizes

All data collected for this study and gathered from other theses are included in Appendix 1. The supplemental data are labeled as sites 83-135, while the first 83 sites are locations visited during fieldwork for this thesis. The original stop names, relabeled as site numbers for consistency, are also listed in Appendix 1. Also, p-values were calculated to statistically test the results of all plots mentioned below in the results section.

Although grain sizes vary by region (Figure 3), no significant correlation was observed between grain size and elevation across the entire study area (Figure 4). Plots of mineral percentages show that there is no significant relationship between quartz and elevation (Figure 5), potassium feldspar and elevation, (Figure 6), or mafic mineral content and elevation (Figure 7). Plagioclase increases as elevation increases, however (Figure 8). Plots reveal a linear relationship between plagioclase and potassium feldspar content (Figure 9). The interpolated maps show that mineral content also varies by region, (Figures 10-12), approximately corresponding to the location of different plutonic units as expressed in Figure 2. An exception is mafic mineral content, for which there is no distinct relationship between location and lithologic unit (Figure 13).

Mineral percentages also vary by lithologic unit (Table 1). For example, the Mount Hoffman Granodiorite (Kh) contains significantly more potassium feldspar than other units. Based on all the data, grain size also varies by unit (Table 1).

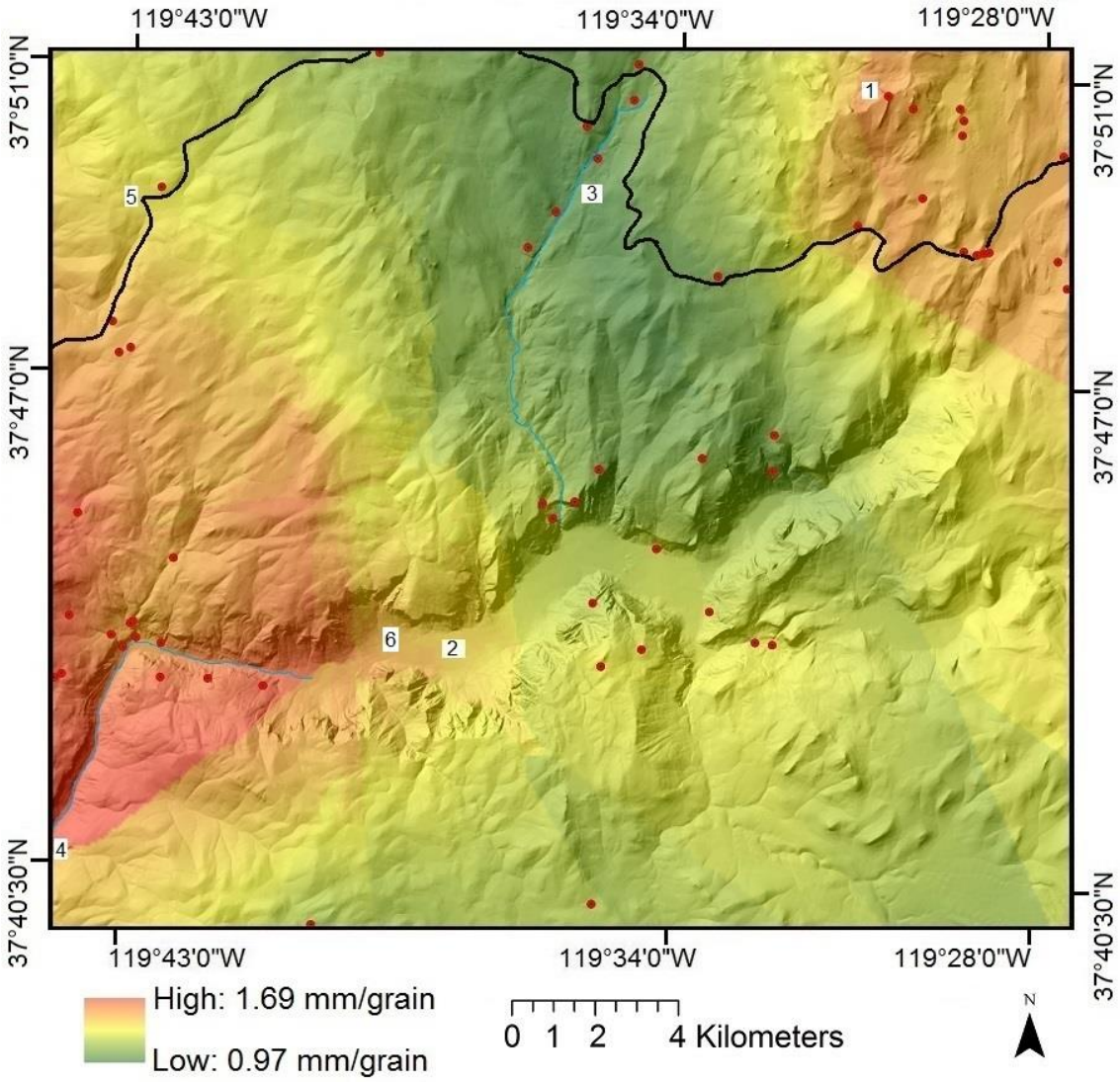

Figure 3. Interpolated map of average grain size. "1" shows the location of Mount Hoffman, "2" Yosemite Valley, "3" Yosemite Creek, "4" the Merced River, "5" Highway 120, and "6" El Capitan/ The Rockslides.

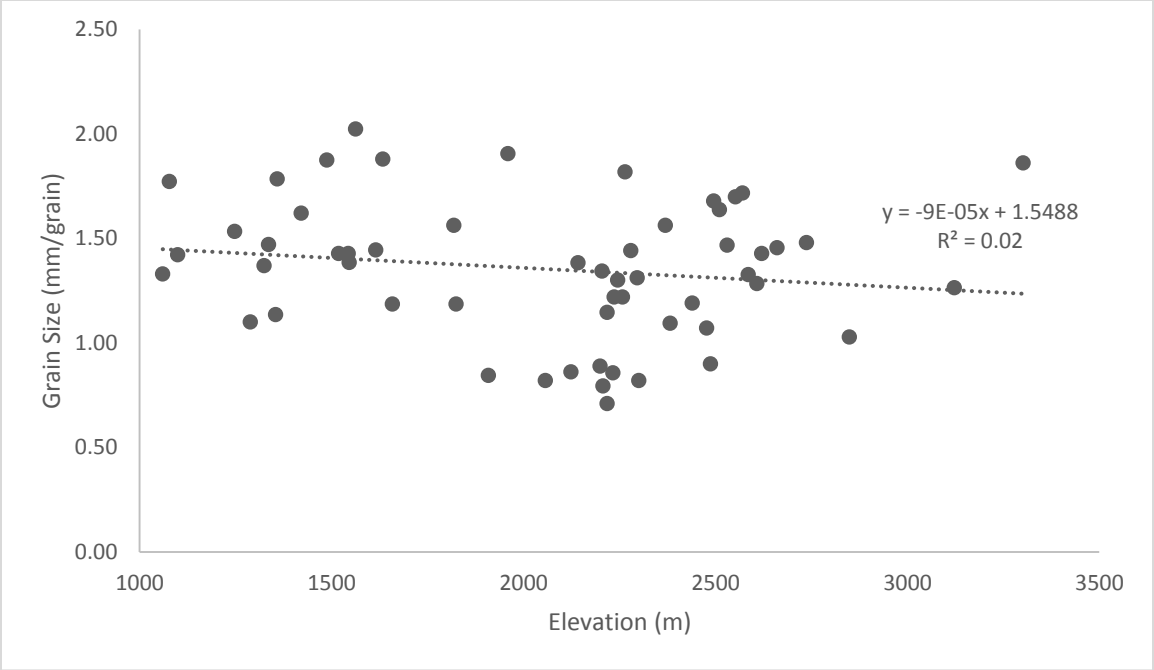

Figure 4. Plot of average grain size versus elevation.

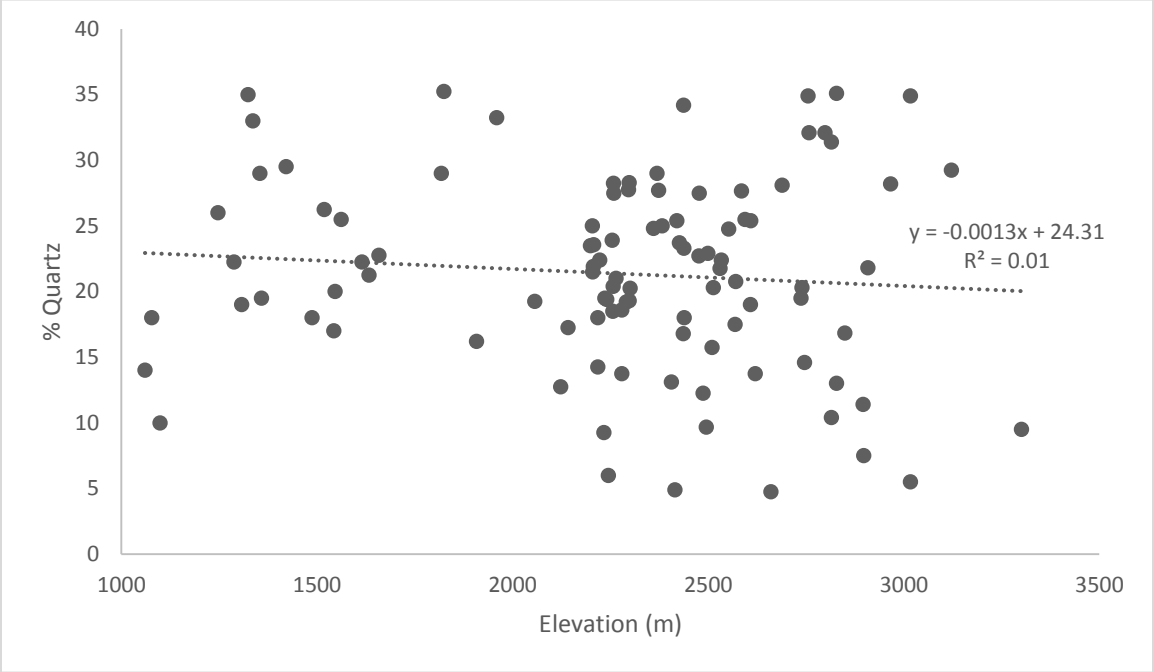

Figure 5. Plot of quartz content versus elevation.

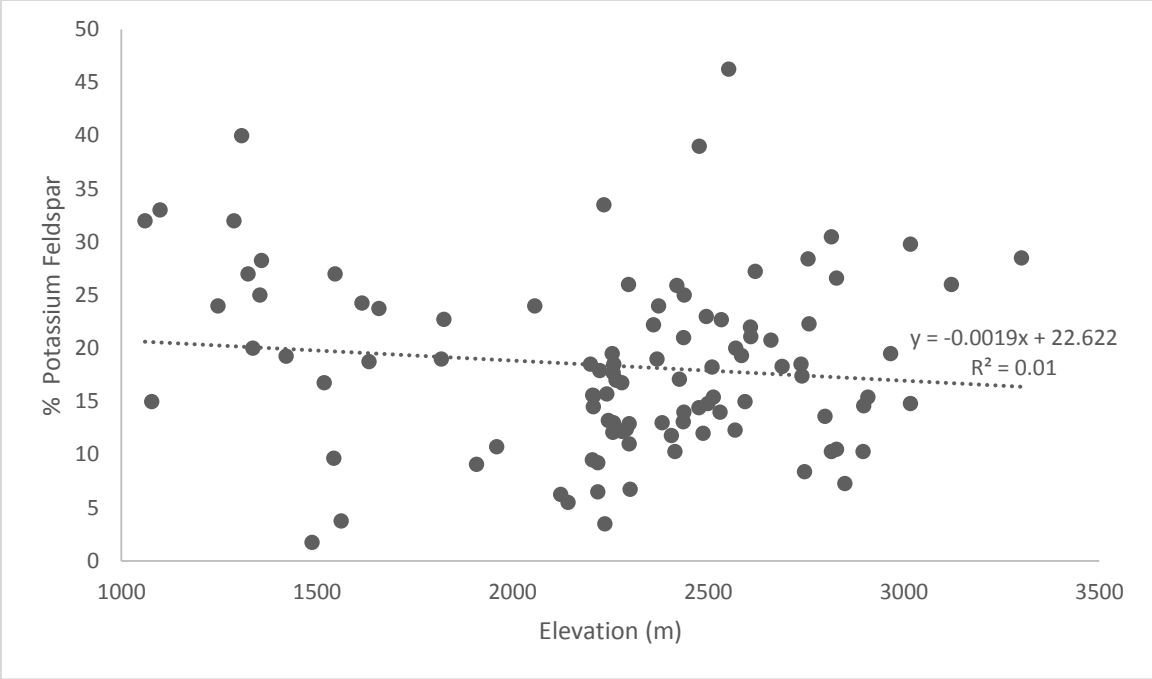

Figure 6. Plot of potassium feldspar content versus elevation.

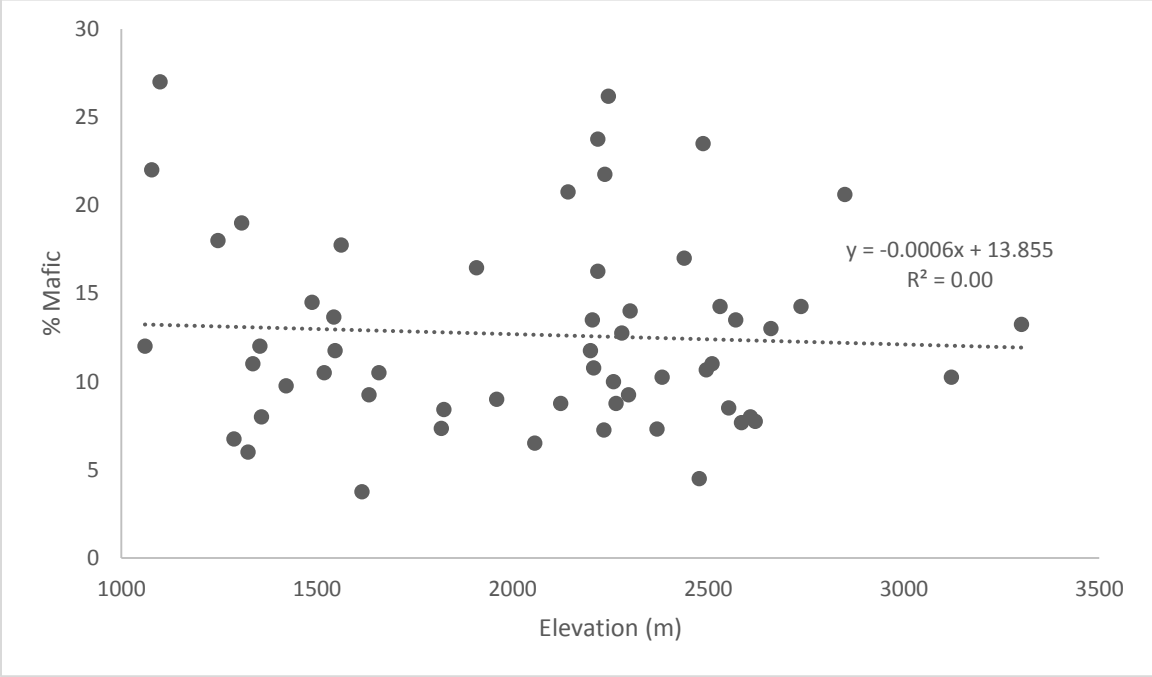

Figure 7. Plot of mafic mineral content versus elevation.

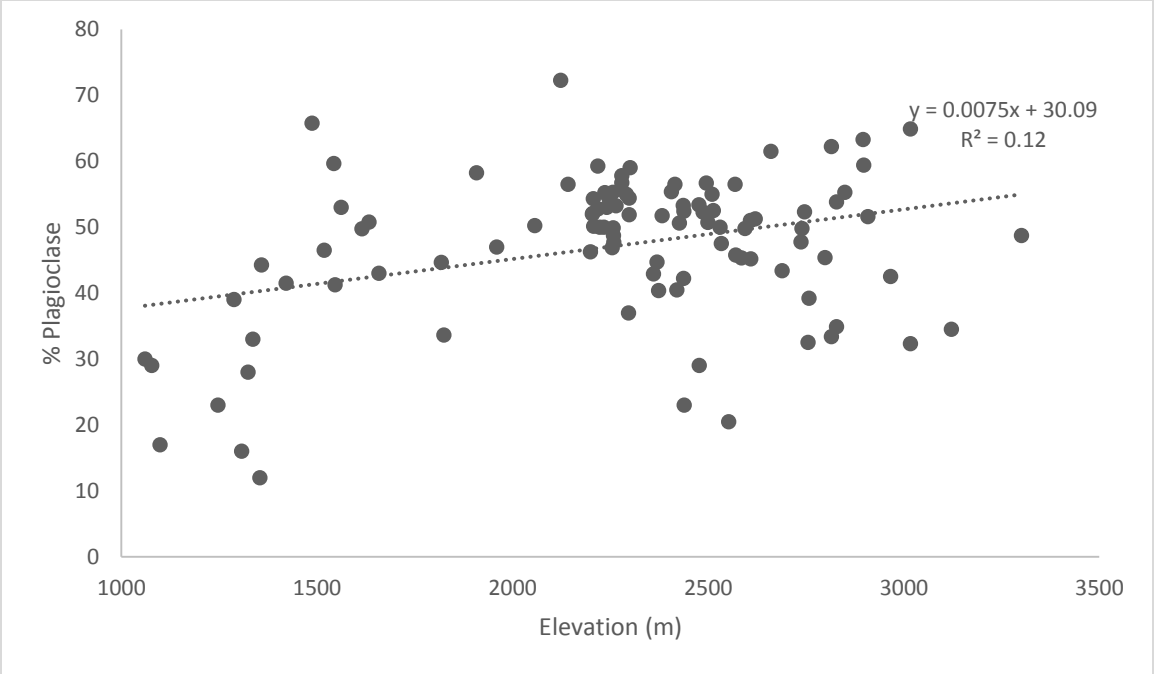

Figure 8. Plot of plagioclase feldspar content versus elevation.

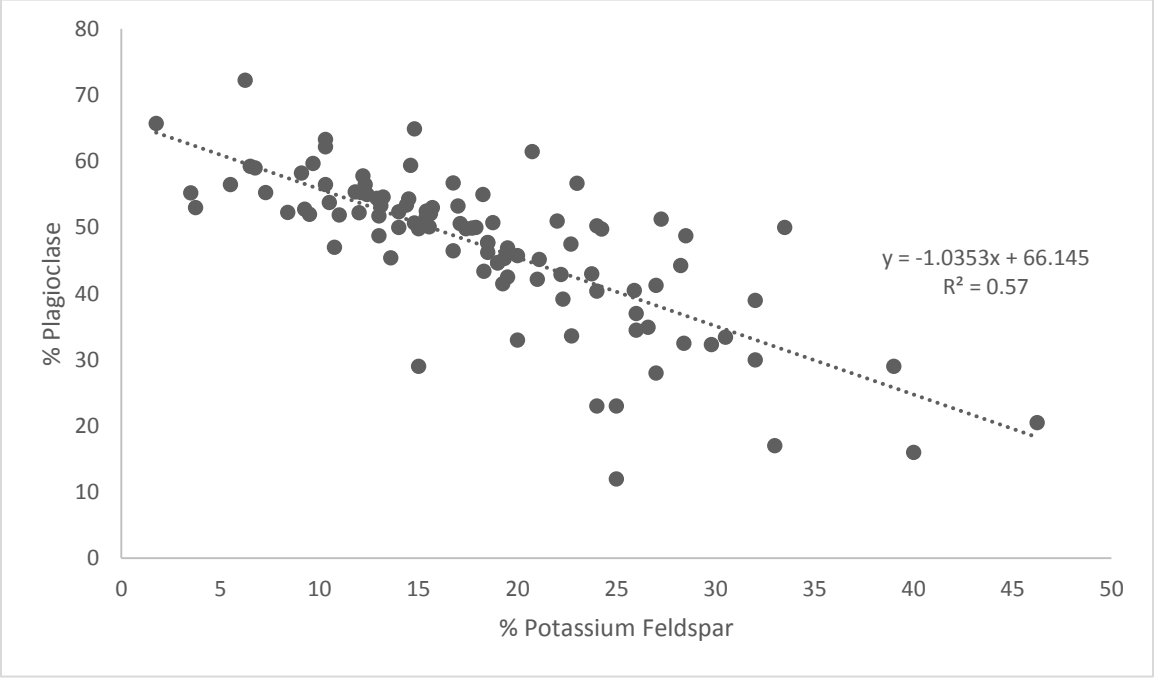

Figure 9. Plot of potassium feldspar content versus plagioclase content.

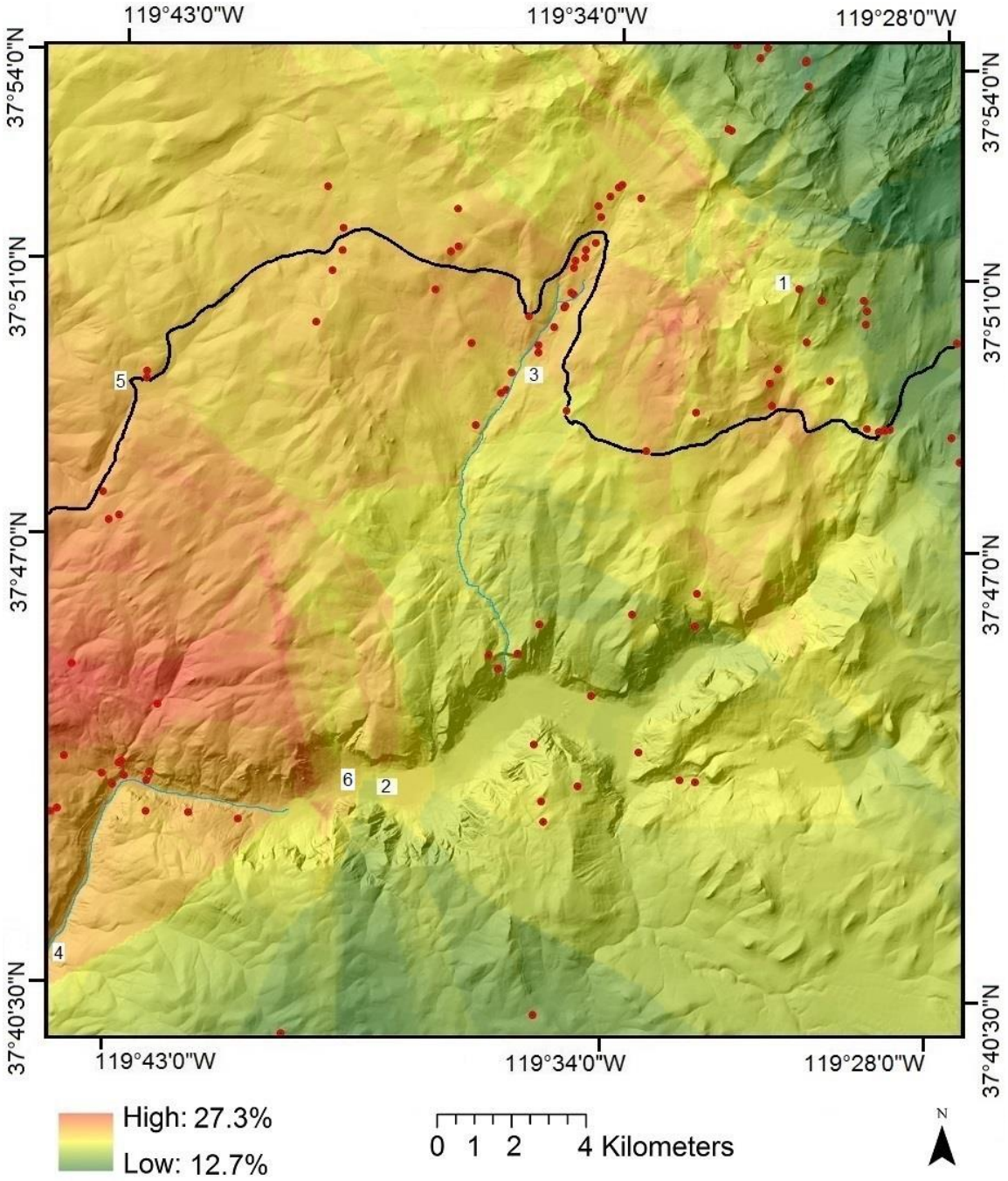

Figure 10. Interpolated map of quartz content. “1” shows the location of Mount Hoffman, “2” Yosemite Valley, “3” Yosemite Creek, “4” the Merced River, “5” Highway 120, and “6” El Capitan/ The Rockslides.

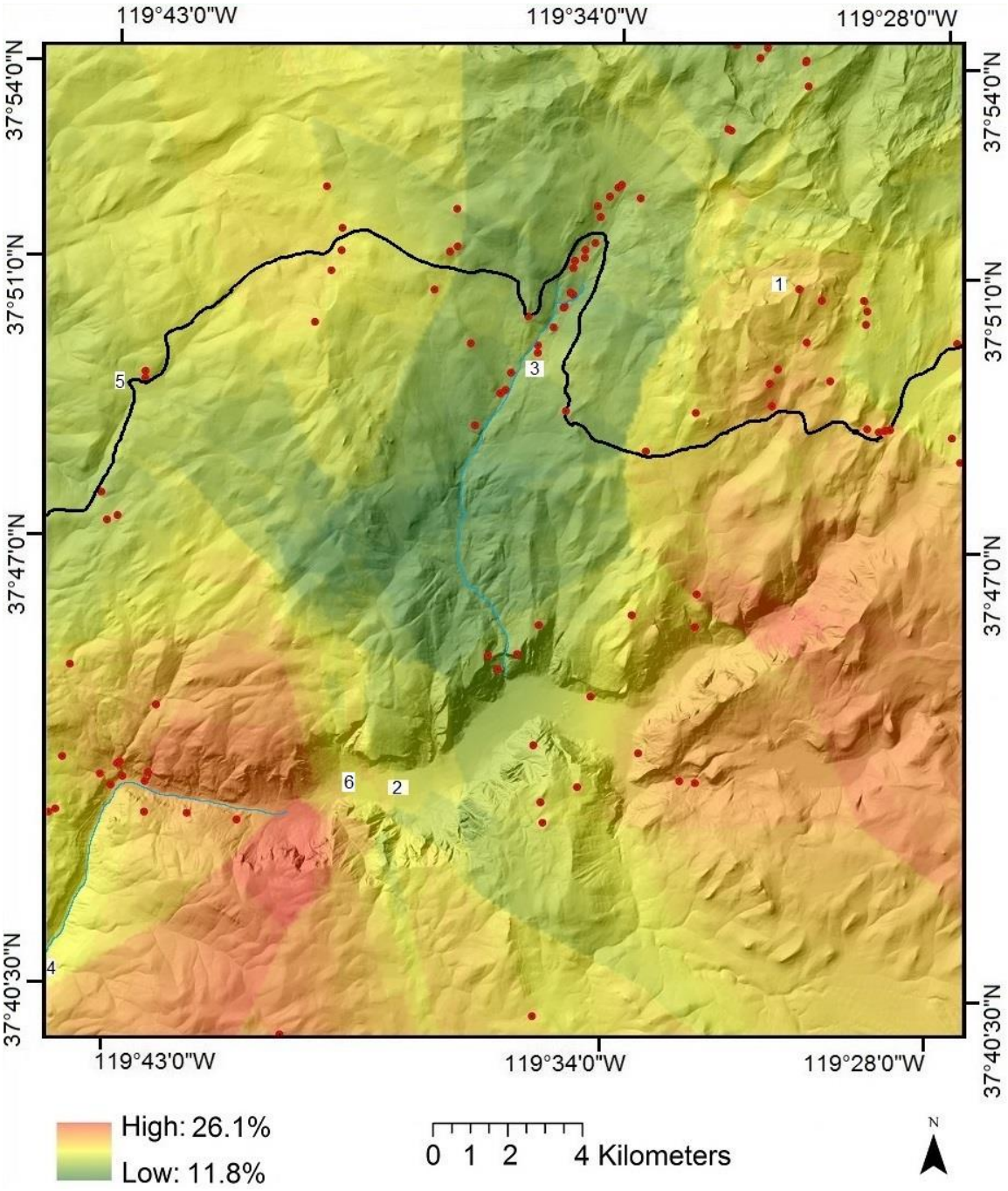

Figure 11. Interpolated map of potassium feldspar content. “1” shows the location of Mount Hoffman, “2” Yosemite Valley, “3” Yosemite Creek, “4” the Merced River, “5” Highway 120, and “6” El Capitan/ The Rockslides.

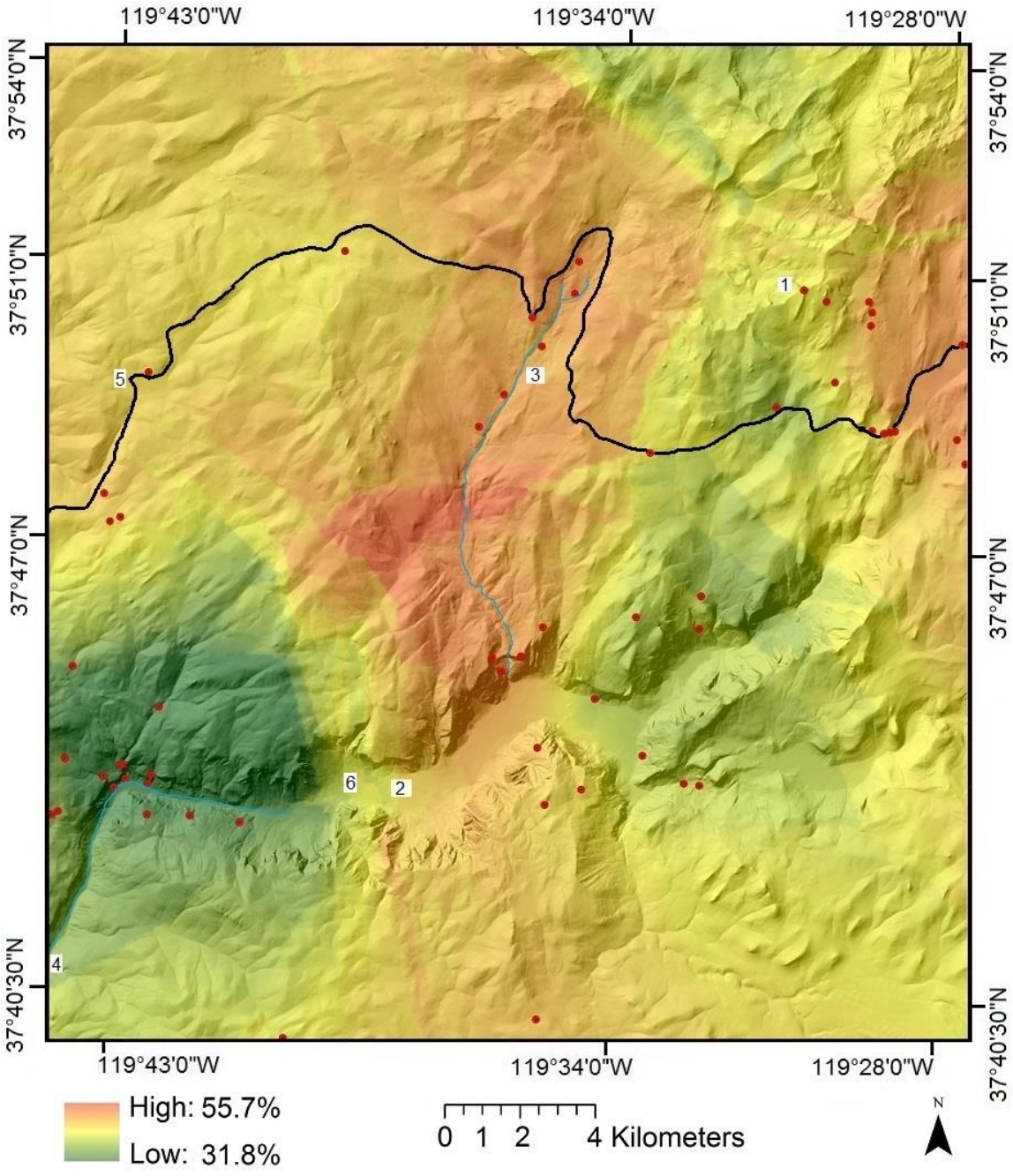

Figure 12. Interpolated map of plagioclase content. “1” shows the location of Mount Hoffman, “2” Yosemite Valley, “3” Yosemite Creek, “4” the Merced River, “5” Highway 120, and “6” El Capitan/ The Rockslides.

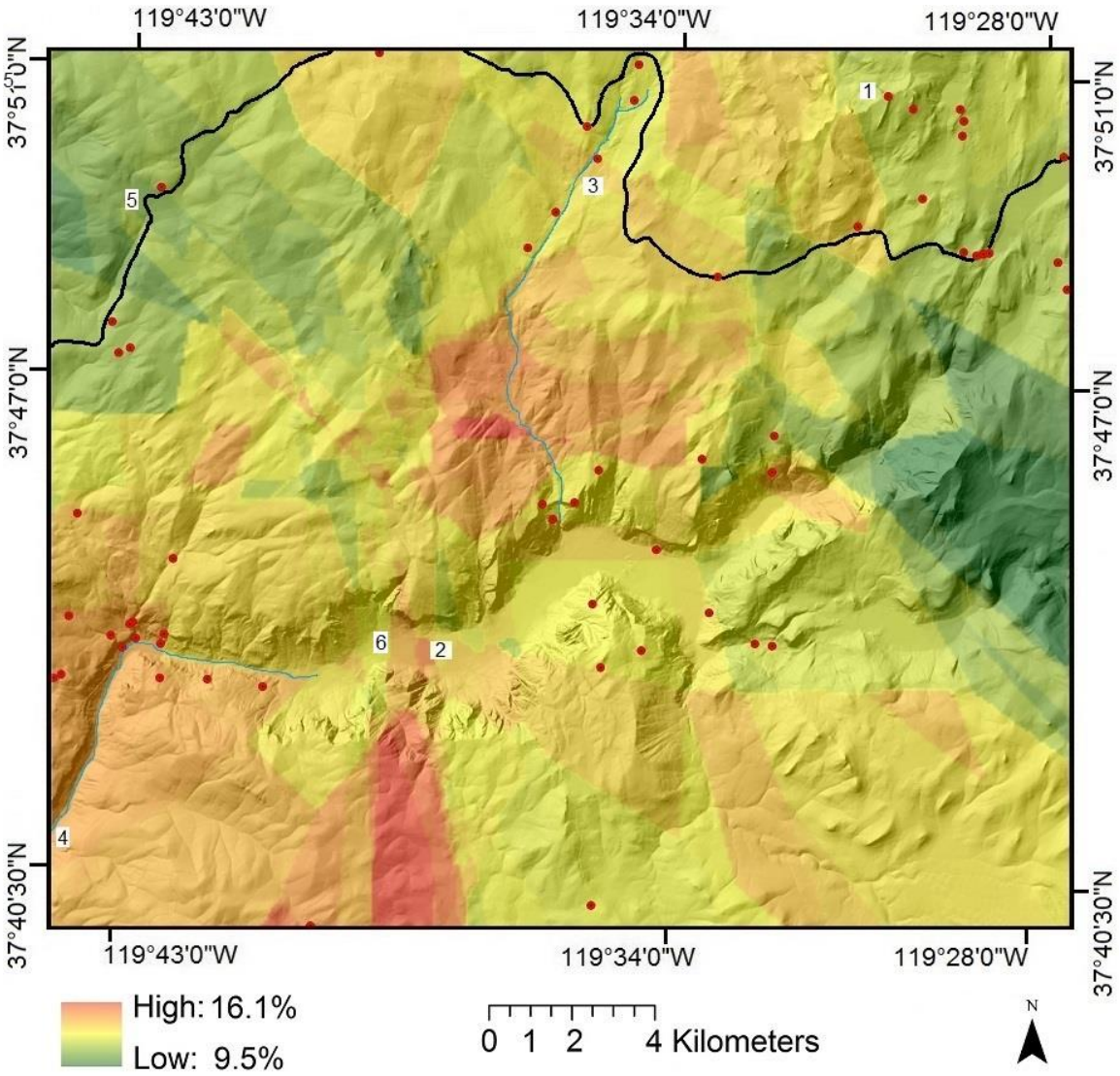

Figure 13. Interpolated map of mafic mineral content. "1" shows the location of Mount Hoffman, "2" Yosemite Valley, "3" Yosemite Creek, "4" the Merced River, "5" Highway 120, and "6" El Capitan/ The Rockslides.

TABLE 1. MOST COMMONLY SAMPLED UNITS COMPARED, RANKED BY ELEVATION

Unit	Elev (m)	Schmidt	Foliation	Joint Density	%Kspar	%Plag	%Mafic	%Quartz	Mm/grain
Kh	3144	41.2	0.5	0.1	27.3	41.6	11.8	19.4	1.51
Kyc	2492	44.4	1.0	0.8	16.4	49.7	10.0	22.0	4.88
Kkc	2430	44.9	1.2	0.6	13.8	49.3	22.0	20.2	0.98
Ks	2337	41.1	0.6	0.5	16.4	50.1	12.3	22.1	1.10
Khd	2143	42.6	0.6	0.3	23.8	44.1	10.7	19.8	1.36
Ka	1913	41.2	1.0	0.6	13.8	53.7	13.8	18.8	1.59
Kec	1756	37.9	0.9	0.3	19.7	40.8	12.0	23.6	1.12

Note: Kspar=potassium feldspar, Plag=plagioclase

Joint Density

Although no significant relationship exists between joint density and elevation (Table 1; Figure 14), joint density varies by region (Figure 15). The most jointed rocks are found in a region near the center of the field area in the Yosemite Creek granodiorite (Figure 15), corresponding to the location of Yosemite Creek ("3," Figure 15) and the large master joint it follows ("4," Figure 15). This links regional master joints to areas of high joint density at the outcrop scale.

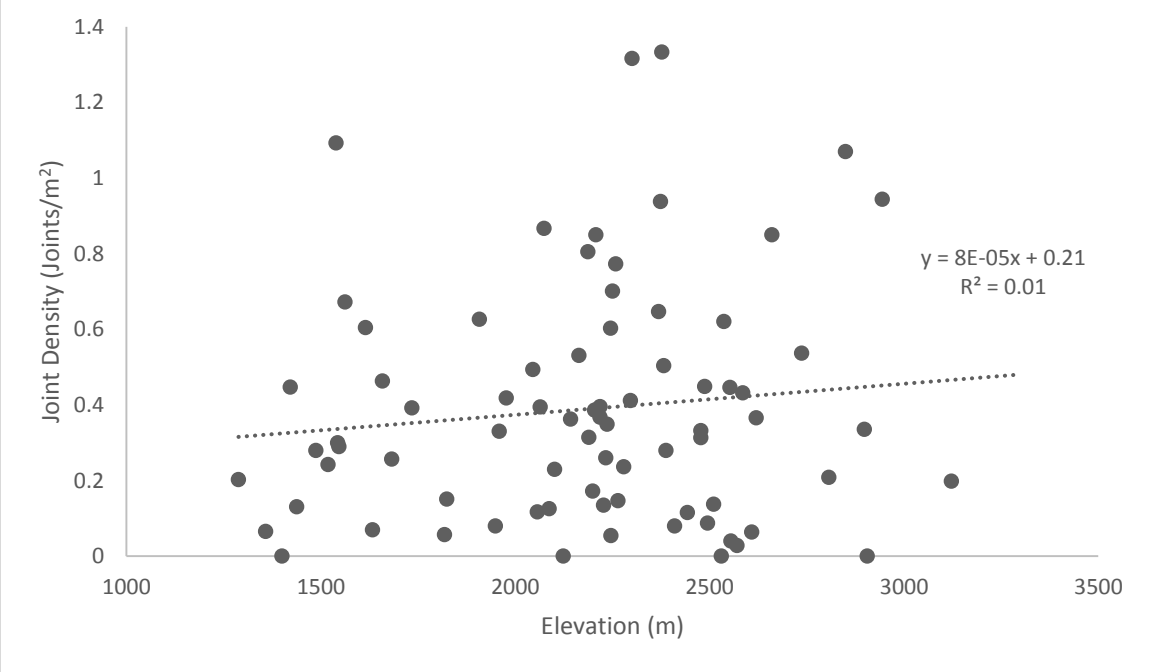

Figure 14. Plot of joint density versus elevation.

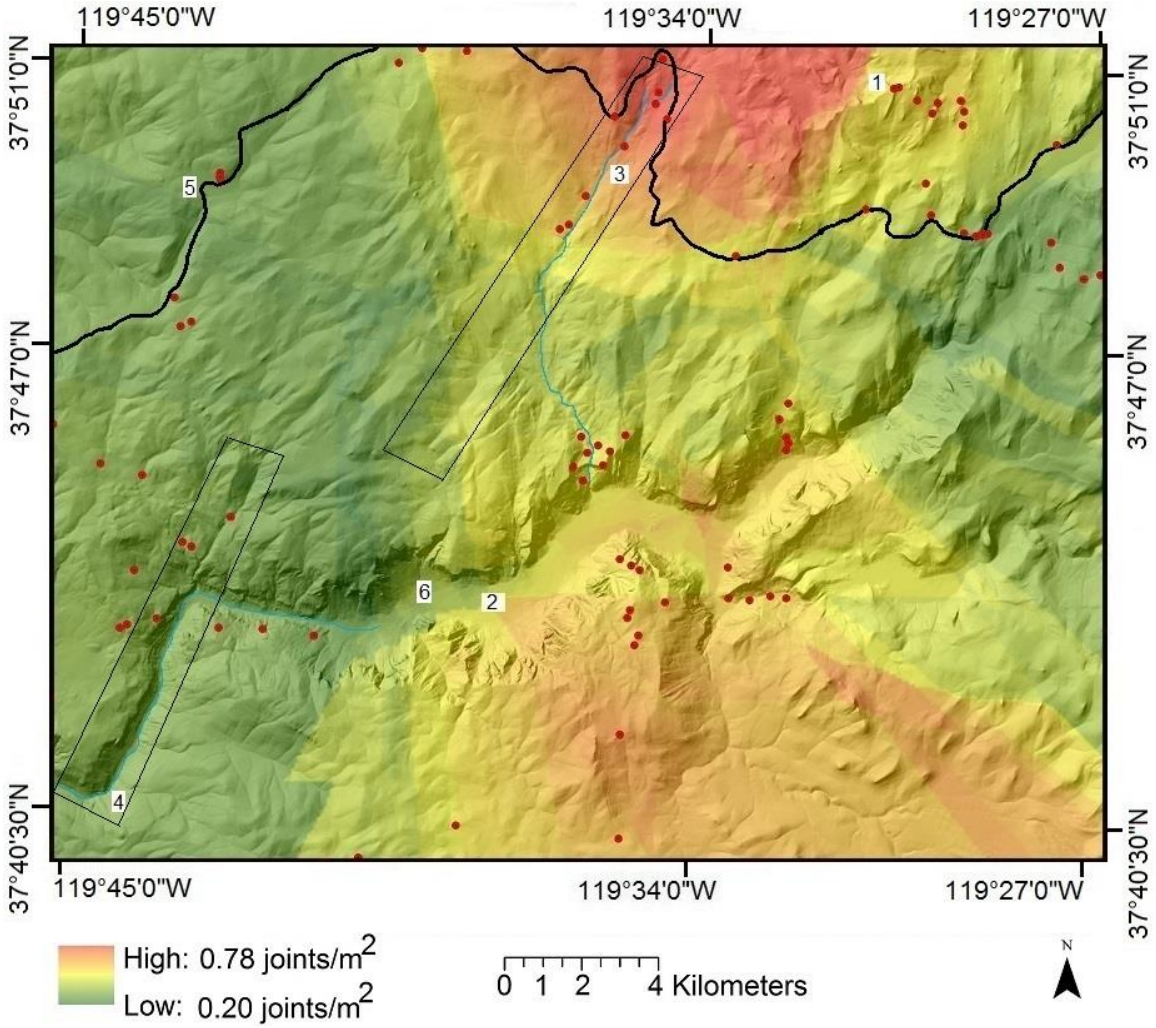

Figure 15. Interpolated map of joint density. "1" shows the location of Mount Hoffman, "2" Yosemite Valley, "3" Yosemite Creek, "4" the Merced River, "5" Highway 120, and "6" El Capitan/ The Rockslides. The rectangles surrounding "3" and "4" outline locations of master joints.

Foliation

Foliation varies by region (Figure 16), but no significant relationship exists between foliation and elevation (Figure 17). Some of the most highly-foliated rocks are observed in a metamorphic pendant at the base of Mount Hoffman (next to "1" in Figure 2), although data was only recorded at 1 site (site 53) in this location. Other highly foliated rocks are located in the Granodiorite of Kuna Crest and the region including Yosemite

Creek (“3,” Figure 16) and Mount Hoffman (“1,” Figure 16). However, as foliation was only visually analyzed using a simple ranking system, all foliation results should be interpreted with caution.

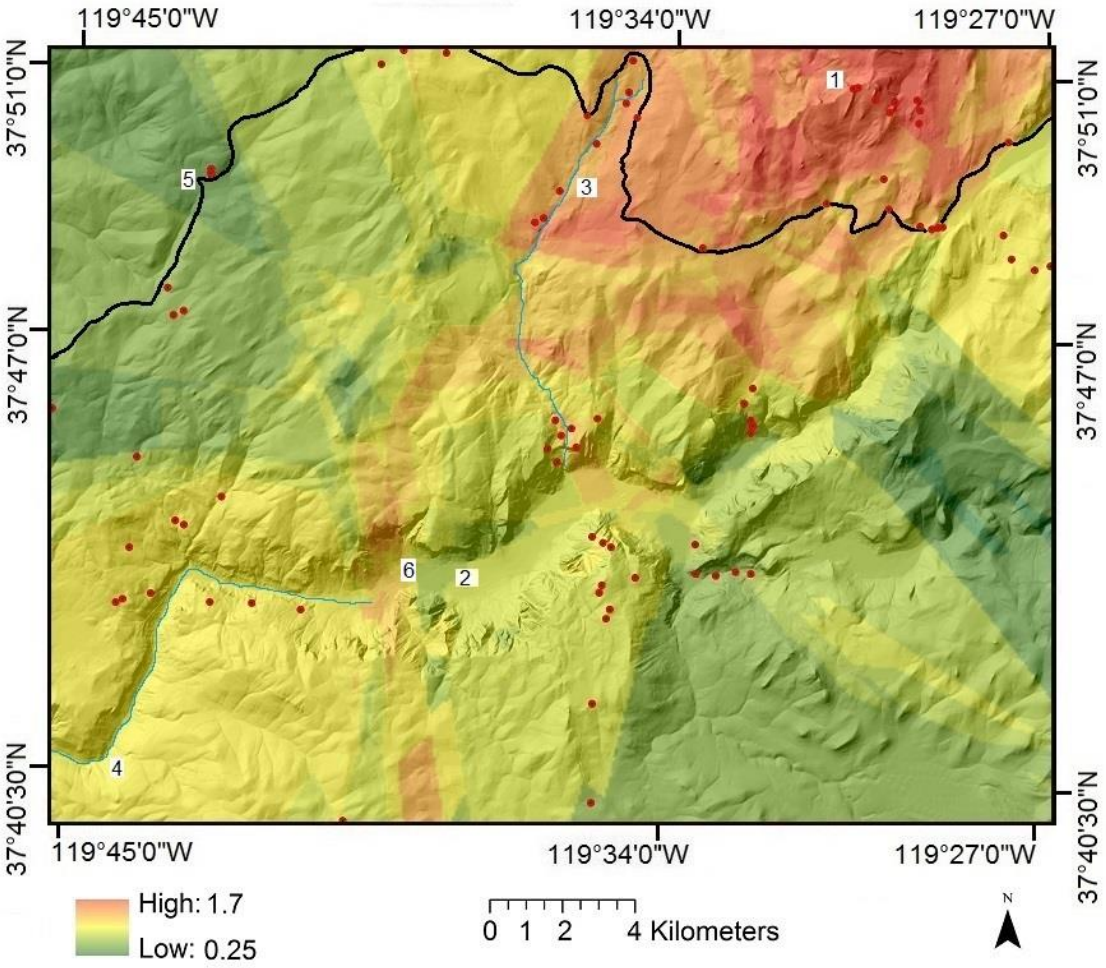

Figure 16. Interpolated map of foliation. A higher number means that rocks at the site are more foliated than those at sites with lower value. “1” shows the location of Mount Hoffman, “2” Yosemite Valley, “3” Yosemite Creek, “4” the Merced River, “5” Highway 120, and “6” El Capitan/ The Rockslides.

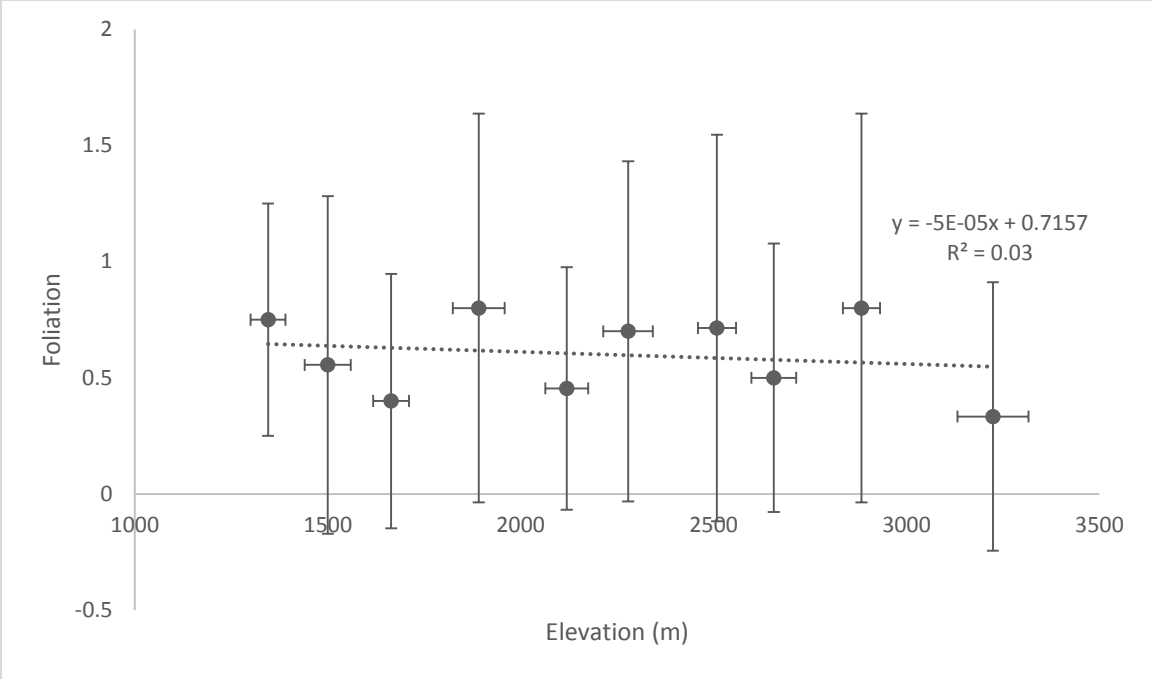

Figure 17. Plot of foliation versus elevation. Foliation data were binned into groups for every 200 meters of elevation, then the average of each group was plotted.

Schmidt Hammer Data

The highest elevations of the study area are found in the northeast and the majority of the sites with the highest 20 Schmidt rebound values are also mostly located in the northeast. Also, the areas of the lowest elevations on average are found in the southwest of the study area and the majority of the sites with the lowest 20 rebound values are located in the southwest half of the area (Figure 18). Plots and maps of all Schmidt hammer data display a poor correlation with elevation (Table 1; Figures 19-21), although binning Schmidt measurements into groups for every 200 m of elevation shows that rebounds increase with elevation (Figure 21). A single exception to the observations above occurred on Mount Hoffman, which featured some of the lowest 20 rebound values despite featuring the highest elevations in the study area, although the Granodiorite of

Mount Hoffman (Kh) has average rebound values (Table 1). Average rebound values for all units are similar, except for the El Capitan Granite (Kec), which features slightly lower rebound values than all other units (Table 1, Figures 18-21).

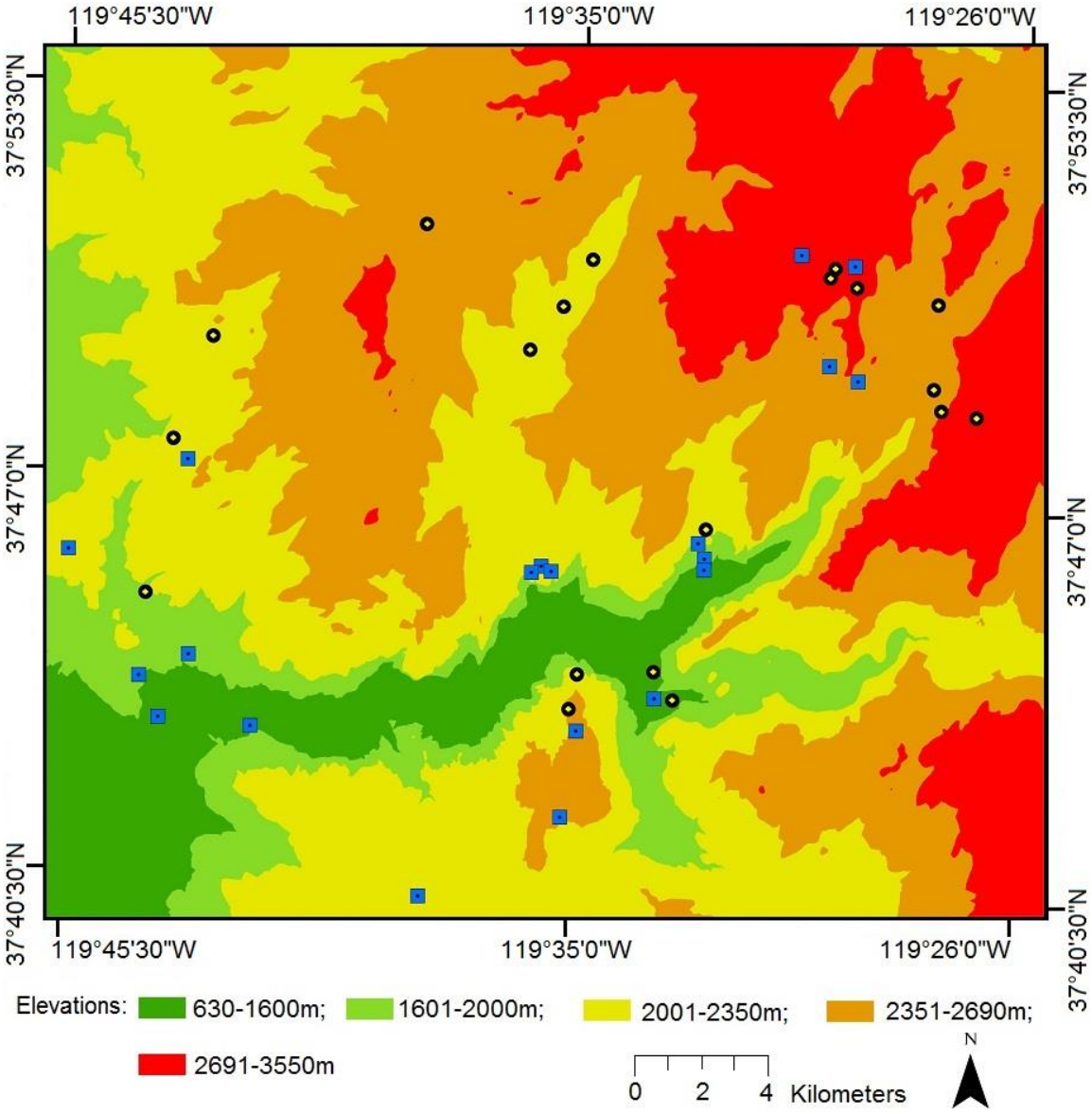

Figure 18. Plot of highest 20 Schmidt values (black and yellow circles) and lowest 20 Schmidt values (blue squares), demonstrating that the highest and lowest rebounds are typically found at the highest and lowest elevations, respectively.

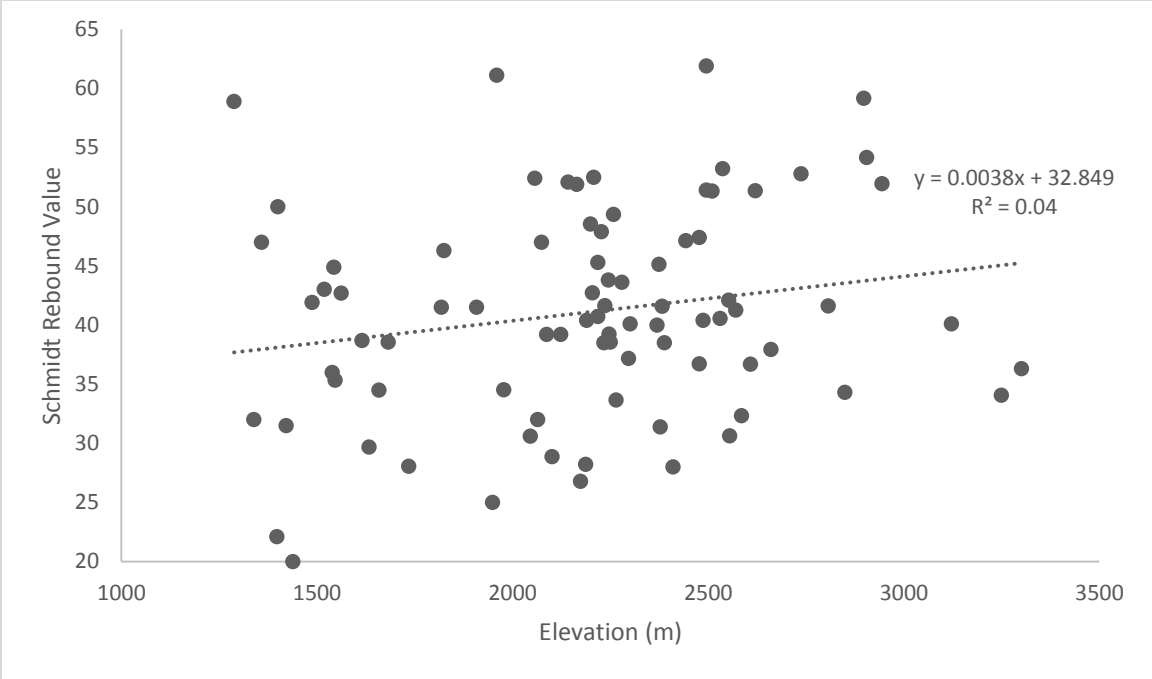

Figure 19. Plot of Schmidt rebound values versus elevation.

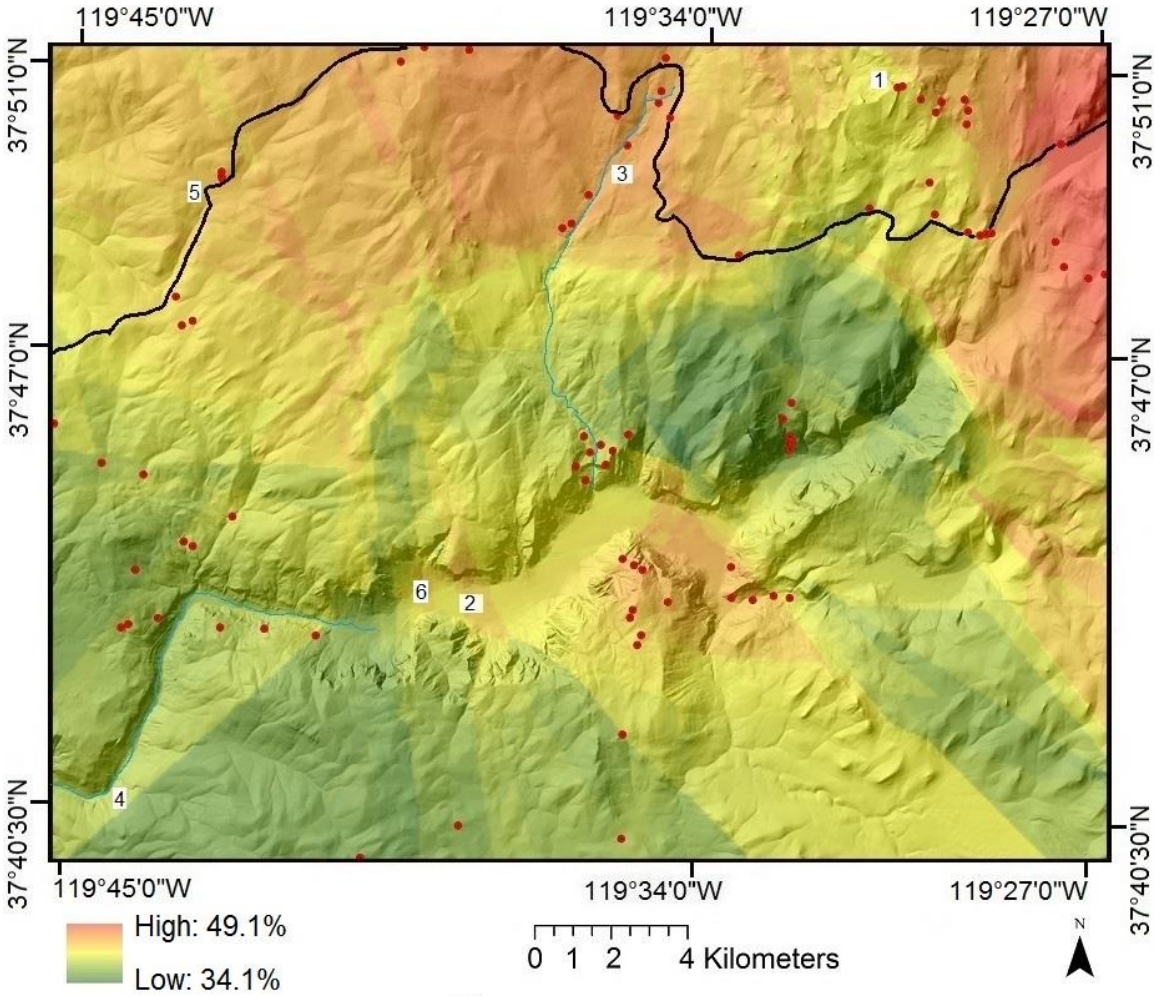

Figure 20. Interpolated map of Schmidt hammer rebound values. "1" shows the location of Mount Hoffman, "2" Yosemite Valley, "3" Yosemite Creek, "4" the Merced River, "5" Highway 120, and "6" El Capitan/ The Rockslides.

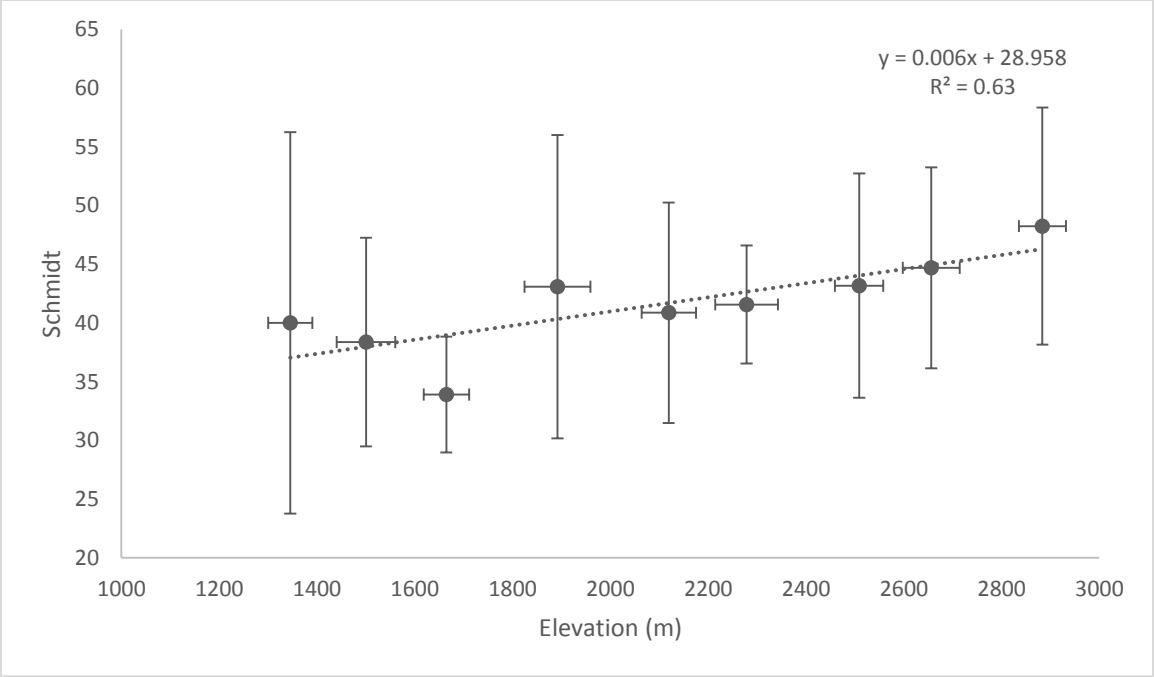

Figure 21. Plot of Schmidt rebound values versus elevation, where Schmidt data were binned into groups for every 200 m of elevation. Since only 3 measurements were taken above 3000 m, no binned group was included above that elevation.

McCarroll (1991) described that surface texture, which may correlate with the degree of weathering on a surface, influences rebound values. Although no correlation between grain size and rebound values was observed in Yosemite, the single highest Schmidt rebound value was recorded at the easternmost site of the study area on a large aplite dike (site 34), indicating that surface texture, also controlled by grain size, may lead to some variations in Schmidt rebound values. No correlation was observed between rebound values and mineral percentages and joint density (Figures 22-27). Schmidt rebound values typically increased with increasing foliation, however (Figure 28).

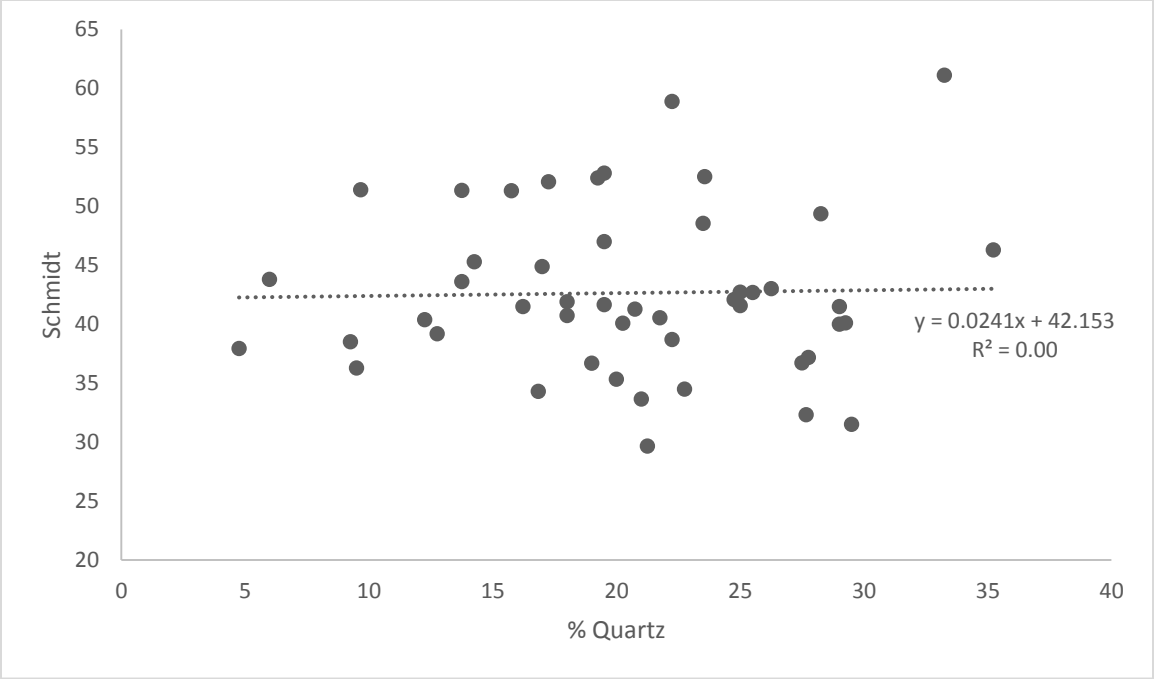

Figure 22. Plot of Schmidt rebound values versus quartz.

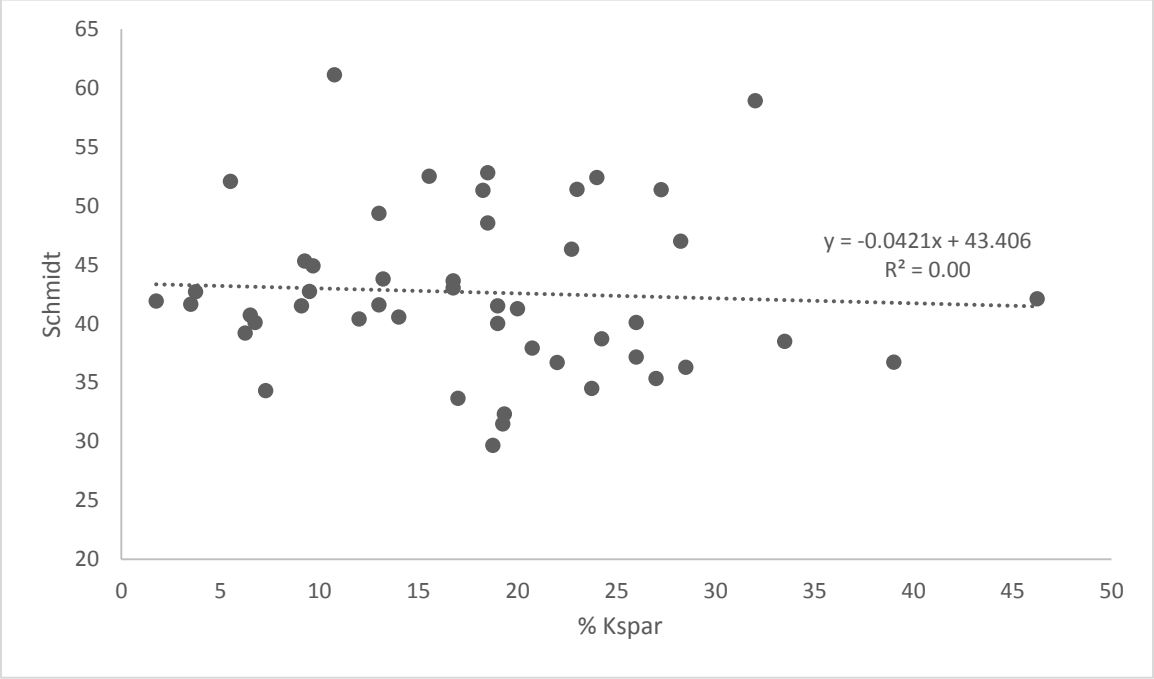

Figure 23. Plot of Schmidt rebound values versus potassium feldspar.

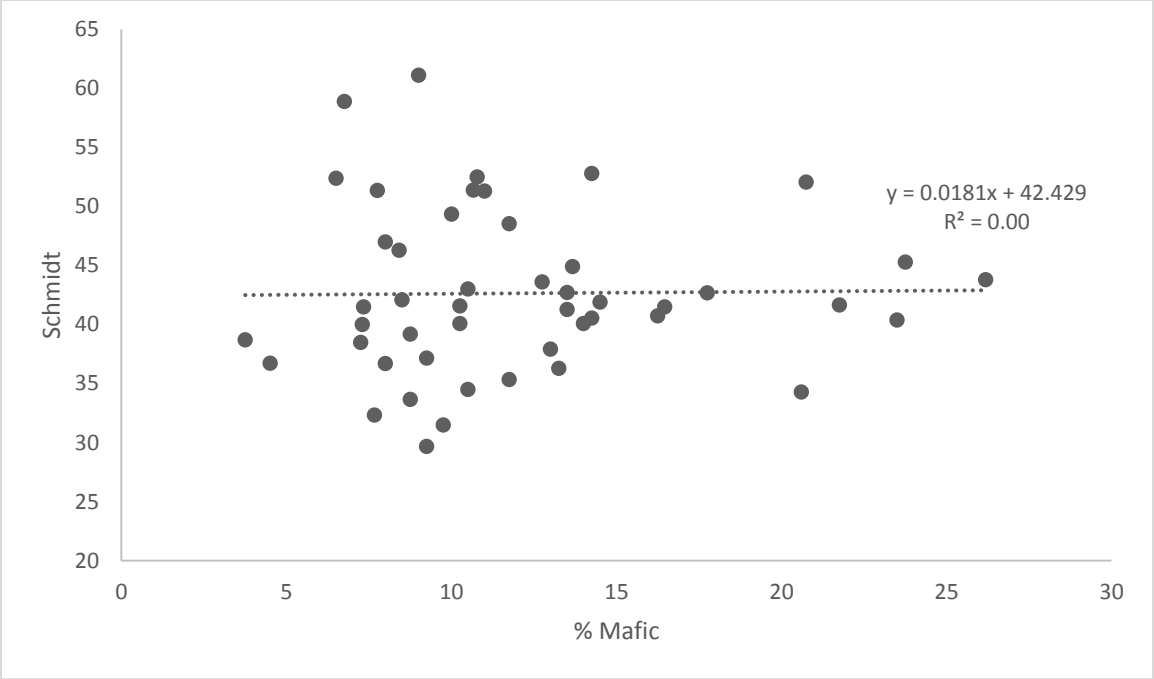

Figure 24. Plot of Schmidt rebound values versus mafic mineral content.

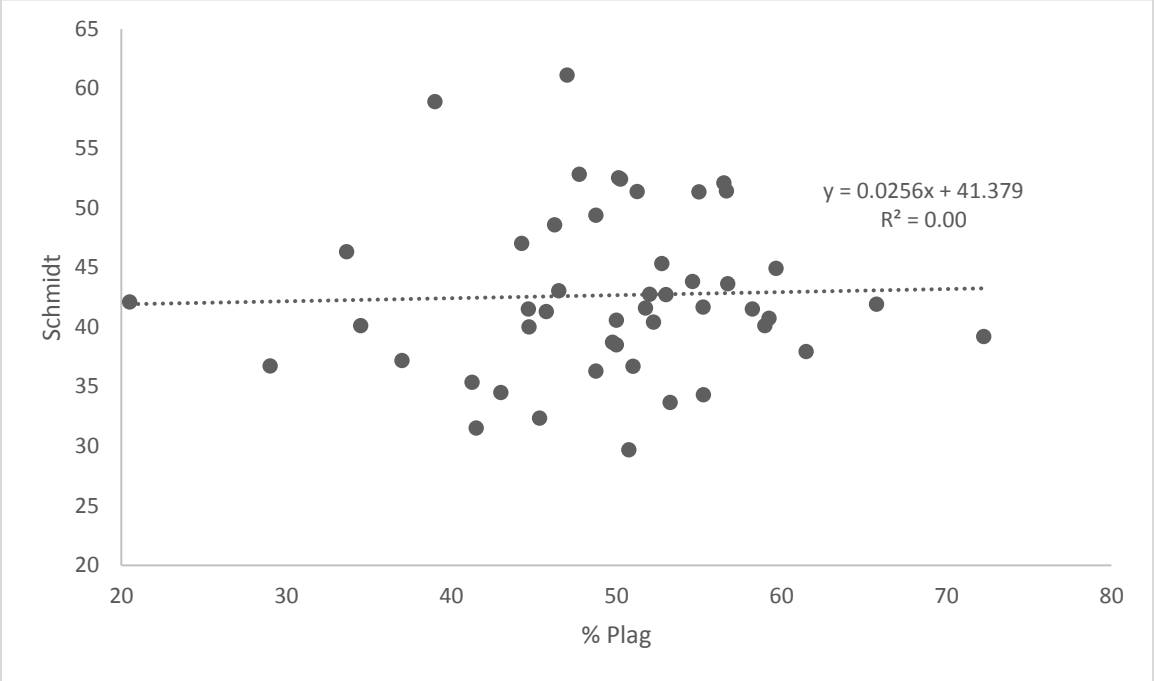

Figure 25. Plot of Schmidt rebound values versus plagioclase.

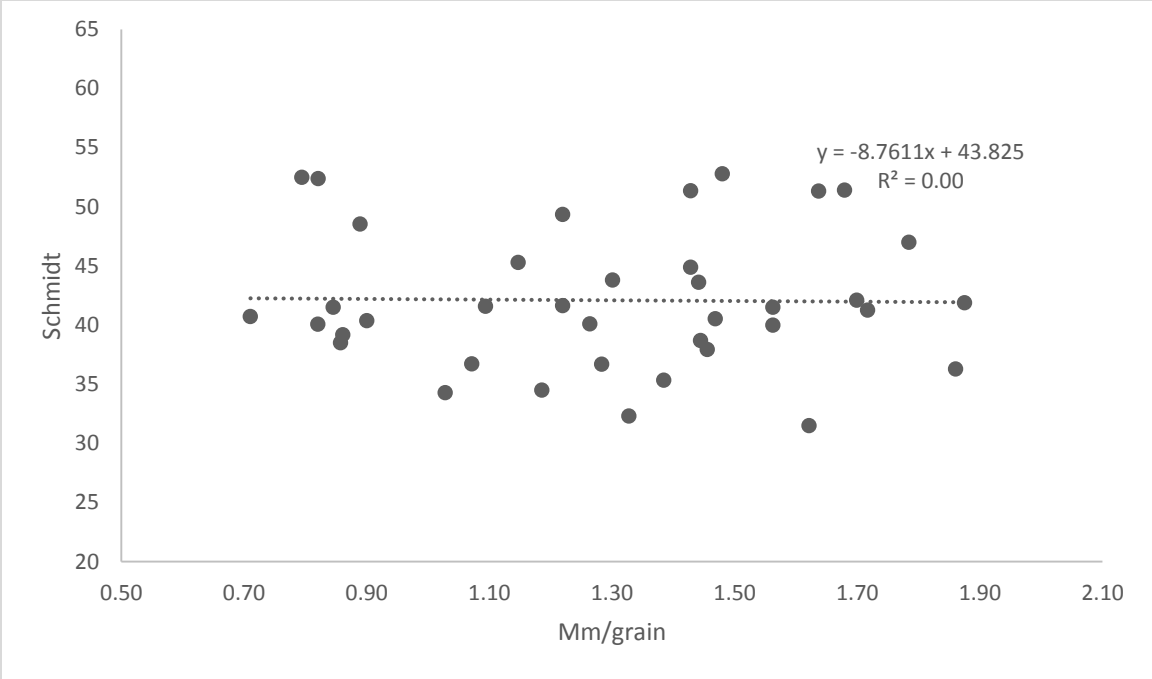

Figure 26. Plot of Schmidt hammer rebound values versus average grain size.

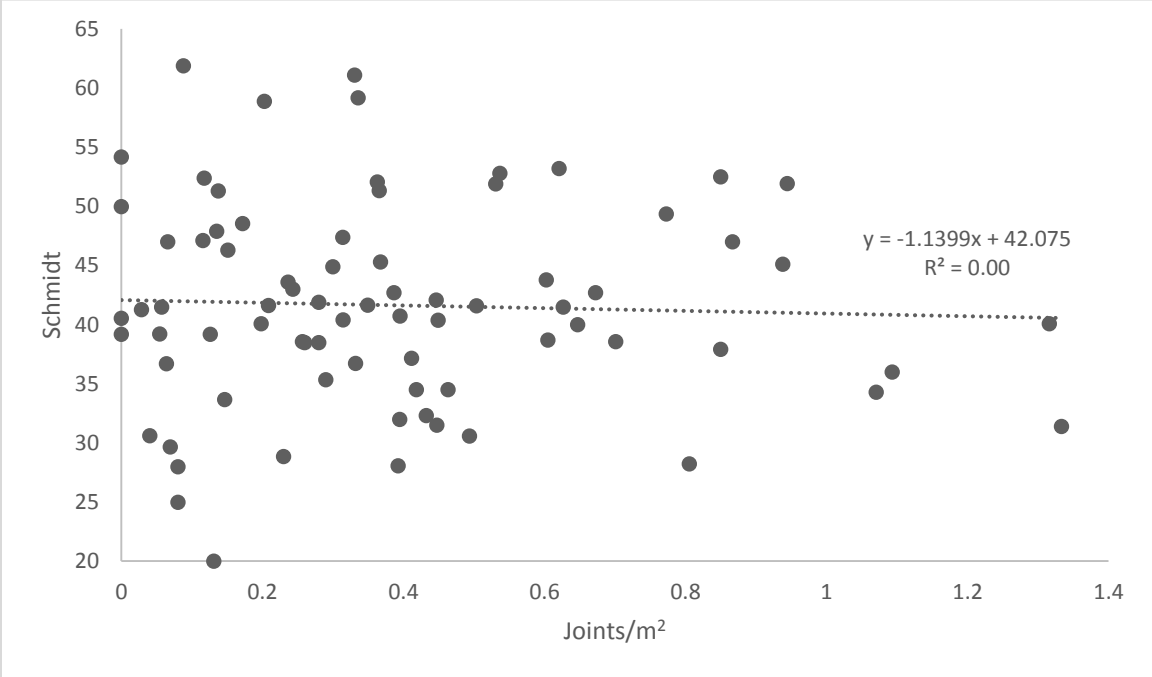

Figure 27. Plot of Schmidt hammer rebound values versus joint density.

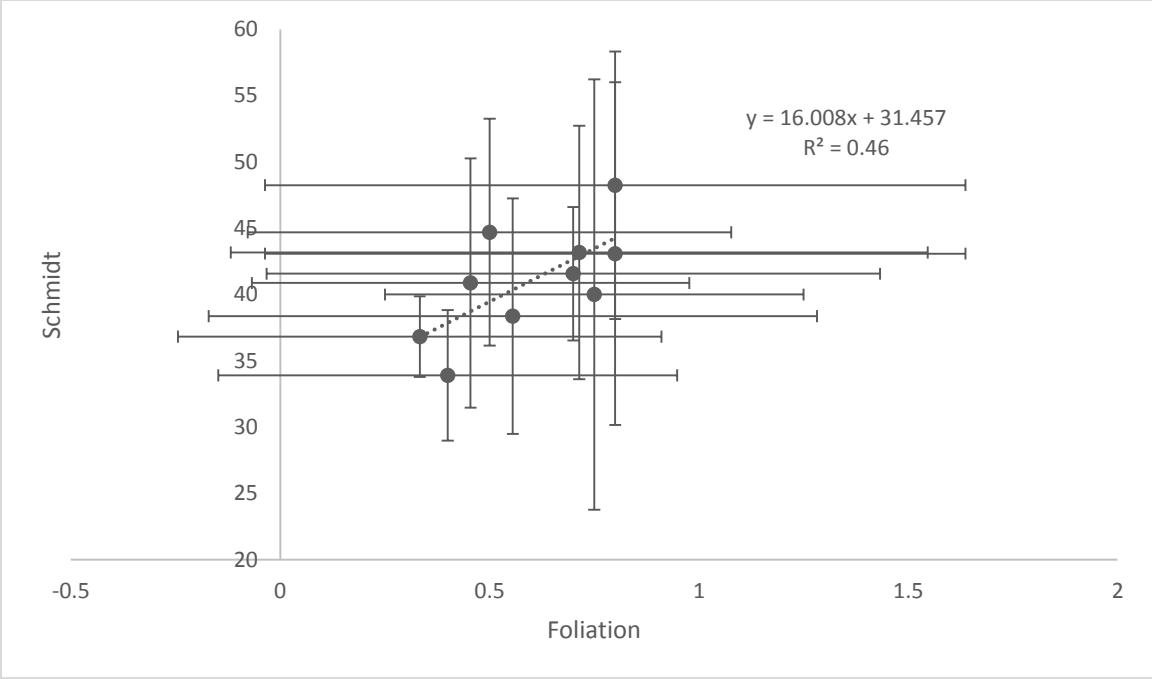

Figure 28. Plot of binned Schmidt hammer results versus foliation.

Topographic Profiles

Overall, no significant regional trend was observed for any data from all topographic profiles (Figures 29-32). Based on the hypothesis presented in this study's introduction, mineral composition, Schmidt rebound values, and other factors would be expected to consistently increase or decrease with elevation, but the topographic profiles below indicate that this is typically not the case. Two exceptions occur that indicate a possible local-scale correlation between variations in lithology and topography. In Profile 1 (Figure 29B), Schmidt rebounds mostly increase with elevation, and in Profile 2 (Figure 30I), grain size typically decreases with elevation. Therefore, although no relationships exist across the entire study area or between profiles, rock strength may play a role in shaping topography at local scales.

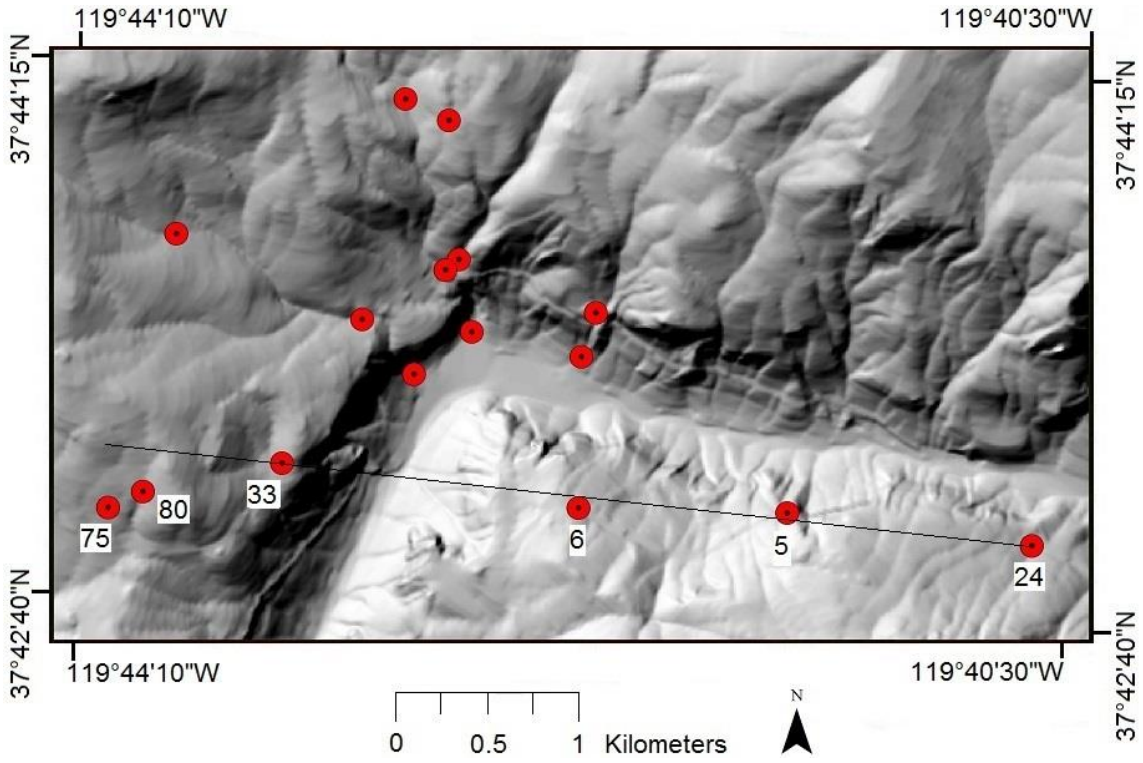
119°44'10"W
119°40'30"W
37°44'15"N
37°42'40"N
75
80
33
6
5
24
0
0.5
1 Kilometers
N

(A)

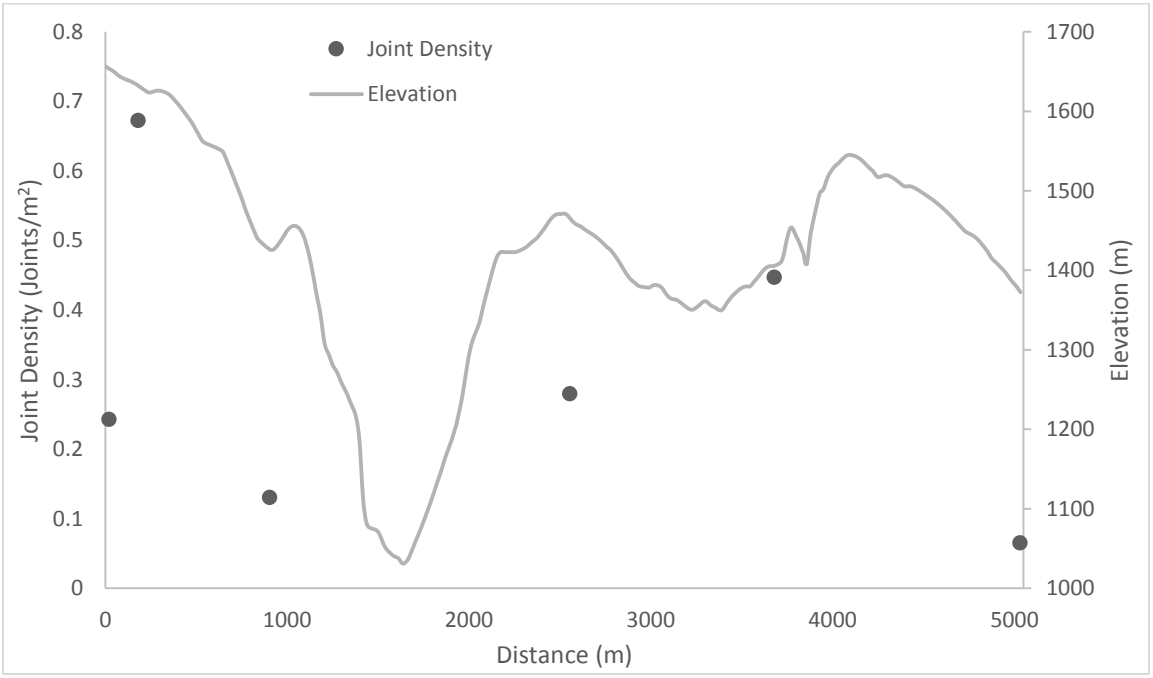
Joint Density
Elevation
Joint Density (Joints/m²)
Elevation (m)
Distance (m)
0
0.1
0.2
0.3
0.4
0.5
0.6
0.7
0.8
1000
1100
1200
1300
1400
1500
1600
1700
0
1000
2000
3000
4000
5000

(B)

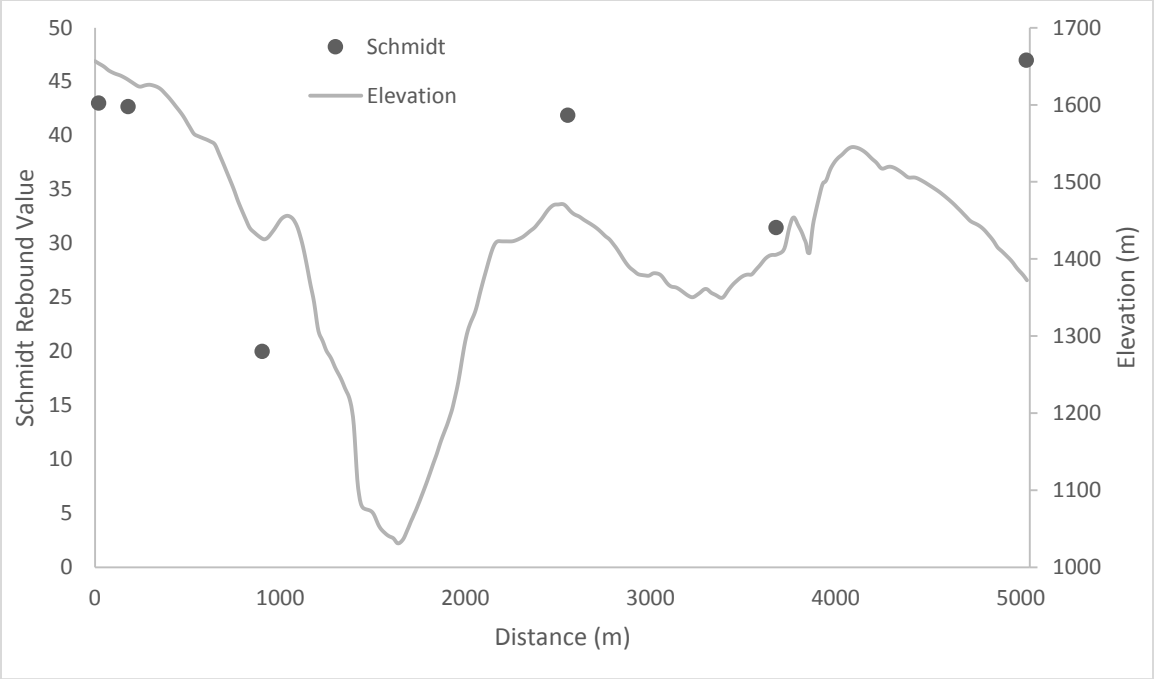
Schmidt
Elevation
Schmidt Rebound Value
Elevation (m)
Distance (m)
0
5
10
15
20
25
30
35
40
45
50
1000
1100
1200
1300
1400
1500
1600
1700
0
1000
2000
3000
4000
5000

(C)

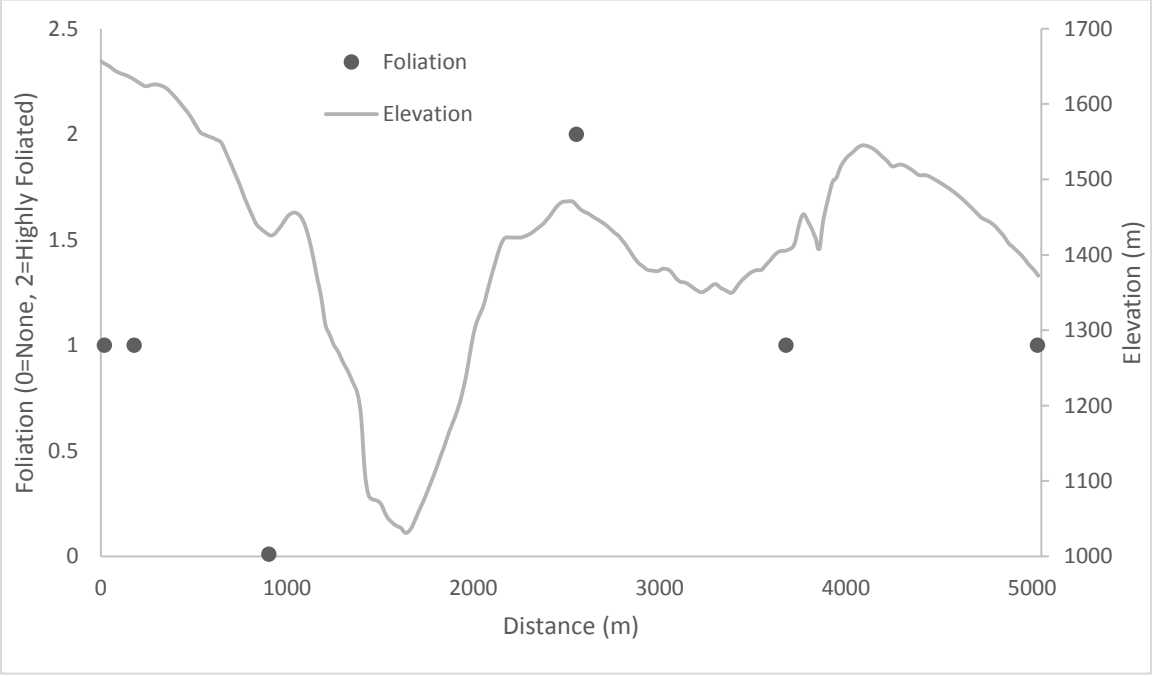
Foliation
Elevation
Foliation (0=None, 2=Highly Foliated)
Elevation (m)
Distance (m)
0
0.5
1
1.5
2
2.5
1000
1100
1200
1300
1400
1500
1600
1700
0
1000
2000
3000
4000
5000

(D)

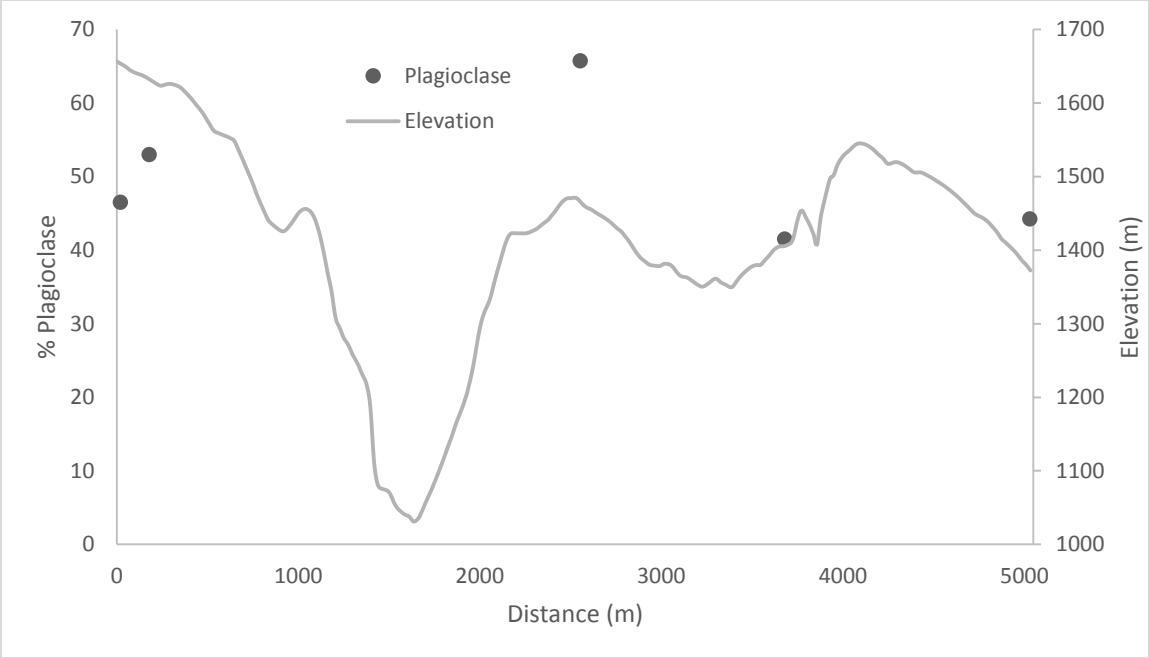
Plagioclase
Elevation
% Plagioclase
Elevation (m)
Distance (m)
0
10
20
30
40
50
60
70
1000
1100
1200
1300
1400
1500
1600
1700
0
1000
2000
3000
4000
5000

(E)

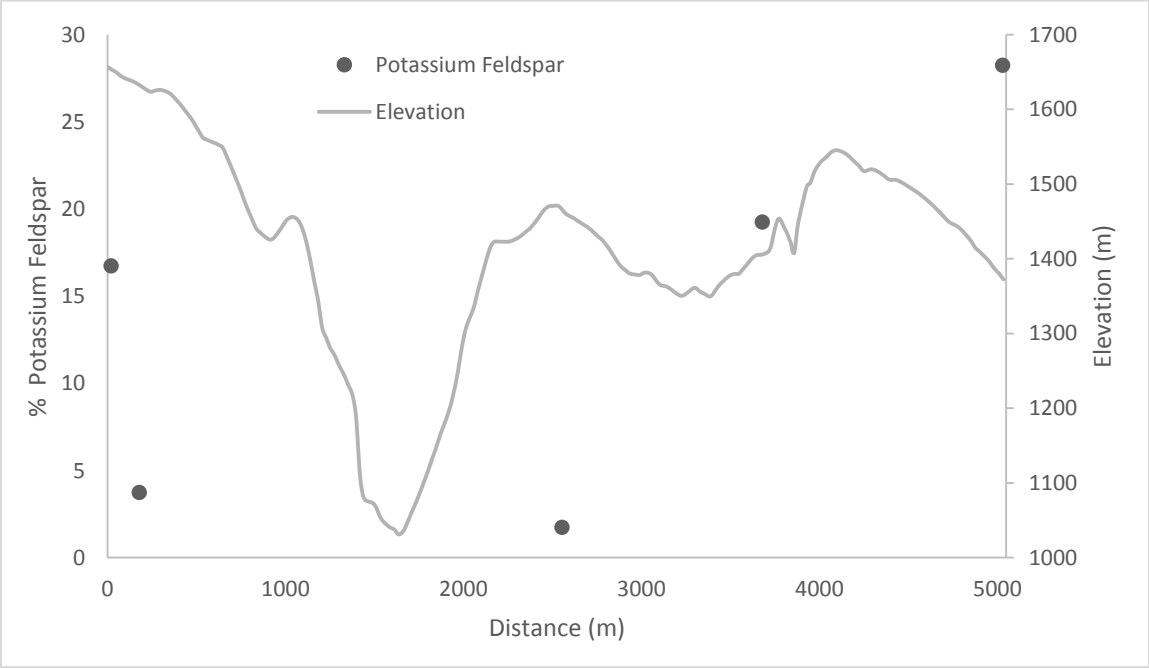
Potassium Feldspar
Elevation
% Potassium Feldspar
Elevation (m)
Distance (m)
0
5
10
15
20
25
30
1000
1100
1200
1300
1400
1500
1600
1700
0
1000
2000
3000
4000
5000

(F)

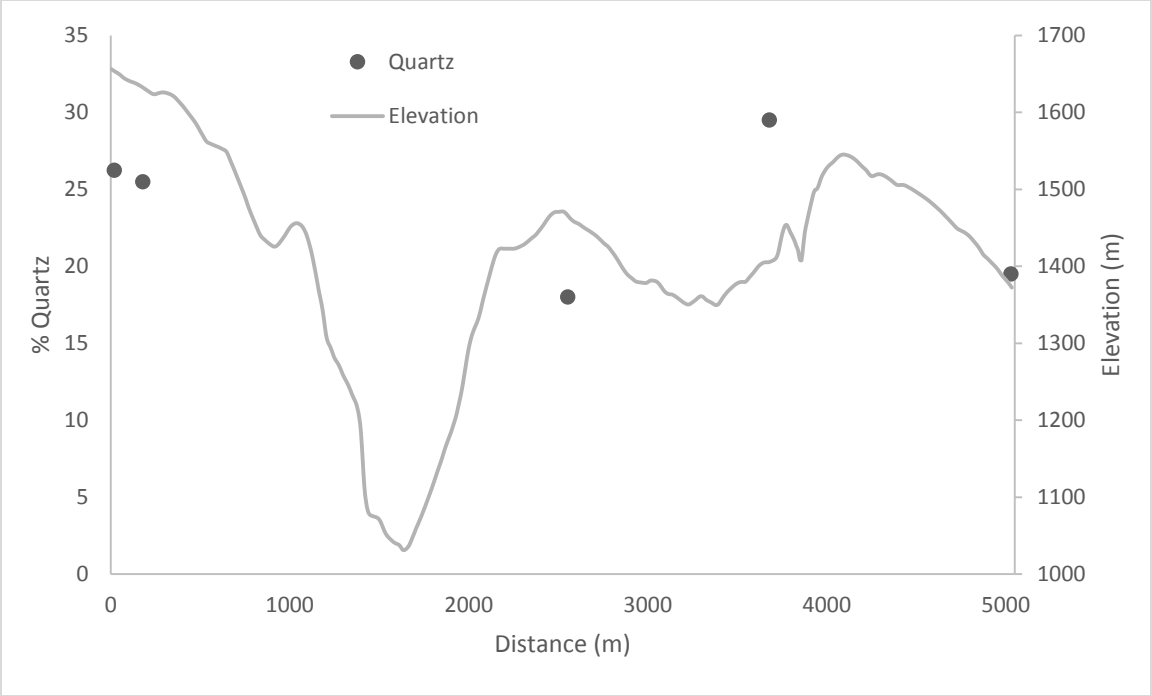

(G)

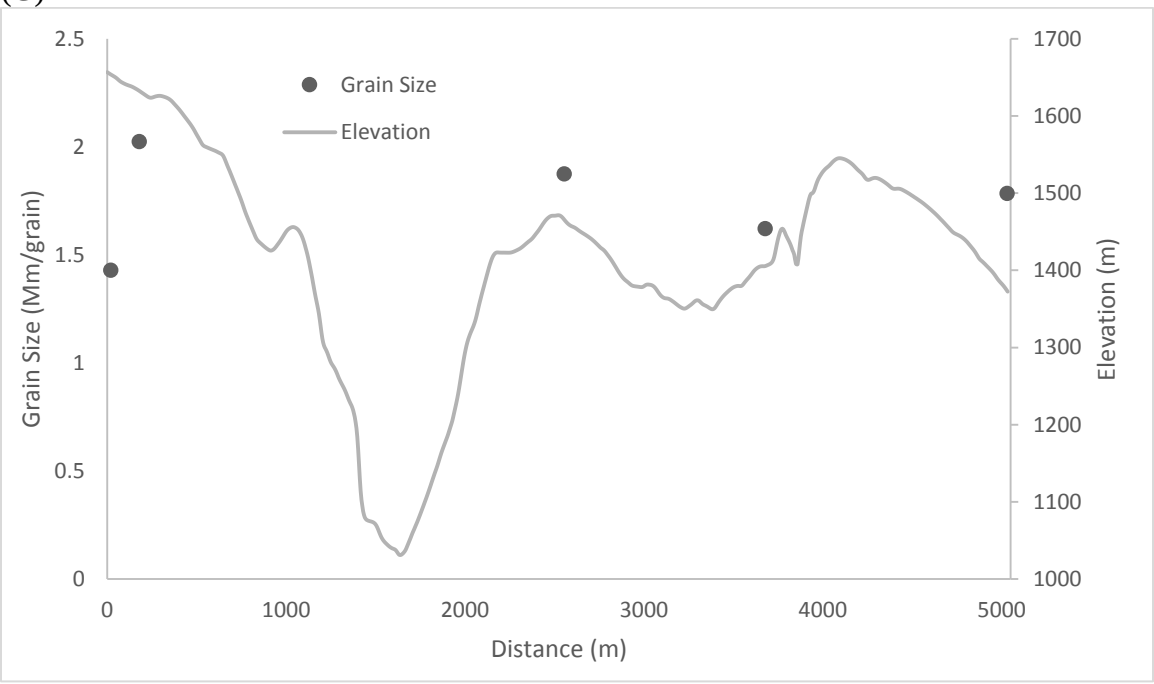

(H)

Figure 29. Profile 1. The area in the figure is outlined by box "A" in Figure 1. Part (A) shows the location of profile 1, while (B) through (C) document how different factors change between site 75 in the west and site 24 at the eastern end of the profile. (D) through (H) only involves sites where no rock samples were taken. The profile goes through the Granodiorite of Arch Rock, diorite and gabbro, and El Capitan Granite units.

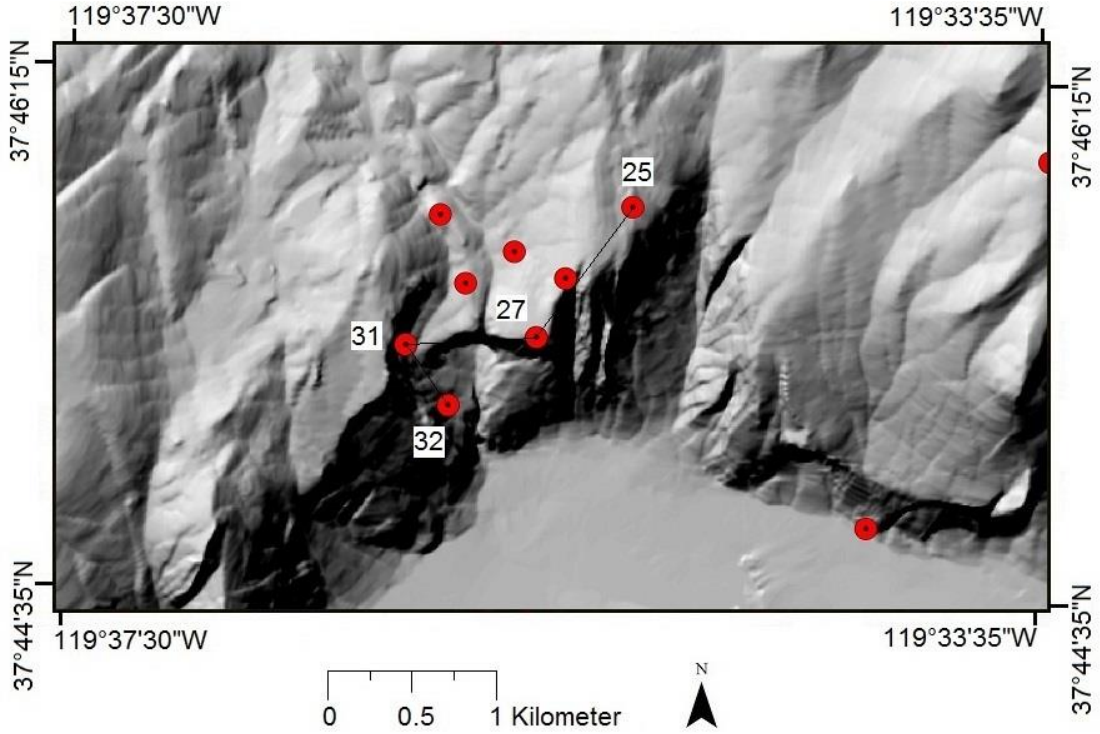
119°37'30"W
119°33'35"W
37°46'15"N
37°44'35"N
25
27
31
32
0
0.5
1 Kilometer
N

(A)

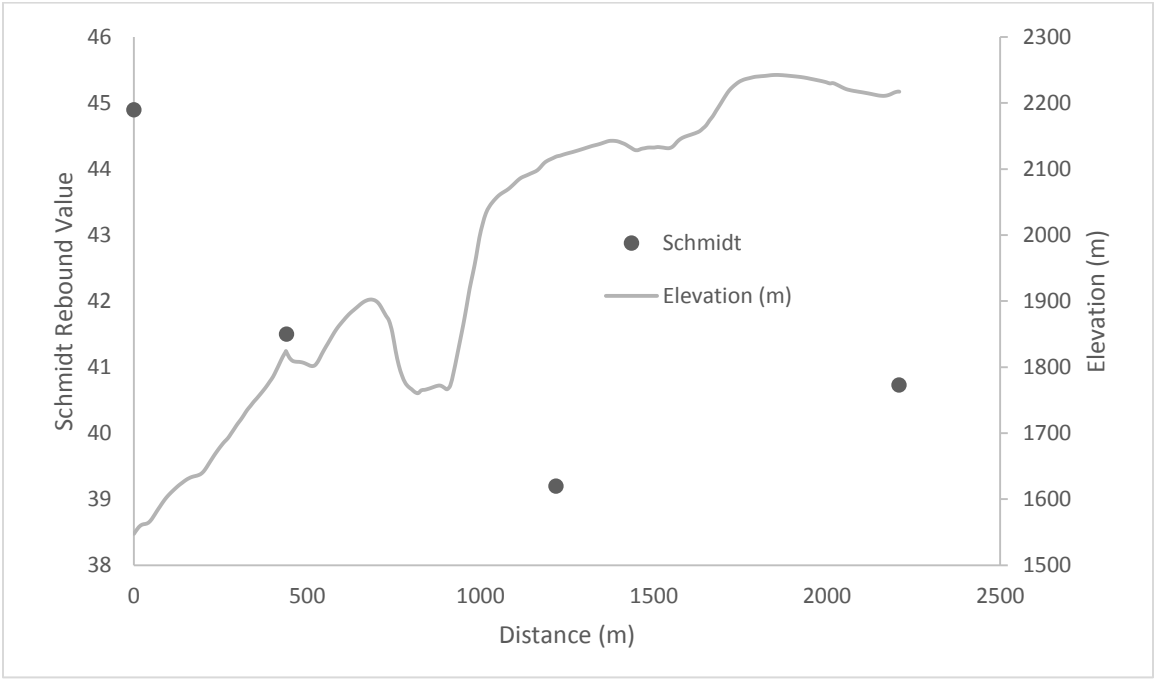
Schmidt Rebound Value
Elevation (m)
Distance (m)
Schmidt
Elevation (m)
46
45
44
43
42
41
40
39
38
2300
2200
2100
2000
1900
1800
1700
1600
1500
0
500
1000
1500
2000
2500

(B)

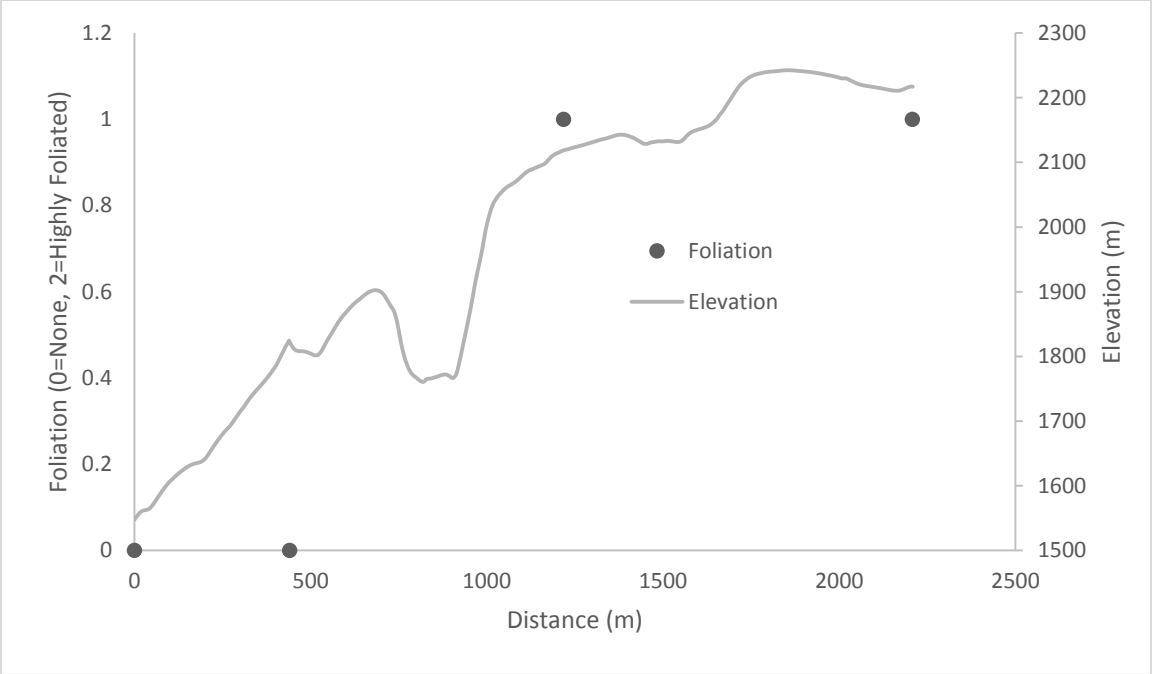
Foliation (0=None, 2=Highly Foliated)
1.2
1
0.8
0.6
0.4
0.2
0
0
500
1000
1500
2000
2500
Distance (m)
Foliation
Elevation
Elevation (m)
2300
2200
2100
2000
1900
1800
1700
1600
1500

(C)

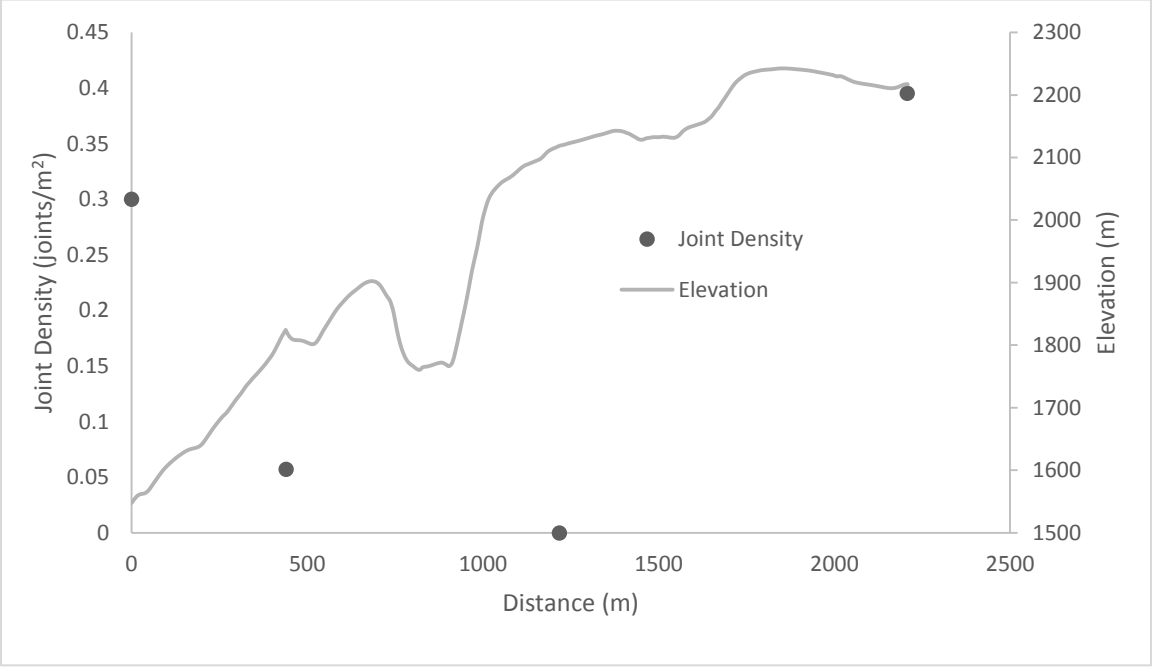
Joint Density (joints/m²)
0.45
0.4
0.35
0.3
0.25
0.2
0.15
0.1
0.05
0
0
500
1000
1500
2000
2500
Distance (m)
Joint Density
Elevation
Elevation (m)
2300
2200
2100
2000
1900
1800
1700
1600
1500

(D)

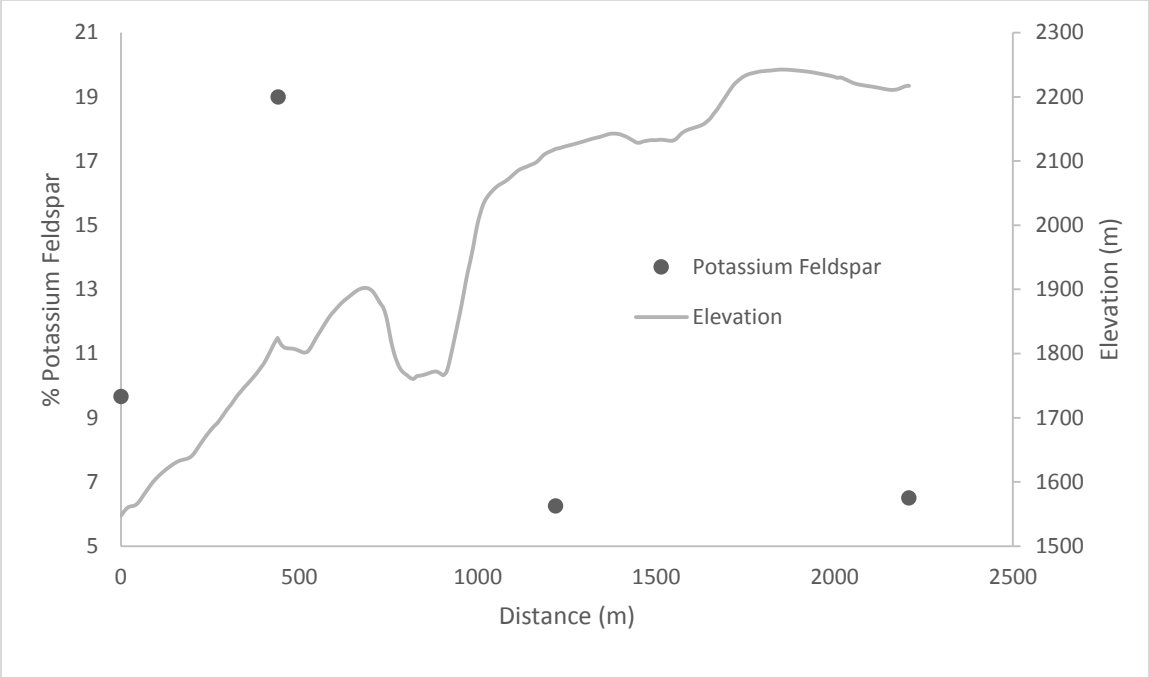
% Potassium Feldspar
Elevation (m)
Distance (m)
Potassium Feldspar
Elevation
21
19
17
15
13
11
9
7
5
2300
2200
2100
2000
1900
1800
1700
1600
1500
0
500
1000
1500
2000
2500

(E)

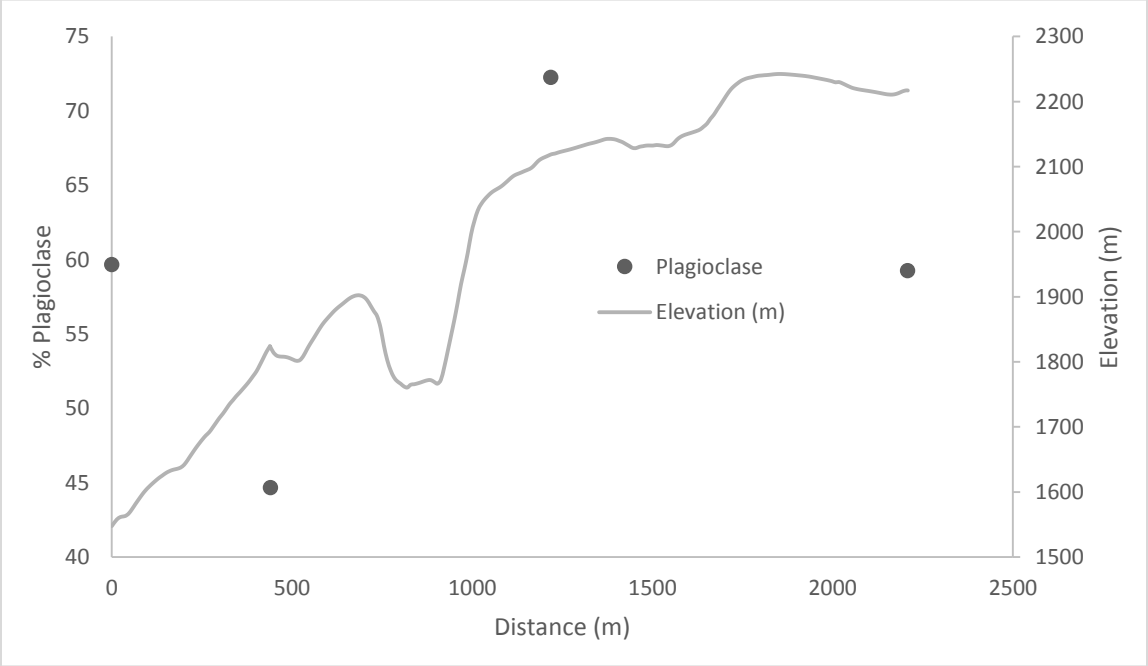
% Plagioclase
Elevation (m)
Distance (m)
Plagioclase
Elevation (m)
75
70
65
60
55
50
45
40
2300
2200
2100
2000
1900
1800
1700
1600
1500
0
500
1000
1500
2000
2500

(F)

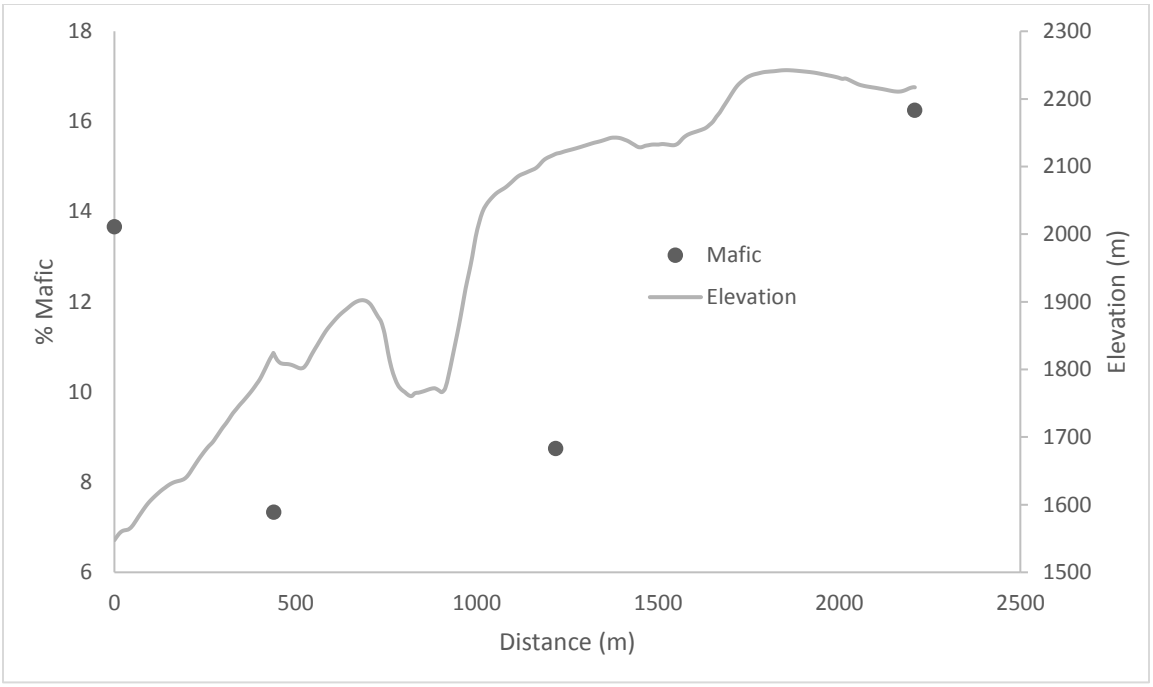
% Mafic
Elevation (m)
Distance (m)
Mafic
Elevation
18
16
14
12
10
8
6
2300
2200
2100
2000
1900
1800
1700
1600
1500
0
500
1000
1500
2000
2500

(G)

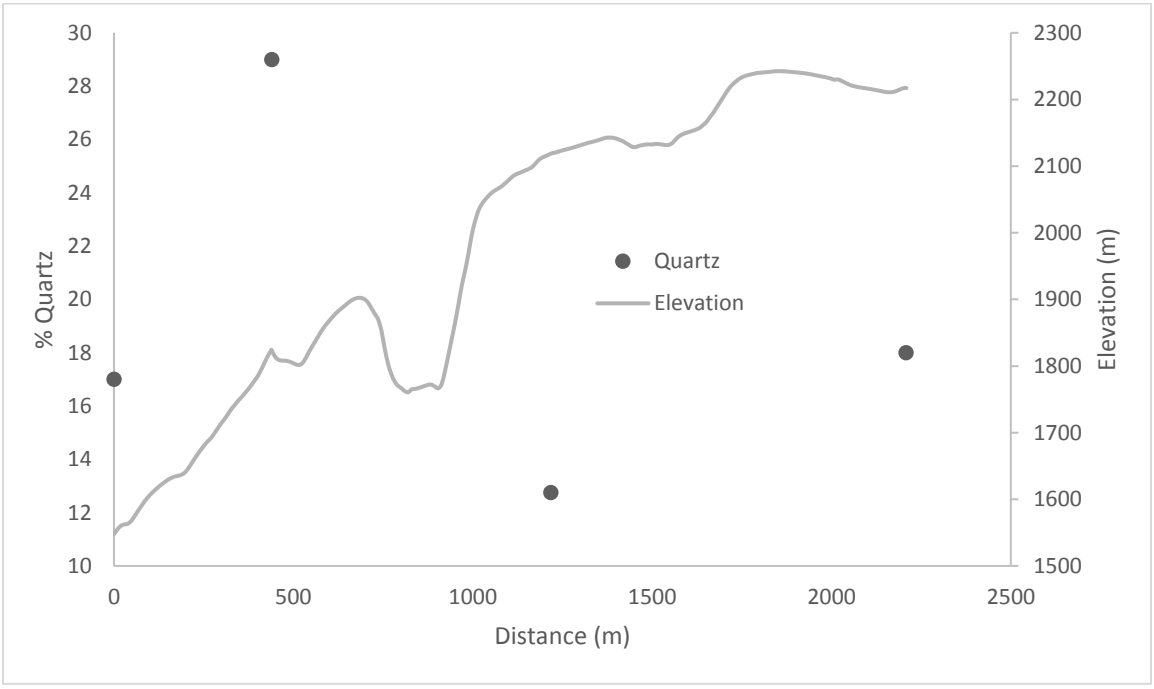
% Quartz
Elevation (m)
Distance (m)
Quartz
Elevation
30
28
26
24
22
20
18
16
14
12
10
2300
2200
2100
2000
1900
1800
1700
1600
1500
0
500
1000
1500
2000
2500

(H)

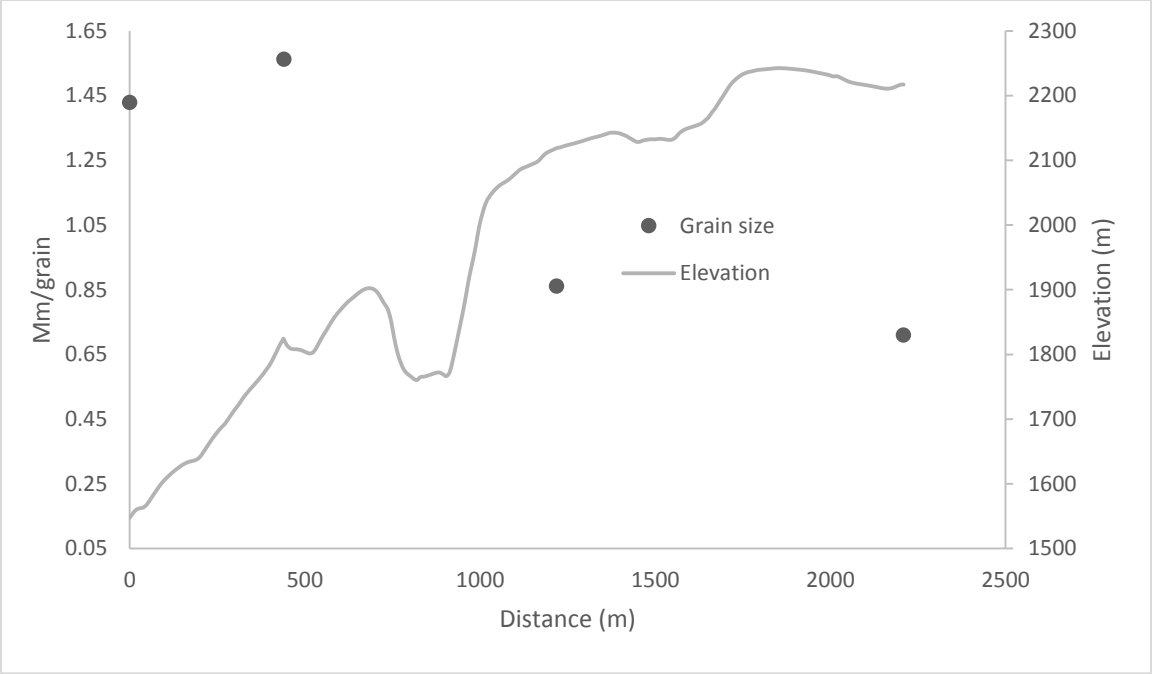

(I)

Figure 30. Profile 2. The area in (A) is outlined by box "B" in Figure 1. Sites 32, 31, 27, 25 were used for the topographic profile. The profile starts at site 32 at the middle of the cliff face and ends at site 25. The profile goes through the El Capitan Granite and Sentinel Granodiorite.

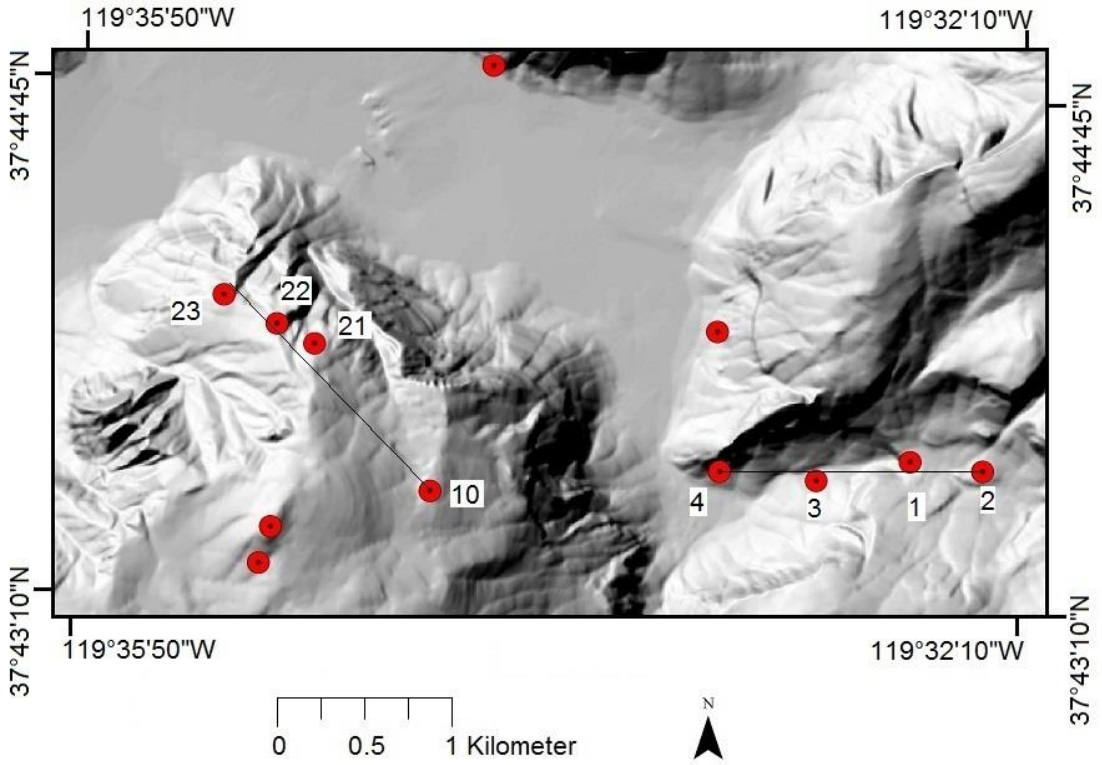
119°35'50"W
119°32'10"W
37°44'45"N
37°43'10"N
23
22
21
10
4
3
1
2
0
0.5
1 Kilometer
N

(A)

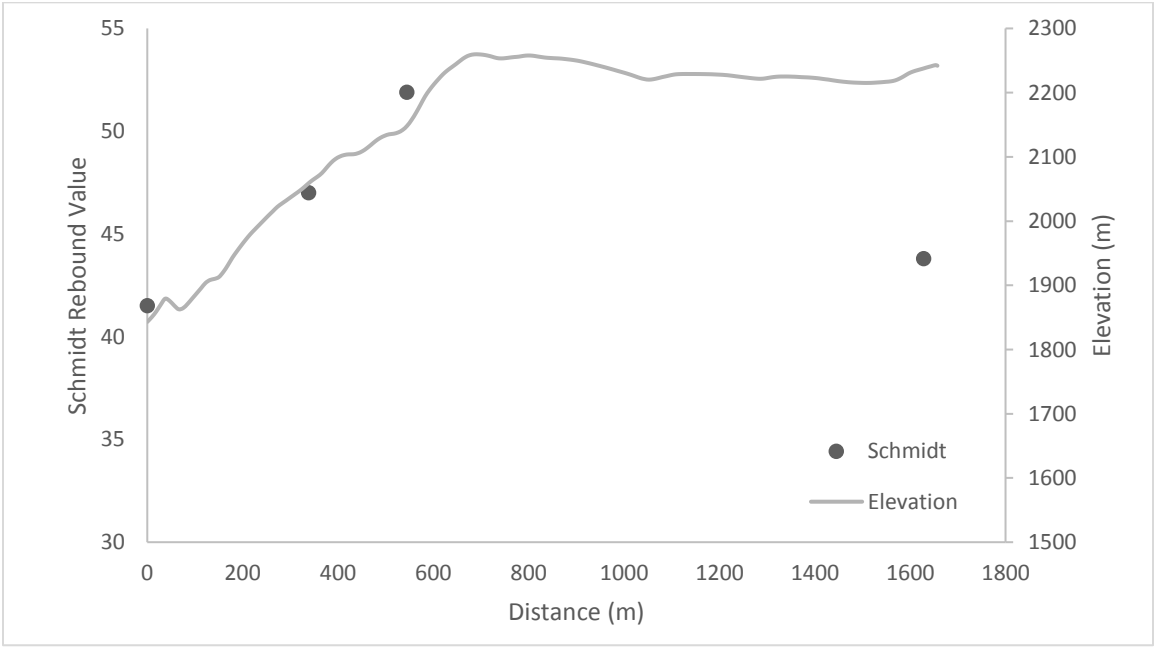
Schmidt Rebound Value
Elevation (m)
Distance (m)
Schmidt
Elevation
55
50
45
40
35
30
2300
2200
2100
2000
1900
1800
1700
1600
1500
0
200
400
600
800
1000
1200
1400
1600
1800

(B)

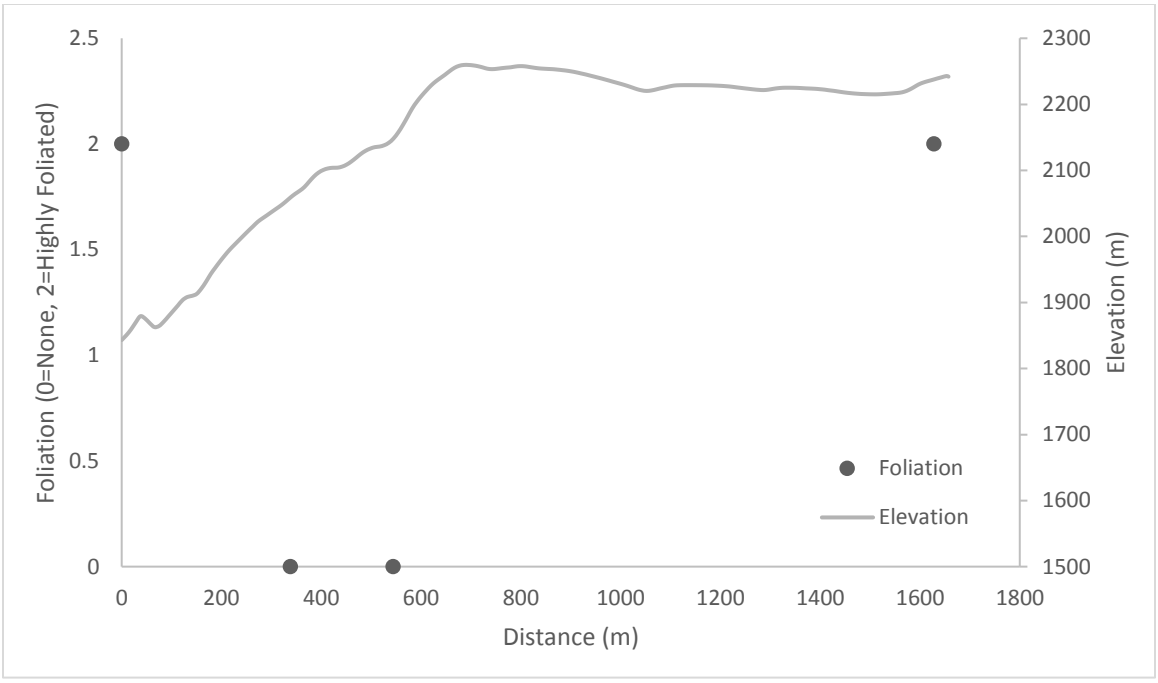
Foliation (0=None, 2=Highly Foliated)
Elevation (m)
Distance (m)
Foliation
Elevation
0
0.5
1
1.5
2
2.5
1500
1600
1700
1800
1900
2000
2100
2200
2300
0
200
400
600
800
1000
1200
1400
1600
1800

(C)

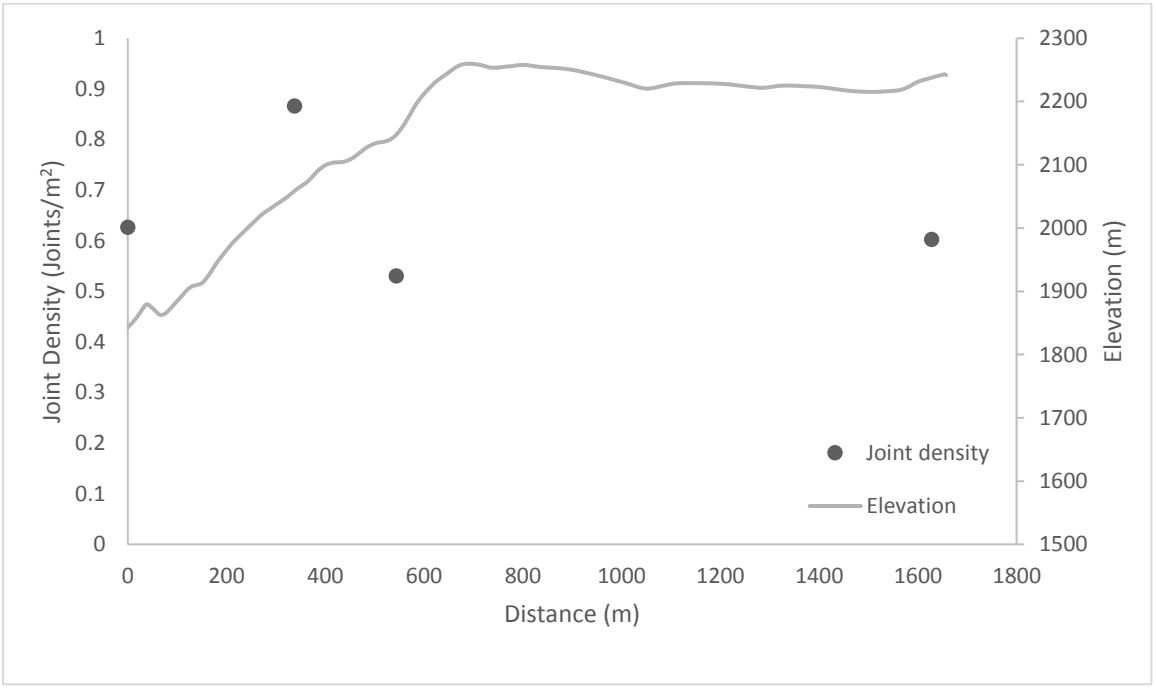
Joint Density (Joints/m²)
Elevation (m)
Distance (m)
Joint density
Elevation
0
0.1
0.2
0.3
0.4
0.5
0.6
0.7
0.8
0.9
1
1500
1600
1700
1800
1900
2000
2100
2200
2300
0
200
400
600
800
1000
1200
1400
1600
1800

(D)

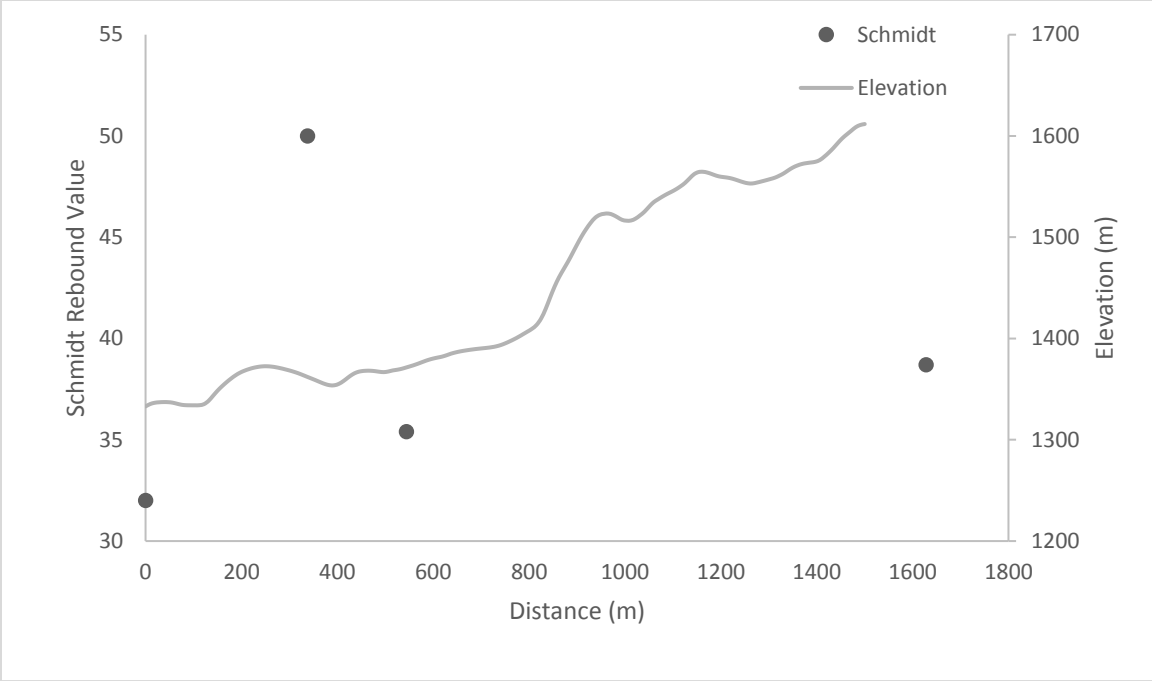
Schmidt
Elevation
Schmidt Rebound Value
Elevation (m)
Distance (m)
55
50
45
40
35
30
1700
1600
1500
1400
1300
1200
0
200
400
600
800
1000
1200
1400
1600
1800

(E)

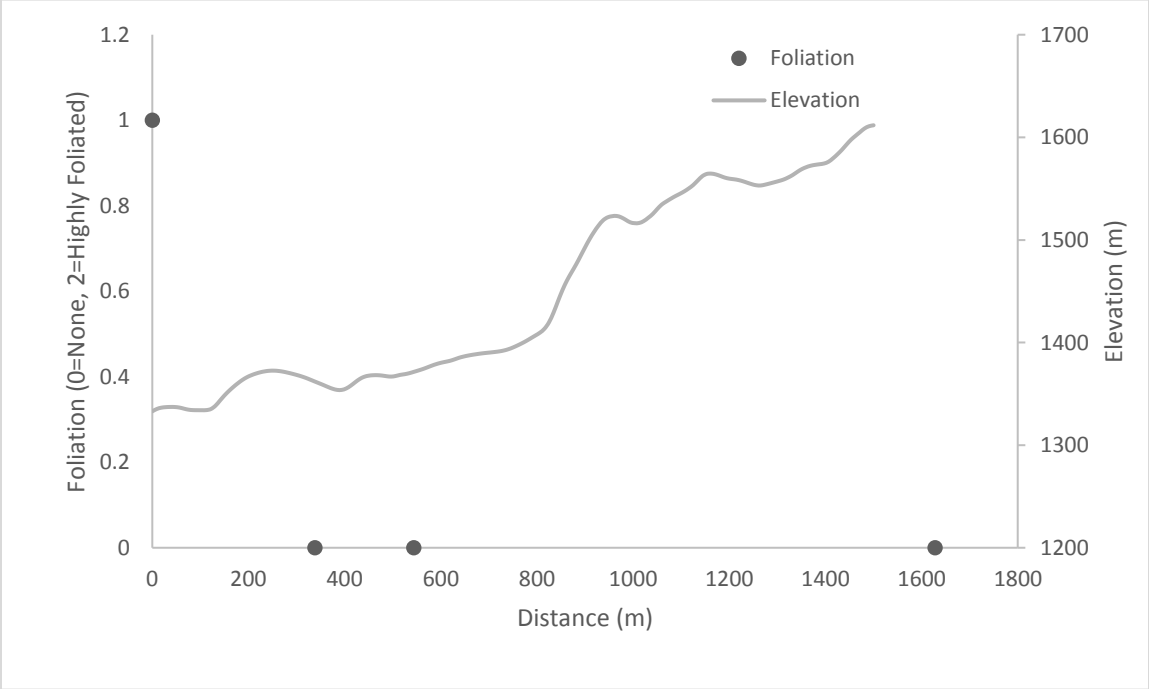
Foliation
Elevation
Foliation (0=None, 2=Highly Foliated)
Elevation (m)
Distance (m)
1.2
1
0.8
0.6
0.4
0.2
0
1700
1600
1500
1400
1300
1200
0
200
400
600
800
1000
1200
1400
1600
1800

(F)

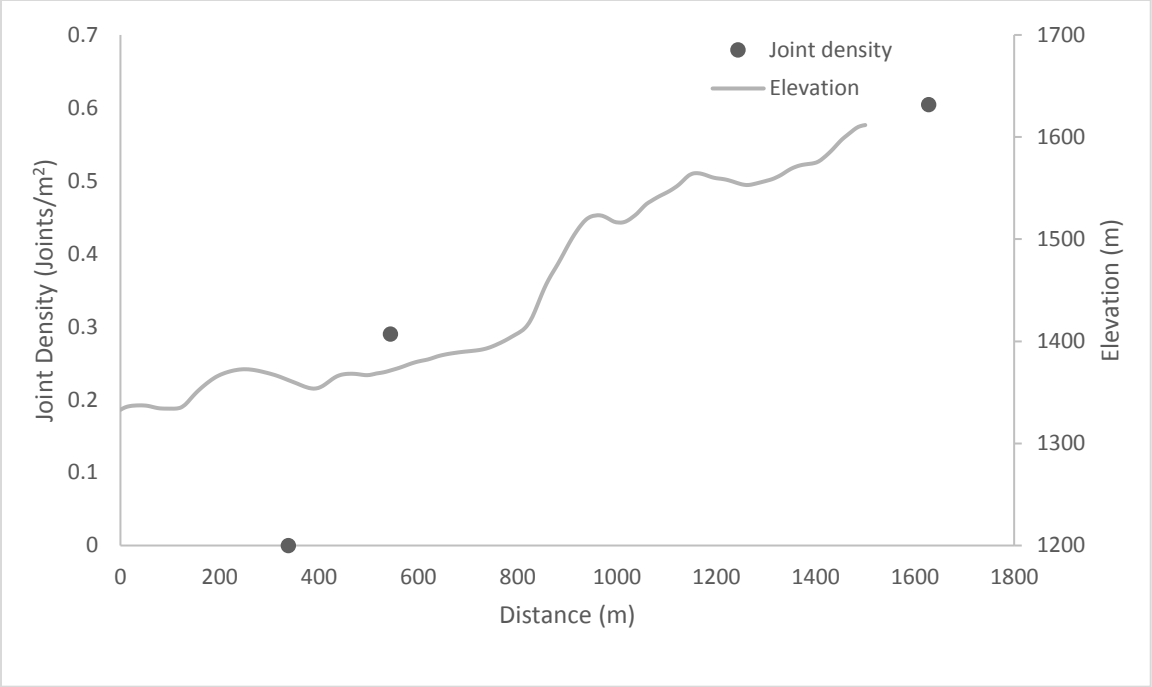

(G)

Figure 31. The area in the figure is outlined by box "C" in Figure 1. (A) shows the geographic location of the profiles. Profile 3 (B-D) consists of sites 23, 22, 21, and 10, and goes through the Granodiorite of Kuna Crest. Profile 4 (E-G) consists of sites 4, 3, 2, and 1 and goes through the Half Dome Granodiorite.

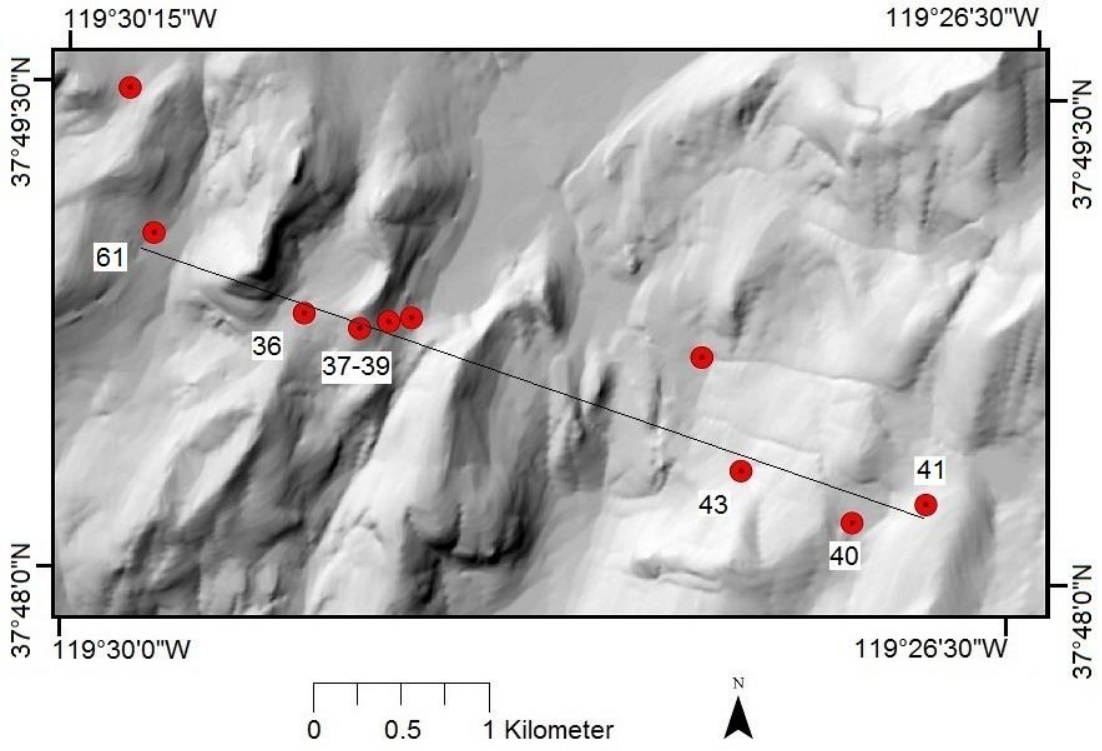
119°30'15"W
119°26'30"W
37°49'30"N
37°48'0"N
61
36
37-39
43
41
40
119°30'0"W
119°26'30"W
0
0.5
1 Kilometer
N

(A)

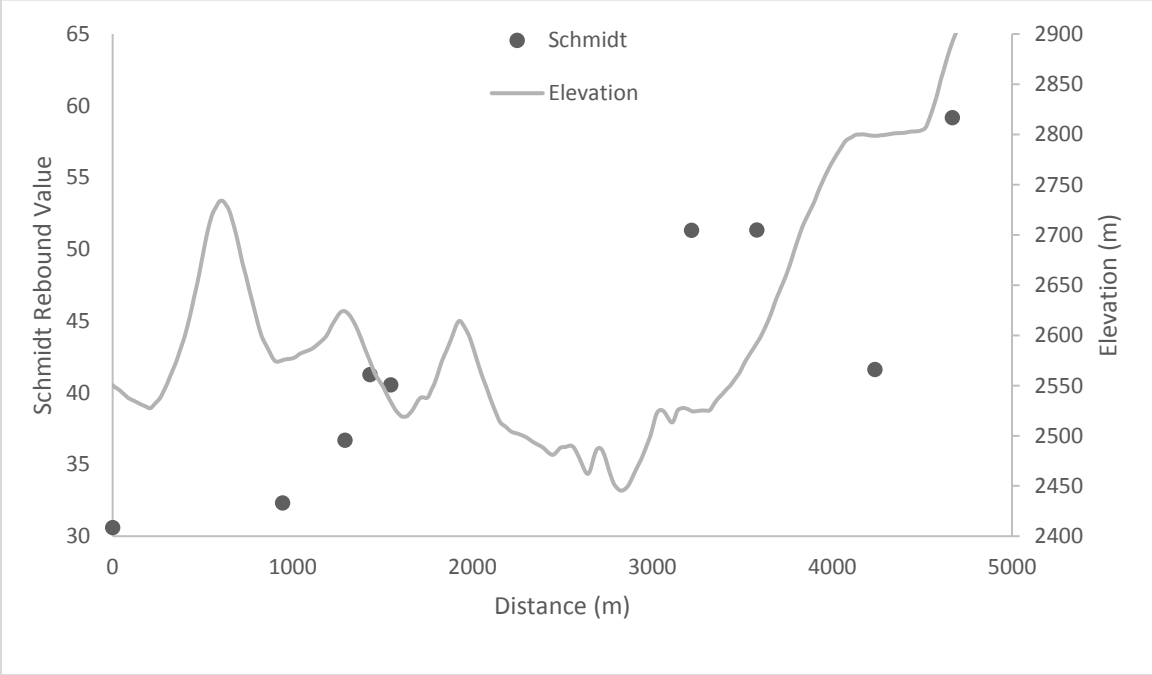
Schmidt
Elevation
Schmidt Rebound Value
Elevation (m)
Distance (m)
65
60
55
50
45
40
35
30
2900
2850
2800
2750
2700
2650
2600
2550
2500
2450
2400
0
1000
2000
3000
4000
5000

(B)

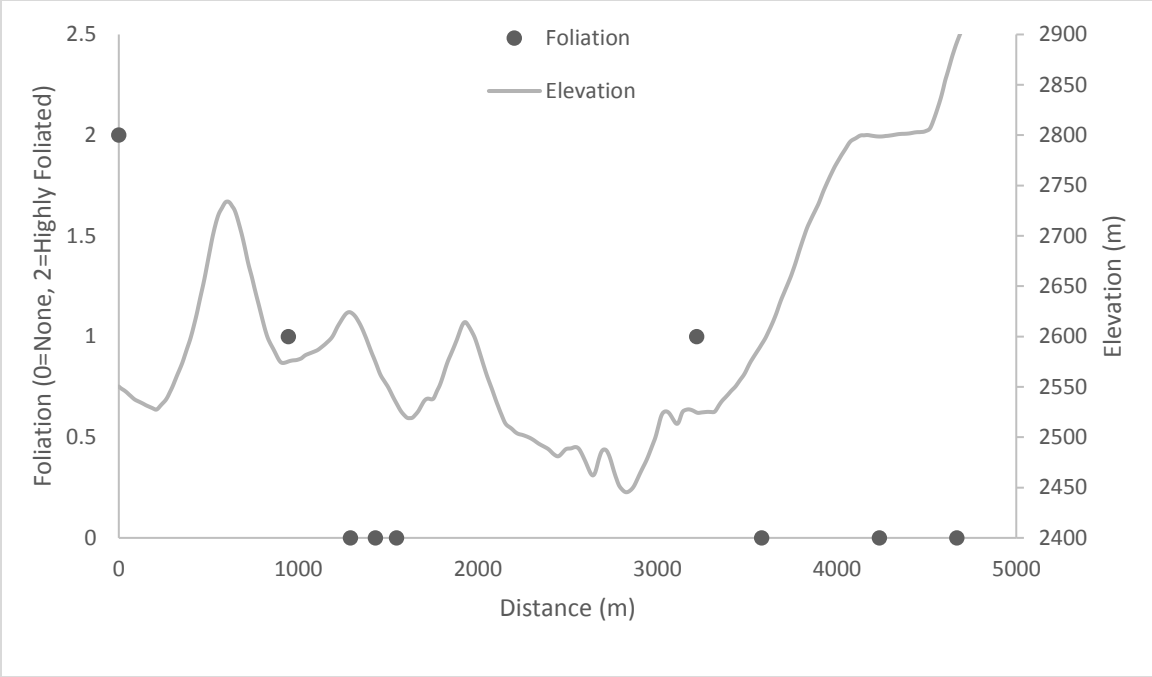
Foliation
Elevation
Foliation (0=None, 2=Highly Foliated)
Elevation (m)
Distance (m)
2.5
2
1.5
1
0.5
0
2900
2850
2800
2750
2700
2650
2600
2550
2500
2450
2400
0
1000
2000
3000
4000
5000

(C)

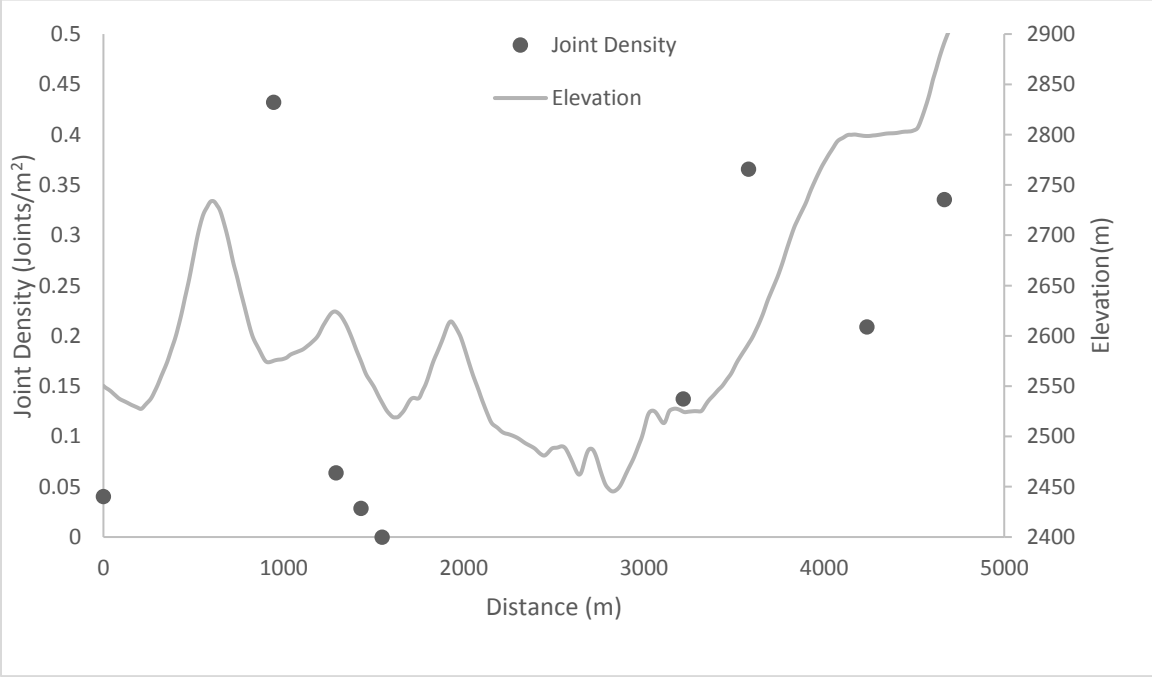
Joint Density
Elevation
Joint Density (Joints/m²)
Elevation(m)
Distance (m)
0.5
0.45
0.4
0.35
0.3
0.25
0.2
0.15
0.1
0.05
0
2900
2850
2800
2750
2700
2650
2600
2550
2500
2450
2400
0
1000
2000
3000
4000
5000

(D)

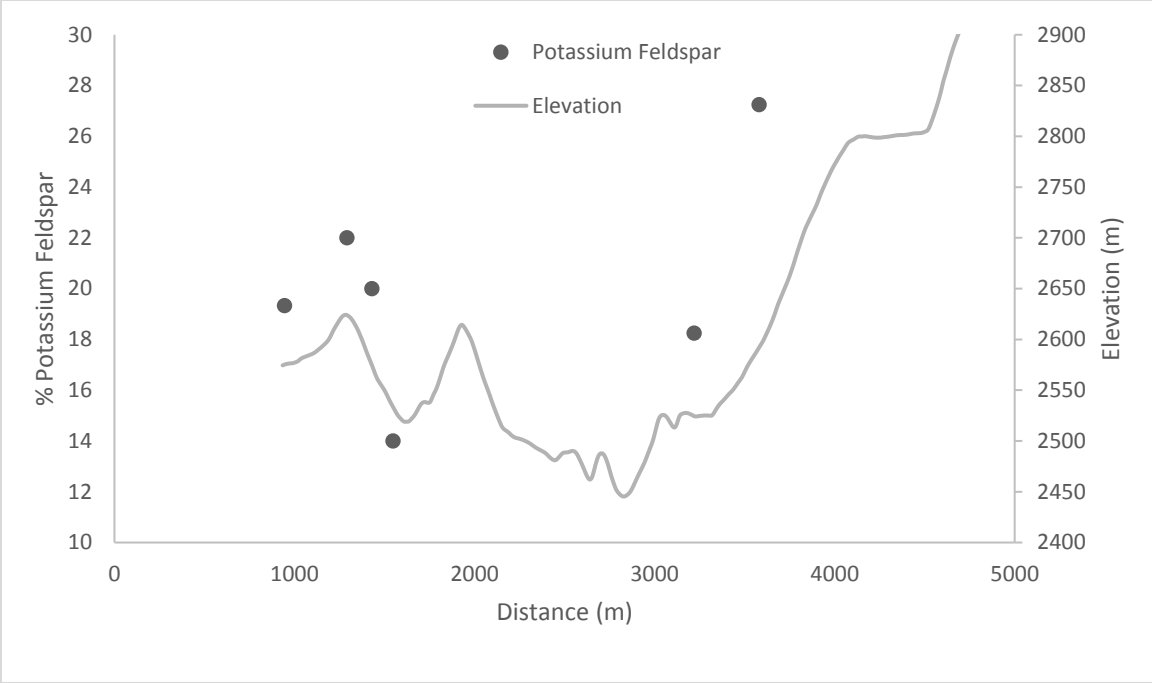
Potassium Feldspar
Elevation
% Potassium Feldspar
Elevation (m)
Distance (m)
30
28
26
24
22
20
18
16
14
12
10
2900
2850
2800
2750
2700
2650
2600
2550
2500
2450
2400
0
1000
2000
3000
4000
5000

(E)

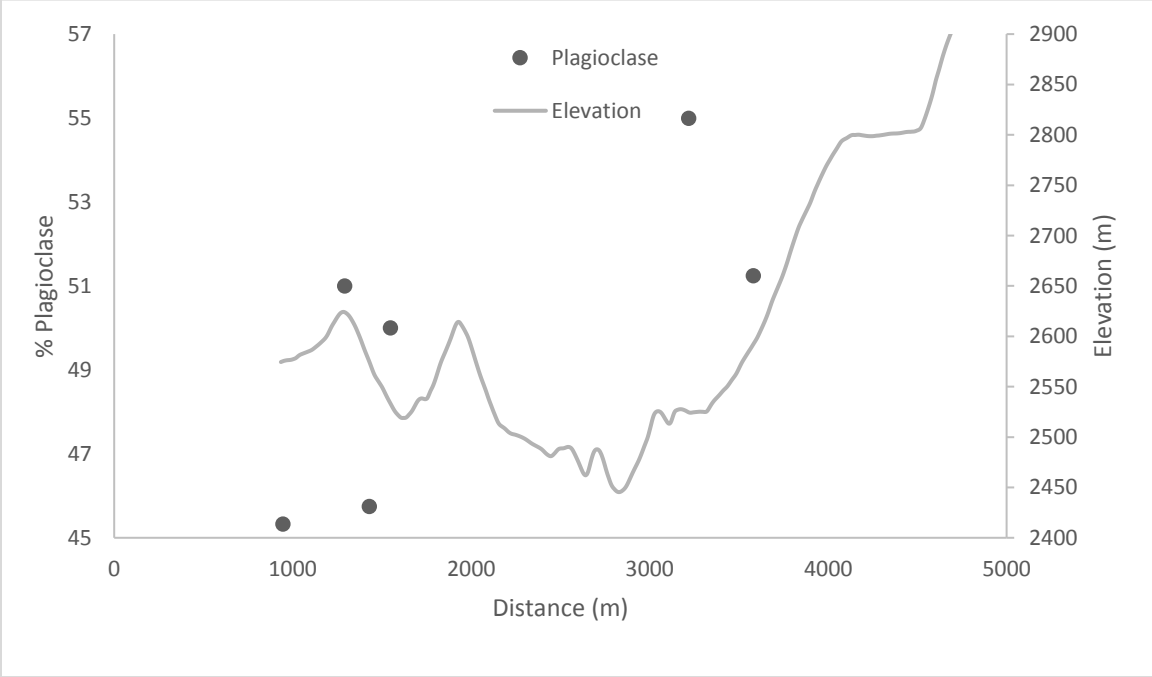
Plagioclase
Elevation
% Plagioclase
Elevation (m)
Distance (m)
57
55
53
51
49
47
45
2900
2850
2800
2750
2700
2650
2600
2550
2500
2450
2400
0
1000
2000
3000
4000
5000

(F)

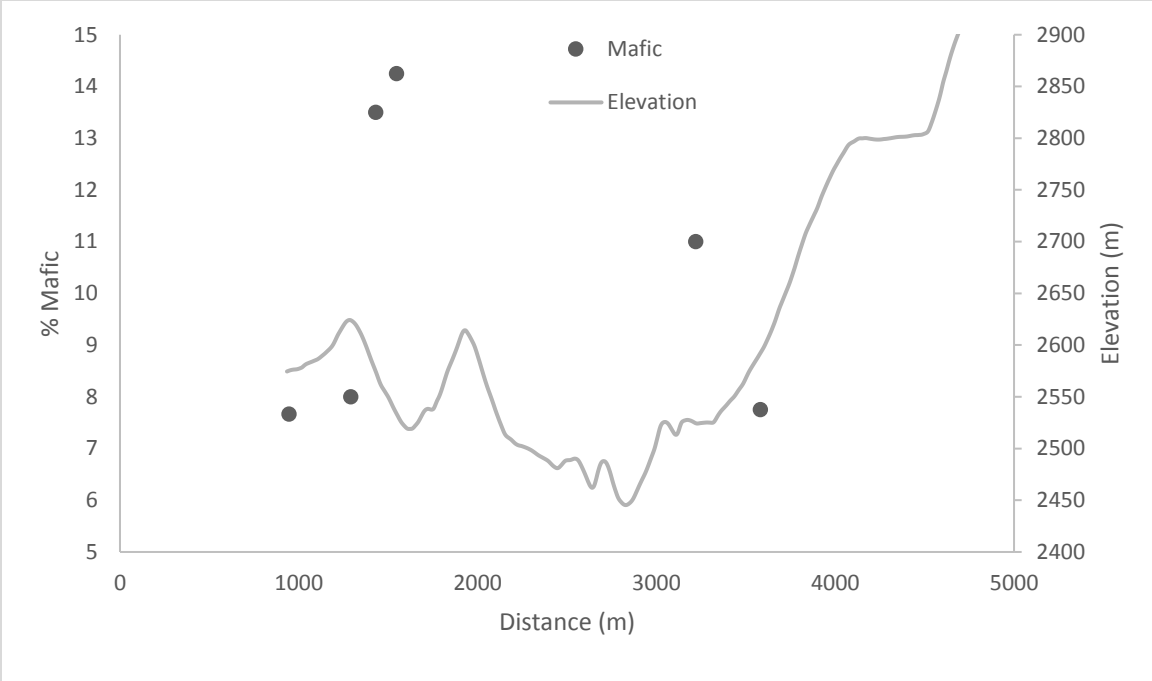
Mafic
Elevation
% Mafic
Elevation (m)
Distance (m)
15
14
13
12
11
10
9
8
7
6
5
2900
2850
2800
2750
2700
2650
2600
2550
2500
2450
2400
0
1000
2000
3000
4000
5000

(F)

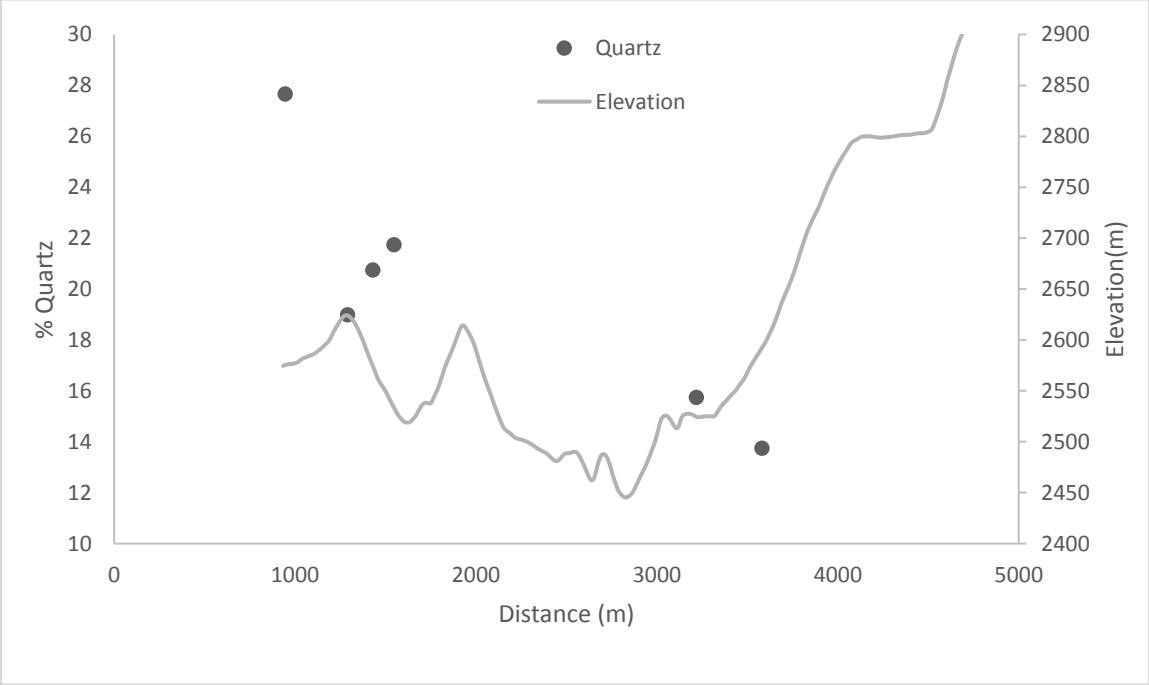
Quartz
Elevation
% Quartz
Elevation(m)
Distance (m)
30
28
26
24
22
20
18
16
14
12
10
2900
2850
2800
2750
2700
2650
2600
2550
2500
2450
2400
0
1000
2000
3000
4000
5000

(G)

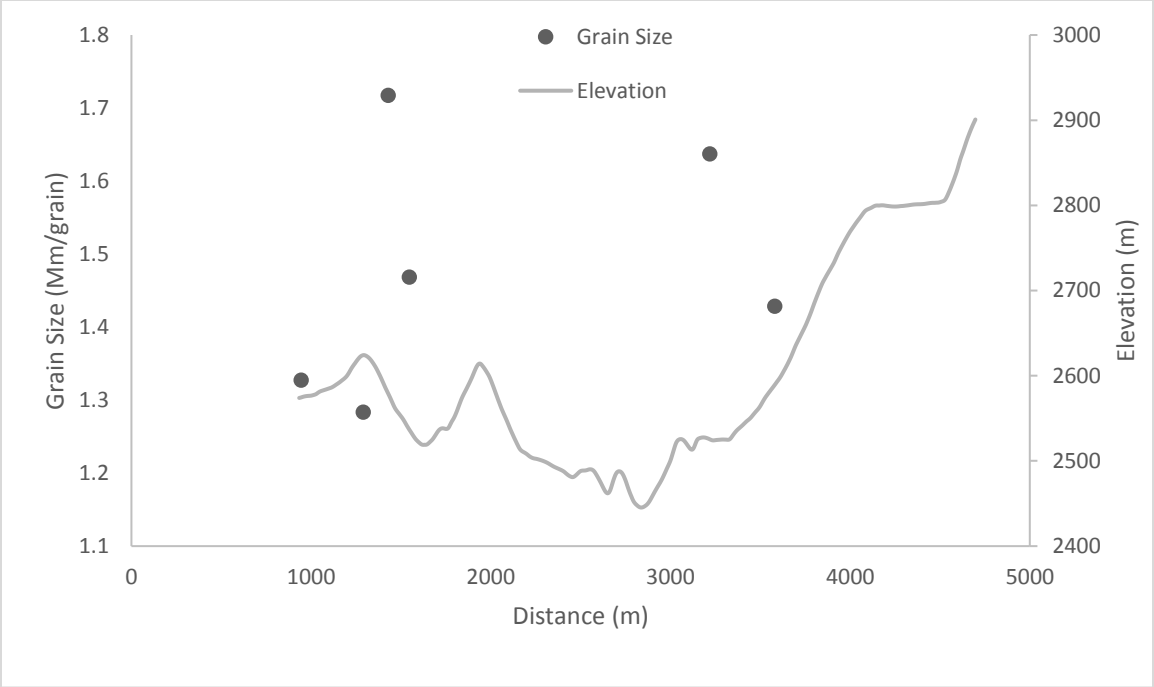

(H)

Figure 32. Profile 5. The area in the figure is outlined by box "D" in Figure 1. (A) shows the geographic location of the profile. (B-D) start at site 61 while E-H start at site 36 as no sample was collected at site 61. Profile 5 goes through the Half Dome Granodiorite.

DISCUSSION

Based on the varied behavior of all properties between regions and lithologic units, noticeable changes in elevation would be expected at contacts between units across Yosemite, but this is generally not observed. Although there are clear differences in slope properties between the granites in El Capitan and the neighboring diorite, no significant differences in morphology exist between the mapped granite and granodiorite units in Yosemite, as explained in Migón (2006). Rather, Migón (2006) suggests that lithologic differences in these units may only be important if landscape development persists over a long time, which would allow for uninterrupted selective weathering of the different rock units. Similarly, Yosemite Valley's slopes remain steep after 10,000 years of ice-free conditions (Migón, 2006) and it may take an additional tens of thousands of years until slope angles are reduced. Migón (2006) also notes that most massive landslides in the granitic units have originated above the vertical extent of ice from the last glaciation period, further evidence that age of exposure is an important factor in landscape development. Therefore, the landscape in Yosemite may not display a significant correlation between rock strength and topography at a regional scale simply because the rocks in Yosemite have not been exposed long enough for erosive processes to make contrasts in strength apparent.

Several caveats exist to these observations. First, measurements were not uniformly distributed across the landscape or taken from every region due to the scale of the study area and logistics. Without data for every section of the study area, many relationships need to be inferred from interpolated maps, which are subject to appreciable uncertainty.

For example, Figure 16 shows that the Mount Hoffman region is the most foliated, although foliation intensity varies by lithologic unit (Table 1), which is not shown in the interpolated map. As a result, all sources of data must be considered before making a connection between variations in lithology and topography. Additionally, foliation data are reported in this study, but the data were collected using a subjective, imprecise method of foliation intensity ranking. No significant conclusions are drawn between foliation and its effect on topography or rock strength as a result, and all foliation data should be interpreted with caution.

Another caveat is that the weakest rocks in the region may have already eroded away, leaving only the strongest rocks behind. As previously noted, relatively weak diorite in Yosemite Valley has eroded into significant talus piles in 10,000 years while the surrounding granodiorite units have maintained steep slopes. At greater time scales, extending back further than 10,000 years, weaker rocks possibly were removed by erosion, such as by glaciers and rivers. If these rocks had remained intact, the landscape in Yosemite might display a stronger correlation between rock strength and topography.

Additional factors besides those tested in this study may be responsible for the Schmidt hammer readings. Although the top 20 Schmidt rebound values are typically located at higher elevations than the lowest 20 rebound values, none of the factors tested offer a clear explanation for this finding. As shown in Table 2, the top 20 Schmidt rebound values were over 34 rebound units higher than the lower 20 values, although none of the factors measured for this study, such as mineral percent, vary significantly at these sites. Eight of the top 20 rebound values were recorded in the Half Dome

Granodiorite (Khd) unit, while 11 of the lowest 20 rebound values were recorded in the El Capitan Granite (Kec) unit, suggesting that an additional factor within these units may be responsible for the highest and lowest values.

TABLE 2. PROPERTIES OF LARGEST AND SMALLEST 20 REBOUND VALUES COMPARED

Top or Lowest	Schmidt	Elev. (m)	Fol.	Jnt. Dens.	%Kspar	%Plag	%Mafic	%Quartz	Mm/grain
Top 20 Schmidt	53.0	2326	0.6	0.3	18.8	49.9	10.8	20.5	1.29
Lowest 20 Schmidt	29.7	2071	0.6	0.3	17.6	48.2	11.1	23.2	1.41

Note: Fol= foliation; Jnt. Dens.= joint density; Kspar= potassium feldspar; Plag.= plagioclase.

Occasionally, some of the highest and lowest rebound values were recorded a short distance from each other. For example, one of the highest rebound values was recorded at one of the sites near the base of Mount Hoffman on a fresh surface of a large boulder that detached from the side of Mount Hoffman and rolled less than 60 m from its source (Figure 33). In contrast, some of the lowest rebound values were obtained a short distance away on highly weathered, in situ rock on the top of Mount Hoffman (Figure 34). Measurements at both sites were taken on the same lithologic unit, the Granodiorite of Mount Hoffman, further evidence that an additional factor besides lithology is controlling the majority of variation in Schmidt rebound values. Weathering influences rebound values (e.g., McCarroll, 1991) and appears to be responsible for the variations seen above, along with the variations across the entire study area, meaning that the Schmidt hammer may not be a reliable tool for measuring rock strength. Further research is required to precisely determine whether weathering or an additional factor is controlling Schmidt rebound values in Yosemite.

Although the Schmidt hammer readings may not be a reliable indicator of rock strength, several examples confirm that rock strength is important at relatively local

scales. Johnson (2015) described a pattern in Yosemite where quartz-rich, fine-grained rocks were observed at higher elevations in stream channels than rocks with lower quartz content and larger grain sizes, indicating that rock strength has a role in shaping Yosemite's topography. Despite the contrast to observations made by Migón (2006), the observations made by Johnson (2015) are valid and suggest that the effects of rock strength are seen at the local scale (~100 m or less) in bedrock channels regardless of how long the landscape has been exposed. With flowing water, erosion may be significant enough at the local scale for lithologic differences to influence topography. This finding is reinforced by Zimmer and Gabet (2018), who concluded that rock strength in the Sierras was only of importance at local scales in terms of glacial erosion. The distribution of rivers and glaciers are an additional factor to consider as they are unevenly spread across the landscape, possibly leading to differences in erosive forces at different regions in the landscape. This could possibly allow for areas to erode at different rates, even if the mineralogy is similar between them.

Figure 33. Fresh surfaces delivered high Schmidt rebound values at the base of Mount Hoffman, site 53.

Figure 34. Example of weathered and jointed rocks at the top of Mount Hoffman, site 46.

Other examples demonstrate that rock strength has some control over the landscape of Yosemite. At areas such as Yosemite Creek ("3" in Figure 15) or the southwest end of Yosemite Valley ("4" in Figure 15), large master joints influence topography and guide streams. Visible in Figure 15 and from aerial photos, master joints leave an impression on topography as creeks and shape features such as hills. These areas of large master joints correlate with the areas of highest joint densities at the outcrop scale (e.g. Figure 15), demonstrating that master joints affect the landscape at multiple scales. In the Cathedral Peak Granodiorite at Tuolumne Meadows, less than 10 km east of the study area,

variations in fracture densities control topography as they enable differences in erosion rates (Becker et al., 2014). Master joints may shape the topography of the study area in a similar way, creating zones of weak material, enabling higher erosion rates than in the surrounding non-jointed area. In cases such as Yosemite Creek, rivers flowing in master joints increase erosion rates and incise valleys. Becker et al. (2014) hypothesize that fractures control erosion in Tuolumne Meadows more than variations in lithology, a hypothesis which is reinforced by this study.

Fractures may also control the distribution of vegetation in Yosemite. Hahm et al. (2014) suggest that higher fracture densities may be correlated with higher amounts of vegetation, and in Yosemite, the 20 sites with the lowest joint density also plot in relatively unforested areas (Figure 35). While Hahm et al. (2014) found that areas with increased silica content (associated with more quartz and potassium feldspar) had more vegetation, the regions in Yosemite with more forestation had bedrock with less quartz and potassium feldspar but increased plagioclase. Therefore, further research is needed on the correlation between bedrock geochemistry and vegetation in Yosemite.

The final and perhaps most important example of the relationship between rock strength and topography in Yosemite is Mount Hoffman, which rises steeply above the study area. The Granodiorite of Mount Hoffman has distinct mineralogy when compared to the other units in the study area, consisting of less plagioclase than almost any other unit. The Granodiorite of Mount Hoffman is also distinguished by its potassium feldspar phenocrysts (Johnson, 2013), and the unit has more potassium feldspar than any other unit (Table 1). The unit is also the least jointed (Table 1) and aerial photographs show

that it has fewer master joints than the surrounding area. Large grain sizes, which may include phenocrysts, are typically associated with decreased rock strength (e.g., Tuğrul and Zarif, 1999), however, so low joint density is likely the explanation for why the unit rises steeply.

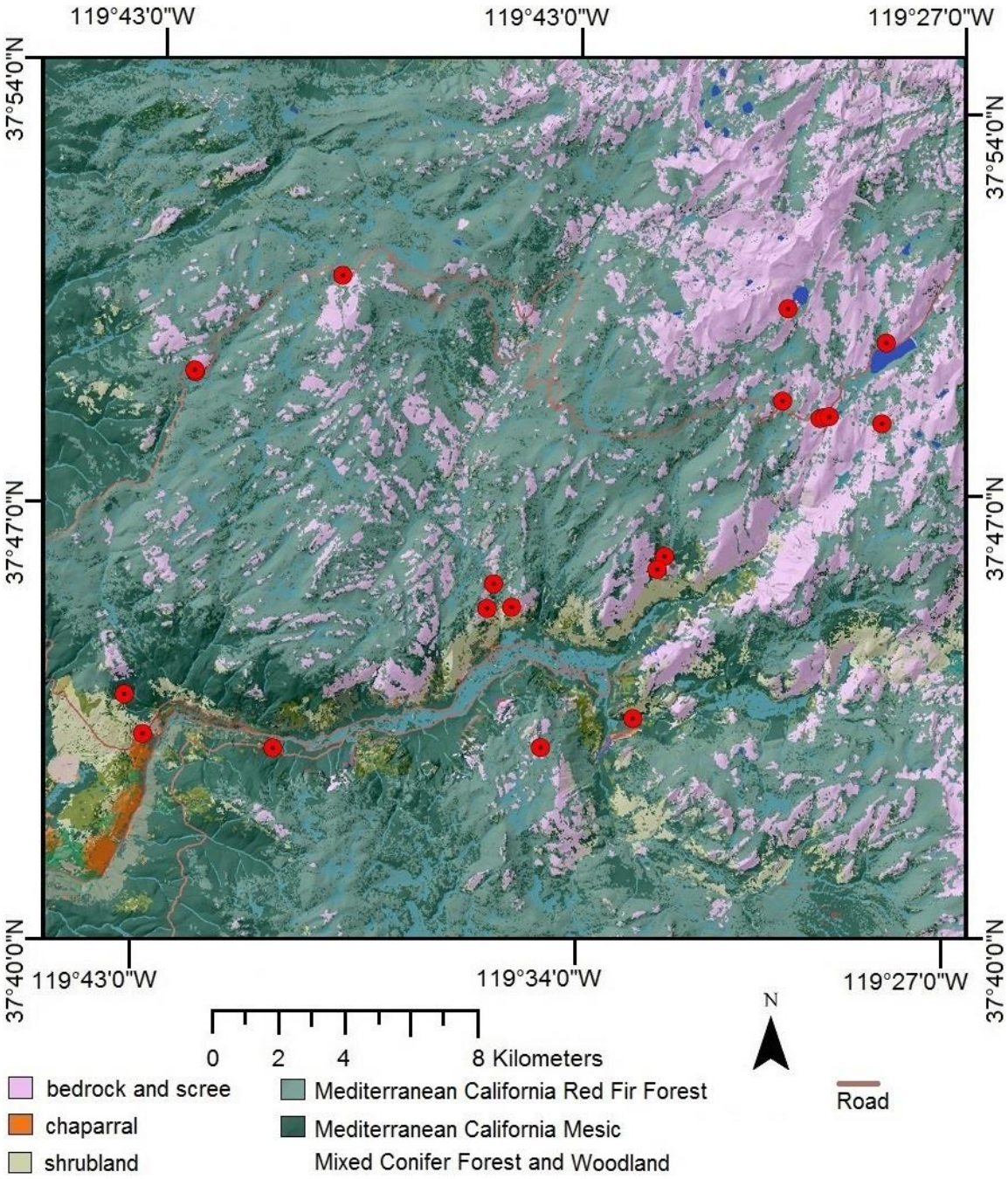

Figure 35. Vegetation cover map of the study area. Red dots represent the 20 sites with the lowest joint density. Data available from the U.S. Geological Survey Gap Analysis Program (2016).

CONCLUSION

This study sought to increase our knowledge of rock strength and its effect on topography by using multiple techniques to analyze rock strength at a regional scale. Within Yosemite, conflicting evidence existed which both refuted and supported rock strength as a major control of topography. Schmidt hammer, mineralogical, joint, and foliation data were collected for 83 locations, 48 of which provided mineral percent and grain size data, then combined with additional mineral percentage and grain size data for a total of 135 sites. Although mineralogy varied between lithologic units and no corresponding differences in topography were observed at a landscape scale, several examples demonstrate that rock strength influences topography at more local scales. Previous studies indicate that mineralogy influences knickpoints, and therefore topography, at a scale of ~100 m or less, and Mount Hoffman demonstrates a connection between mineralogy, joint density, and topography at the kilometer scale. Master joints influence topography at the several-kilometer scale, shaping hills and guiding streams. Across the landscape, increased joint density is also associated with increased forestation. Schmidt hammer readings typically increase with elevation across the landscape, although further research is needed to determine if weathering is controlling rebound values or if some other factor not measured by this study is controlling the readings. No significant correlation was observed between foliation, topography, and any factor measured in this study. Overall, these results show a correlation between rock strength and topography at varying scales, establishing a lithologic control of the topography of Yosemite National Park.

TABLE A1. ALL DATA

Site #	Stop Number	Sample Name	Easting (m)*	Northing (m)*	Elevation (m)	Schmidt	Foliation	Joint Density (joints/m^2)	Kspar %	Plag. %	Mafic %	Quartz %	Mm/grain	Unit†
1	1	N.A.	275889	4178587	1546	35.4	0	0.29	N.A.	N.A.	N.A.	N.A.	N.A.	Khd
1	1 Sample	1	275937	4178574	1548	N.A.	N.A.	N.A.	27.0	41.3	11.8	20.0	1.38	Khd
2	2	2	276304	4178533	1615	38.7	0	0.60	24.3	49.8	3.8	22.3	1.44	Khd
3	3	3	275355	4178482	1400	50.0	0	0.00	N.A.	N.A.	N.A.	N.A.	N.A.	Khd
4	4	4	274803	4178533	1338	32.0	1	N.A.	N.A.	N.A.	N.A.	N.A.	N.A.	Khd
5	5	5	262696	4177739	1421	31.5	1	0.45	19.3	41.5	9.8	29.5	1.62	Kec
6	6	6	261557	4177767	1487	41.9	2	0.28	1.8	65.8	14.5	18.0	1.88	Kec
7	7	7	265185	4171805	2233	38.5	0	0.26	33.5	50.0	7.3	9.3	0.86	Kt
8	8	N.A.	267721	4172635	2174	26.8	N.A.	N.A.	N.A.	N.A.	N.A.	N.A.	N.A.	Kic
9	9	N.A.	271980	4174993	2377	31.4	0	1.33	N.A.	N.A.	N.A.	N.A.	N.A.	Ks
10	10	8	273152	4178425	2245	43.8	2	0.60	13.2	54.6	26.2	6.0	1.30	Kkc
11	11	N.A.	272458	4177567	2410	28.0	0	0.08	N.A.	N.A.	N.A.	N.A.	N.A.	Kec
12	12	N.A.	272361	4177310	2388	38.5	1	0.28	N.A.	N.A.	N.A.	N.A.	N.A.	Kec
13	12	9	276305	4182379	1397	22.1	1	N.A.	N.A.	N.A.	N.A.	N.A.	N.A.	Khd
14	13	N.A.	276367	4182563	1539	36.0	0	1.09	N.A.	N.A.	N.A.	N.A.	N.A.	Khd
15	14	10	276307	4182709	1658	34.5	1	0.46	23.8	43.0	10.5	22.8	1.19	Khd
16	15	11	276358	4183587	2057	52.4	0	0.12	24.0	50.3	6.5	19.3	0.82	Khd
17	16	12 a and b	276128	4183176	1949	25.0	1	0.08	N.A.	N.A.	N.A.	N.A.	N.A.	Khd
18	17	12	271944	4172295	2218	45.3	0	0.37	9.3	52.8	23.8	14.3	1.15	Kic
19	18	N.A.	272242	4178224	2477	47.4	1	0.31	N.A.	N.A.	N.A.	N.A.	N.A.	Kec
20	19	13	272173	4178018	2369	40.0	0	0.65	19.0	44.7	7.3	29.0	1.56	Kec
21	20	N.A.	272494	4179264	2164	51.9	0	0.53	N.A.	N.A.	N.A.	N.A.	N.A.	Kkc
22	21	N.A.	272278	4179379	2074	47.0	0	0.87	N.A.	N.A.	N.A.	N.A.	N.A.	Kkc
23	22	14	271978	4179544	1908	41.5	2	0.63	9.1	58.2	16.5	16.2	0.85	Kkc
24	23	15	264033	4177561	1358	47.0	1	0.07	28.3	44.3	8.0	19.5	1.78	Kec
25	24	16	272126	4182765	2218	40.7	1	0.40	6.5	59.3	16.3	18.0	0.71	Ks
26	25	N.A.	271725	4182341	2187	28.2	N.A.	0.81	N.A.	N.A.	N.A.	N.A.	N.A.	Kec
27	26	17	271550	4181990	2123	39.2	1	0.00	6.3	72.3	8.8	12.8	0.86	Kec
28	27	N.A.	271419	4182499	2064	32.0	1	0.39	N.A.	N.A.	N.A.	N.A.	N.A.	Kec
29	28	N.A.	271130	4182311	2045	30.6	0	0.49	N.A.	N.A.	N.A.	N.A.	N.A.	Ks
30	29	18	270979	4182721	2087	39.2	1	0.13	N.A.	N.A.	N.A.	N.A.	N.A.	Kec
31	30	19	270770	4181946	1818	41.5	0	0.06	19.0	44.7	7.3	29.0	1.56	Kec
32	31	20	271024	4181586	1543	44.9	0	0.30	9.7	59.7	13.7	17.0	1.43	Kec
33	32	N.A.	259941	4178012	1438	20.0	0	0.13	N.A.	N.A.	N.A.	N.A.	N.A.	Kec
34	33 Dike	N.A.	283333	4190300	2495	61.9	N.A.	0.09	N.A.	N.A.	N.A.	N.A.	N.A.	Khd
35	33 Not Dike	21	283333	4190300	2495	51.4	2	N.A.	23.0	56.7	10.7	9.7	1.68	Khd

TABLE A1 CONTINUED. ALL DATA

Site #	Stop Number	Sample Name	Easting (m)*	Northing (m)*	Elevation (m)	Schmidt	Foliation	Joint Density (joints/m^2)	Kspar %	Plag. %	Mafic %	Quartz %	Mm/grain	Unit†
36	33 Olmstead	22	280924	4188012	2585	32.3	1	0.43	19.3	45.3	7.7	27.7	1.33	Khd
37	34	23	281240	4187925	2608	36.7	0	0.06	22.0	51.0	8.0	19.0	1.28	Khd
38	35	24	281405	4187963	2570	41.3	0	0.03	20.0	45.8	13.5	20.8	1.72	Khd
39	36	25	281537	4187984	2530	40.6	0	0.00	14.0	50.0	14.3	21.8	1.47	Khd
40	37	26	284049	4186814	2807	41.6	0	0.21	N.A.	N.A.	N.A.	N.A.	N.A	Khd
41	38	27	284471	4186918	2898	59.2	0	0.34	N.A.	N.A.	N.A.	N.A.	N.A	Khd
42	39	28	283415	4187111	2620	51.4	0	0.37	27.3	51.3	7.8	13.8	1.43	Khd
43	40	29	283193	4187758	2510	51.3	1	0.14	18.3	55.0	11.0	15.8	1.64	Khd
44	41	30	274999	4187416	2487	40.4	2	0.45	12.0	52.3	23.5	12.3	0.90	Kkc
45	42	31	279708	4191451	3122	40.1	0	0.20	26.0	34.5	10.3	29.3	1.26	Kh
46	43	32	279104	4191762	3301	36.3	0	N.A.	28.5	48.8	13.3	9.5	1.86	Kh
47	44	33	280841	4191448	2849	34.3	1	1.07	7.3	55.3	20.6	16.8	1.03	Kkc
48	45	34	280930	4191164	2279	43.6	1	0.24	16.8	56.8	12.8	13.8	1.44	Khd
49	46	35	280896	4190809	2737	52.8	1	0.54	18.5	47.8	14.3	19.5	1.48	Khd
50	47	36	279932	4189298	2660	37.9	1	0.85	20.8	61.5	13.0	4.8	1.46	Kap
51	48	N.A.	279237	4191793	3249	34.1	1	N.A.	N.A.	N.A.	N.A.	N.A.	N.A	Kh
52	49	N.A.	280098	4191115	2944	52.0	2	0.94	N.A.	N.A.	N.A.	N.A.	N.A	Jms
53	50	N.A.	280245	4191382	2905	54.2	1	0.00	N.A.	N.A.	N.A.	N.A.	N.A	Kh
54	51	37	270424	4188119	2236	41.7	1	0.35	3.5	55.3	21.8	19.5	1.22	Ks
55	52	N.A.	270661	4188232	2189	40.4	1	0.31	N.A.	N.A.	N.A.	N.A.	N.A.	Ks
56	53	38	271098	4188976	2199	48.6	1	0.17	18.5	46.3	11.8	23.5	0.89	Ks
57	54	39	272104	4190262	2207	52.5	0	0.85	15.5	50.1	10.8	23.6	0.79	Ks
58	55	N.A.	272911	4191365	2250	38.6	1	0.70	N.A.	N.A.	N.A.	N.A.	N.A.	Kyc
59	56	40	272987	4191669	2258	49.4	2	0.77	13.0	48.8	10.0	28.3	1.22	Kyc
60	57	41	273099	4192524	2300	40.1	2	1.32	6.8	59.0	14.0	20.3	0.82	Ks
61	58	N.A.	280067	4188471	2555	30.6	2	0.04	N.A.	N.A.	N.A.	N.A.	N.A	Khd
62	59	42	278374	4188628	2552	42.1	1	0.45	46.3	20.5	8.5	24.8	1.70	Khd
63	60	N.A.	273213	4190973	2374	45.1	0	0.94	N.A.	N.A.	N.A.	N.A.	N.A	Kyc
64	61	43	271851	4191039	2382	41.6	0	0.50	13.0	51.8	10.3	25.0	1.09	Ks
65	62	N.A.	268007	4192739	2537	53.2	0	0.62	N.A.	N.A.	N.A.	N.A.	N.A	Ks
66	63	44	266850	4192808	2477	36.7	0	0.33	39.0	29.0	4.5	27.5	1.07	Ks
67	64	N.A.	261607	4189402	2227	47.9	1	0.14	N.A.	N.A.	N.A.	N.A.	N.A.	Ks
68	65	N.A.	266239	4192428	2443	47.1	0	0.12	N.A.	N.A.	N.A.	N.A.	N.A	Ks
69	66	N.A.	257259	4183054	2101	28.9	0	0.23	N.A.	N.A.	N.A.	N.A.	N.A	Kec
70	67	N.A.	258485	4182033	1977	34.5	N.A.	0.42	N.A.	N.A.	N.A.	N.A.	N.A	Kec

TABLE A1 CONTINUED. ALL DATA

Site #	Stop Number	Sample Name	Easting (m)*	Northing (m)*	Elevation (m)	Schmidt	Foliation	Joint Density (joints/m^2)	Kspar %	Plag. %	Mafic %	Quartz %	Mm/grain	Unit†
71	68	45	259570	4181735	1959	61.1	0	0.33	10.8	47.0	9.0	33.3	1.91	Kec
72	69	N.A.	261589	4189460	2246	39.2	1	0.05	N.A.	N.A.	N.A.	N.A.	N.A.	Ks
73	70	46	261594	4189578	2296	37.2	1	0.41	26.0	37.0	9.3	27.8	1.31	Ks
74	71	47	274791	4179331	1288	58.9	0	0.20	32.0	39.0	6.8	22.3	1.10	Khd
75	72	48	258990	4177770	1518	43.0	1	0.24	16.8	46.5	10.5	26.3	1.43	Kar
76	73	49	259362	4179262	1633	29.7	0	0.07	18.8	50.8	9.3	21.3	1.88	Kec
77	74	N.A.	260850	4179880	1734	28.1	0	0.39	N.A.	N.A.	N.A.	N.A.	N.A.	Kec
78	75	50	261874	4180643	1824	46.3	1	0.15	22.7	33.6	8.4	35.2	1.19	Kec
79	76	N.A.	260615	4179996	1682	38.6	1	0.26	N.A.	N.A.	N.A.	N.A.	N.A.	Kec
80	77	51	259180	4177856	1562	42.7	1	0.67	3.8	53.0	17.8	25.5	2.02	Kar
81	78	52	260409	4186342	2142	52.1	0	0.36	5.5	56.5	20.8	17.3	1.38	Kec
82	79	53	260844	4185718	2264	33.7	0	0.15	17.0	53.3	8.8	21.0	1.82	Kec
83	80	54	260566	4185598	2204	42.7	0	0.39	9.5	52.0	13.5	25.0	1.34	Kec
84	N.A.	BL-1A	277446	4198310	2828	N.A.	N.A.	N.A.	10.5	53.8	N.A.	13.0	N.A.	Kyc
85	N.A.	BL-1C	277446	4198310	2828	N.A.	N.A.	N.A.	26.6	34.9	N.A.	35.1	N.A.	Kyc
86	N.A.	Bl-2A	278065	4197952	2755	N.A.	N.A.	N.A.	28.4	32.5	N.A.	34.9	N.A.	Kyc
87	N.A.	BL-3C	278262	4198228	2815	N.A.	N.A.	N.A.	10.3	62.2	N.A.	10.4	N.A.	Kt
88	N.A.	BL-3F	278262	4198228	2815	N.A.	N.A.	N.A.	30.5	33.4	N.A.	31.4	N.A.	Kt
89	N.A.	BL-4H	277205	4196050	2908	N.A.	N.A.	N.A.	15.4	51.6	N.A.	21.8	N.A.	Kt
90	N.A.	BL-6A	277291	4196011	2966	N.A.	N.A.	N.A.	19.5	42.5	N.A.	28.2	N.A.	Kt
91	N.A.	BL-7A	273359	4192600	2298	N.A.	N.A.	N.A.	12.9	54.4	N.A.	19.3	N.A.	Ks
92	N.A.	BL-8B	279287	4197839	2898	N.A.	N.A.	N.A.	14.6	59.4	N.A.	7.5	N.A.	Kyc
93	N.A.	BL-8E	279307	4197883	2896	N.A.	N.A.	N.A.	10.3	63.3	N.A.	11.4	N.A.	Kyc
94	N.A.	BL-12A	279356	4197197	3017	N.A.	N.A.	N.A.	29.8	32.3	N.A.	34.9	N.A.	Kt
95	N.A.	BL-12B	279356	4197197	3017	N.A.	N.A.	N.A.	14.8	64.9	N.A.	5.5	N.A.	Kt
96	N.A.	BL-14A	274038	4194243	2406	N.A.	N.A.	N.A.	11.8	55.4	N.A.	13.1	N.A.	Kyc
97	N.A.	BL-14E	274259	4194485	2415	N.A.	N.A.	N.A.	10.3	56.5	N.A.	4.9	N.A.	Kyc
98	N.A.	BL-15B	274359	4194558	2437	N.A.	N.A.	N.A.	21.0	42.2	N.A.	34.2	N.A.	Kyc
99	N.A.	BL-16A	273718	4193987	2420	N.A.	N.A.	N.A.	25.9	40.5	N.A.	25.4	N.A.	Kyc
100	N.A.	BL-17A	274863	4194198	2426	N.A.	N.A.	N.A.	17.1	50.6	N.A.	23.7	N.A.	Kyc
101	N.A.	FKYO-2	279307	4190330	2747	N.A.	N.A.	N.A.	8.4	52.3	N.A.	14.6	N.A.	Kkc
102	N.A.	FKYO-4	278533	4189609	2689	N.A.	N.A.	N.A.	18.3	43.4	N.A.	28.1	N.A.	Kkc
103	N.A.	FKYO-5	278317	4189233	2758	N.A.	N.A.	N.A.	22.3	39.2	N.A.	32.1	N.A.	Kkc
104	N.A.	FKYO-8	272800	4191268	2256	N.A.	N.A.	N.A.	12.1	55.3	N.A.	18.5	N.A.	Kyc
105	N.A.	FKYO-9	272825	4191310	2254	N.A.	N.A.	N.A.	19.5	46.9	N.A.	23.9	N.A.	Ks

TABLE A1 CONTINUED. ALL DATA

Site #	Stop Number	Sample Name	Easting (m)*	Northing (m)*	Elevation (m)	Schmidt	Foliation	Joint Density (joints/m^2)	Kspar %	Plag. %	Mafic %	Quartz %	Mm/grain	Unit†
106	N.A.	FKYO-13c	273052	4191620	2259	N.A.	N.A.	N.A.	18.5	47.7	N.A.	27.5	N.A.	Kyc
107	N.A.	FKYO-15a	273785	4193692	2373	N.A.	N.A.	N.A.	24.0	40.4	N.A.	27.7	N.A.	Kyc
108	N.A.	FKYO-16	273648	4193000	2298	N.A.	N.A.	N.A.	11.0	51.9	N.A.	28.3	N.A.	Kyc
109	N.A.	FKYO-17	269948	4193920	2569	N.A.	N.A.	N.A.	12.3	56.5	N.A.	17.5	N.A.	Kyc
110	N.A.	FKYO-19	269961	4192911	2594	N.A.	N.A.	N.A.	15.0	49.8	N.A.	25.5	N.A.	Kyc
111	N.A.	FKYO-21c	269754	4192776	2609	N.A.	N.A.	N.A.	21.1	45.2	N.A.	25.4	N.A.	Ks
112	N.A.	FKYO-25a	269337	4191753	2499	N.A.	N.A.	N.A.	14.8	50.7	N.A.	22.9	N.A.	Ks
113	N.A.	FKYO-29	273379	4192819	2291	N.A.	N.A.	N.A.	12.4	55.0	N.A.	19.2	N.A.	Kyc
114	N.A.	FKYO-30	273058	4192329	2279	N.A.	N.A.	N.A.	12.2	57.8	N.A.	18.6	N.A.	Ks
115	N.A.	FKYO-31a	272107	4190063	2222	N.A.	N.A.	N.A.	17.9	50.0	N.A.	22.4	N.A.	Ks
116	N.A.	FKYO-33	272528	4190744	2257	N.A.	N.A.	N.A.	17.7	49.9	N.A.	20.4	N.A.	Ks
117	N.A.	FKYO-40	266870	4193406	2477	N.A.	N.A.	N.A.	14.4	53.4	N.A.	22.7	N.A.	Ks
118	N.A.	FKYO-42a	271390	4189524	2206	N.A.	N.A.	N.A.	14.5	54.3	N.A.	21.9	N.A.	Ks
119	N.A.	FKYO-45	271247	4189065	2205	N.A.	N.A.	N.A.	15.6	52.1	N.A.	21.5	N.A.	Ks
120	N.A.	FKYO-47	270308	4190317	2437	N.A.	N.A.	N.A.	14.0	52.4	N.A.	23.3	N.A.	Ks
121	N.A.	FKYO-53c	261589	4189389	2241	N.A.	N.A.	N.A.	15.7	53.0	N.A.	19.4	N.A.	Ks
122	N.A.	FKYO-54	272229	4177472	2360	N.A.	N.A.	N.A.	22.2	42.9	N.A.	24.8	N.A.	Ks
123	N.A.	FKYO-55b	266577	4192270	2533	N.A.	N.A.	N.A.	22.7	47.5	N.A.	22.4	N.A.	Ks
124	N.A.	FKYO-58b	266135	4190889	2740	N.A.	N.A.	N.A.	17.4	49.8	N.A.	20.3	N.A.	Ks
125	N.A.	FKYO-62	272855	4188504	2513	N.A.	N.A.	N.A.	15.4	52.5	N.A.	20.3	N.A.	Ks
126	N.A.	FKYO-63	276337	4188448	2798	N.A.	N.A.	N.A.	13.6	45.4	N.A.	32.1	N.A.	Kkc
127	N.A.	FKYO-64	266456	4194522	2437	N.A.	N.A.	N.A.	13.1	53.3	N.A.	16.8	N.A.	Ks
128	N.A.	Wildcat Cr-Top	260378	4178795	1354	N.A.	N.A.	N.A.	25.0	12.0	12.0	29.0	0.11	Kec
129	N.A.	Cascade Cr-Top	260906	4179121	1336	N.A.	N.A.	N.A.	20.0	33.0	11.0	33.0	0.15	Kec
130	N.A.	Tamarack Cr-Top	260833	4179065	1324	N.A.	N.A.	N.A.	27.0	28.0	6.0	35.0	0.14	Kec
131	N.A.	M.R. Trib 22 C-Top	261653	4178832	1307	N.A.	N.A.	N.A.	40.0	16.0	19.0	19.0	N.A.	Kec
132	N.A.	North Dome	274615	4183030	2439	N.A.	N.A.	N.A.	25.0	23.0	17.0	18.0	0.12	Khd
133	N.A.	Wildcat Cr-Base	260659	4178496	1077	N.A.	N.A.	N.A.	15.0	29.0	22.0	18.0	0.18	Kec
134	N.A.	Cascade- Tamarack Cr-Base	260977	4178728	1060	N.A.	N.A.	N.A.	32.0	30.0	12.0	14.0	0.13	Kec
135	N.A.	M.R. Trib 22 C-Base	261574	4178592	1099	N.A.	N.A.	N.A.	33.0	17.0	27.0	10.0	0.14	Kec
136	N.A.	17B	273517	4180848	1247	N.A.	N.A.	N.A.	24.0	23.0	18.0	26.0	0.15	Khd

Notes: Stop 33 measurements were taken on a dike, and 34 measurements were taken on the surrounding outcrop. Kspar= Potassium Feldspar, Plag.=Plagioclase. Sites 84-100 are sourced from Bliekendaal (2012) and Van der Linde (2012), 101-127 from Fulmer and Kruijer (2009), and 128-136 from Johnson (2015).

*All sites are located in UTM Zone 11S.

† All unit identifications are based on Figure 2.

N.A.= not applicable.

REFERENCES CITED

Bateman, P. C., and Wahrhaftig, C., 1966, Geology of the Sierra Nevada, *in* Bailey, E. H., ed., Geology of Northern California: California Division of Mines and Geology Bulletin 190, p. 107–172.

Bateman, P.C., Ronald, K.W., and Busacca, A., 1983, Geologic map of the Tuolumne Meadows quadrangle, Yosemite National Park, California: U.S. Geological Survey, scale 1:62,500.

Bateman, P.C., 1992, Plutonism in the central part of the Sierra Nevada batholith, California: U.S. Geological Survey Professional Paper 1483, Washington, D.C, United States Government Printing Office, 186 p., https://pubs.usgs.gov/pp/1483/report.pdf

Becker, R.A, Tikoff, B., Riley, P.R., and Iverson, N.R., 2014, Preexisting fractures and the formation of an iconic American landscape: Tuolumne Meadows, Yosemite National Park, USA: Geological Society of America Today v. 24, p. 4–10, doi: 10.1130/gsatg203a.1.

Bliekendaal, E., 2012, Formation of the Yosemite Creek Granodiorite: A field and geochemical study [M.S. thesis]: Vrije University, Amsterdam, 155 p.

Cross, W., Iddings J.P., Pirsson L.V., and Washington, H.S., 1902, A quantitative chemico-mineralogical classification and nomenclature of igneous rocks: The Journal of Geology, Vol. 10, No. 6, p. 555-690.

Ericson, K., Migón, P., and Olvmo, M., 2005, Fractures and drainage in the granite mountainous area: A study from Sierra Nevada, USA: Geomorphology, v. 64, p. 97–116, doi: 10.1016/j.geomorph.2004.06.003.

Fulmer, E.C., and Kruijer, T., 2009, The nature of batholith formation: Detailed field, geochemical and isotopic constraints on the assembly of the Sentinel Granodiorite, Sierra Nevada Batholith, USA [M.S. thesis]: Vrije University, Amsterdam, 272 p.

Flageollet, J.C., 1977, Origine des reliefs, altérations et formations superficielles; contribution à l'étude géomorphologique des massifs anciens cristallins: l'exemple du Limousin et de la Vendée du Nord-Ouest [PhD Thesis]: Paris Diderot University, Paris, 491 p.

Gabet, E.J., 2014, Late Cenozoic uplift of the Sierra Nevada, California? A critical analysis of the geomorphic evidence: American Journal of Science, v. 314, p. 1224–1257, doi: 10.2475/08.2014.03.

Glazner, A.F., Bartley, J.M., Coleman, D.S., Gray, W., and Taylor, R.Z., 2004, Are plutons assembled over millions of years by amalgamation from small magma chambers?: GSA Today, v. 14, p. 4–12, doi: 10 .1130 /1052 -5173 (2004)014 <0004:APAOMO>2.0.CO;2.

Godard, A., 1965, *in* Godard, A., Godard, J. J., and Yannick L.(Eds.), Recherches de geomorphologie en Ecosse du Nord-Ouest: These Doct. Etat, Univ. Paris, Les Belles Lettres, Paris, p. 343-347.

Godard, A., Lagasquie, J. J., and Yannick L. ed., 2001, Basement Regions: Springer-Verlag Berlin Heidelberg, 306 p.

Hahm, W.J., Riebe, C.S., Lukens, C.E., and Araki, S., 2014, Bedrock composition regulates mountain ecosystems and landscape evolution: Proceedings of the National Academy of Sciences, v. 111, p. 3338–3343, doi: 10.1073/pnas.1315667111.

Huber, N.K., 1987, The geologic story of Yosemite National Park: USGS Numbered Series, v. 1595, p. 1–64.

Huber, N. K., Bateman, P.C., and Wahrhaftig, C., 1989, Geological map of Yosemite National Park and Vicinity, California: U.S. Geological Survey, scale 1:125,000, https://pubs.usgs.gov/imap/i1874/.

Johnson, B.D., 2015, Lithologic controls on knickpoint formation in Sierra Nevada bedrock channels [M.S. thesis]: San Jose State University, California, 62 p.

Johnson, B.L., 2013, Structure, construction, and emplacement of the Yosemite Valley intrusive suite and the Yosemite Creek granodiorite in the Central Sierra Nevada batholith [M.S. thesis]: San Jose State University, California, 89 p.

Karaman, K., and Kesimal, A., 2014, A comparative study of Schmidt hammer test methods for estimating the uniaxial compressive strength of rocks: Bulletin of Engineering Geology and the Environment, v. 74, p. 507–520, doi: 10.1007/s10064-014-0617-5.

Kistler, R.W., 1973, Geologic map of the Hetch Hetchy quadrangle, Yosemite National Park, California: U.S. Geological Survey, scale 1:62,500.

Kühni, A. and Pfiffner, O.A., 2001, The relief of the Swiss Alps and adjacent areas and its relation to lithology and structure: Topographic analysis from a 250-m DEM: Geomorphology, v. 41, p. 285–307, doi: 10.1016/s0169-555x(01)00060-5.

McCarroll, D., 1991, The Schmidt hammer, weathering and rock surface roughness: Earth Surface Processes and Landforms, v. 16, p. 477–480, doi: 10.1002/esp.3290160510.

Migón, P., 2006, Granite Landscapes of the World: Oxford, Oxford University Press, 384 p.

Migón, P. and Vieira, G., 2014, Granite geomorphology and its geological controls, Serra da Estrela: Geomorphology, v. 226, p. 1-14.

Mulch, A., Sarna-Wojcicki, A. M., Perkins, M. E., and Chamberlain, C. P., 2008, A Miocene to Pleistocene climate and elevation record of the Sierra Nevada (California): Proceedings of the National Academy of Sciences of the United States of America V. 105, No. 19 (May 13, 2008), p. 6819-6824.

Onodera, T.F., and Asoka Kumara, H.M., 1980, Relation between texture and mechanical properties of crystalline rocks: Bulletin of the International Association for Engineering Geology, v. 22, p. 173–177.

Pitcher, W.S., and Berger, A.R., 1972, The Geology of Donegal: A Study of Granite Emplacement and Unroofing: New York, Wiley, 435 p.

Schaffer, J. P., 1997, Sierra Nevada uplift— When did it occur?: Yearbook of the Association of Pacific Coast Geographers, Vol. 59, p. 101-119.

Scott, D.N., and Wohl, E.E., 2018, Bedrock fracture influences on geomorphic process and form across process domains and scales: Earth Surface Processes and Landforms, doi: 10.1002/esp.4473.

Segall, P., McKee, E.H., Martel, S.J., and Turrin B.D., 1990, Late Cretaceous age of fractures in the Sierra Nevada batholith, California: Geology, v. 18, p. 1248-1251.

Segall, P., and Pollard, D. D., 1983, Joint formation in granitic rock of the Sierra Nevada: Geological Society of America Bulletin, v. 94, p. 563-575.

Stutenbecker, L., Costa, A., and Schlunegger, F., 2016, Lithological control on the landscape form of the upper Rhône Basin, Central Swiss Alps: Earth Surface Dynamics., v. 4, p. 253-272, doi: 10.5194/esurf-4-253-2016.

Tuğrul, A., and Zarif, I. H., 1999, The correlation of mineralogical and textural characteristics with engineering properties of selected granitic rocks from Turkey: Engineering Geology, v. 51, p. 303-317.

U.S. Geological Survey, 2014, National Elevation Dataset: http://nationalmap.gov/viewer.html.

U.S. Geological Survey Gap Analysis Program, 2016, GAP/LANDFIRE National Terrestrial Ecosystems 2011: https://doi.org/10.5066/F7ZS2TM0.

van der Linde, M., 2012, The Formation of the Yosemite Creek granodiorite: A field and geochemical study [M.S. thesis]: Vrije University, Amsterdam, 196 p.

Wahrhaftig, C., 1965, Stepped Topography of the Southern Sierra Nevada, California: Geological Society of America Bulletin, v. 76, p. 1165–1189.

Zhang, W., Oguchi, T., Hayakawa, Y.S., and Peng, H., 2013, Morphometric analyses of Danxia landforms in relation to bedrock geology: A case of Mt. Danxia, Guangdong Province, China: The Open Geology Journal, 2013, 7, 54−62, 10.2174/1874262901307010054.

Zimmer, P., and Gabet, E.J., 2018, Assessing glacial modification of bedrock valleys using a novel approach: Geomorphology, v. 318, p. 336-347.